SLURRY LEAKOFF CONTROL IN NATURALLY FRACTURED RESERVOIRS USING SOLID FLUID LOSS ADDITIVES

by

Hossein Hosseini

ProQuest LLC.
789 East Eisenhower Parkway
P.O. Box 1346
Ann Arbor, MI 48106 – 1346

A thesis submitted to the Faculty and Board of Trustees of the Colorado School of Mines in partial fulfillment of the requirements for the degree of Doctor of Philosophy (Petroleum Engineering).

Golden, Colorado

Date April 4, 2001

Signed: Hossein Hosseini
Hossein Hosseini

Approved: Ramona M. Graves
Dr. Ramona M. Graves
Thesis Advisor

Golden, Colorado

Date April 4, 2001

Craig W. Van Kirk
Dr. Craig W. Van Kirk
Professor and Head,
Department of
Petroleum Engineering

ABSTRACT

Hydraulic fracturing is a means of enhancing hydrocarbon production, particularly for low permeability formations. During the fracturing process, injected liquids leakoff through fracture walls to adjacent formations. Excessive fluid leakoff will result in fluid pressure loss inside the induced fracture, inhibiting fracture propagation and possibly bridging the fracture with proppant. Leakoff and its consequences are magnified for naturally fractured reservoirs.

The goal of this research is to improve technical and economic performance for hydraulic fracturing of naturally fractured reservoirs. The objective of this project is to better understand slurry leakoff and the parameters which influence this process in naturally fractured reservoirs. The emphasis of this research is on fluid flow experiments conducted in small plexiglass models of 12 x 1 x 1/4 inches dimensions. The structure of the models represent induced and natural fractures 0.01, 0.03, 0.05, 0.06, and 0.08 inches wide. The injected slurries consisted of aqueous solutions of guar and polyacrylamide mixed with 20-40 mesh sand and solid fluid loss additives such as silica flour, starch, 100 mesh sand, and oil soluble resin. Pressure drop, fluid leakoff, polymer fluid rheological data, and the videos of the experiments are used for analysis of the results.

The results from the slurry flow experiments show that addition of solid particles to a polymer solution may inhibit fluid leakoff if the particle diameter is sufficiently large to bridge the simulated natural fracture. Solid concentration (20-40 mesh) of 1 lb/gal

mixed with 60 lb/Mgal guar solution was sufficient to form a sand node at the round leakoff site of 0.0625 inch diameter. However, 3 lb/gal solid concentration would inhibit slurry leakoff through simulated natural fractures of up to 0.06 inch wide. Experimental observations indicate that a sand node forms at or below a slurry velocity in the model. This velocity is referred to as the "critical velocity" for a given slurry. For example, for a 60 lb/Mgal guar slurry with 5 lb/gal 20-40 mesh, a sand node formed at a critical velocity of 0.33 ft/sec. Successive runs below this velocity will result in sand node formation at the leakoff site.

A total of 240 flow experiments were completed. The results show that fluid properties have a significant role in determining sand node formation. In particular, the viscoelasticity of the slurry strongly influences the sand node build up at the leakoff site. Dimensionless groups, such as Reynolds number and Weissenberg number, were used to characterize this phenomenon. The calculations indicate that sand node formed for Reynolds number and Weissenberg number less than 3 and 6, respectively.

The results also indicate that viscoelastic slurries would form a sand node at lower slurry velocities in the induced fracture. The lower the viscoelasticity of the slurry, the higher the injection rates can be in order to effectively block the natural fractures of up to 0.06 inches wide with a minimum 20-40 mesh sand concentration of 3 lb/gal.

Analysis indicates that the mechanism of the sand node formation is related to the particle migration during the slurry flow. Particles migrate to the low velocity gradient region (toward the center of the model) for the viscoelastic slurries (i.e. polyacrylamide)

whereas particles migration is toward the high velocity gradient region (toward the model wall) for pseudoplastic slurries (i.e. guar). When a sand node forms, initially, the particles accumulate at the walls by the leakoff site entrance. This process continues until sand node enlarges from the walls toward the center and ultimately blocks the entire leakoff site.

A spreadsheet set was developed to predict hydraulic fracture dimensions using the Perkins-Kern-Nordgren (PKN) model. Simulated fracture dimensions are used to calculate the corresponding Weissenberg and Reynolds number and regions of node formation are identified. This approach can be utilized for planning and design of hydraulic fracturing of the naturally fractured reservoirs.

In conclusion, slurry leakoff can be controlled by the fluid rheology and the flow rate in the fracture channel. This process is influenced by the size, concentration, and distribution of the solid fluid loss additives, and the natural fracture dimensions. The findings of this investigation promises cost reduction due to chemical leakoff prevention, and revenue enhancement due to better extension of fracture and thus increased hydrocarbon production.

TABLE OF CONTENTS

Page

LIST OF FIGURES

Page

LIST OF TABLES

Page

ACKNOWLEDGEMENTS

I take this opportunity to express my deep appreciation to Dr. Ramona Graves, my advisor, for her guidance, supervision, and advice in the completion of this dissertation. I am indebted to her tenacity for finishing this dissertation.

I also extend my appreciation to Dr. Jon Carlson for his technical contributions and his assistance during this investigation. I thank Dr. Robert Thompson for his continual positive encouragement during this research investigation and recognize Dr. Mark Miller's support and encouragement all along during the completion of this research.

I am indebted to Dr. Will Fleckenstein for his review of this dissertation. He has greatly facilitated the completion of this work.

I would also extend my appreciation to the remaining two members of my committee, Professors Don Dickinson and John Stermole for their selfless willingless to serve on my defense committee and for being available at any opportunity to make finishing this work a reality. I sincerely appreciate the efforts of all the committee members on my behalf.

I acknowledge the partial financial support from PERFORM Consortium at the Colorado School of Mines for the support of this research. The plexiglass models provided by Amoco are also appreciated.

Finally, I take this opportunity to dedicate this work to the ones who have encouraged me and have patiently waited for this moment to be realized. I dedicate this dissertation to my parents, my brother, my sisters, and specially my three children, Amir, Amin, and Laila.

Chapter I. Introduction

Hydraulic fracturing has been used in oil and gas industry for almost half a century. It is a means of stimulating formations to increase oil and gas production. A formation of interest is hydraulically fractured by injecting frac fluids. Frac fluids usually consist of suspension of solids in liquids. Suspended solids keep the induced fracture open such that effective formation permeability increases and hydrocarbon production is enhanced.

One of the major concerns in hydraulic fracturing is loss of fluids to the formation. Loss of frac fluid inhibits fracture growth. This effect is more pronounced in naturally fractured reservoirs where severe fluid loss to the formation may take place due to existing channels in the formation.

To remedy this problem, different types of solid additives are included in the injected slurry to prevent fluid leakoff. Silica flour, starch, and 100 mesh sand are examples of fluid loss additives (FLA) in field applications.

There are three main mechanisms which affect fluid leakoff rates to the formation: i) Fracturing fluid properties and relative permeability to the filtrate, ii) Viscosity and compressibility of the reservoir fluids, and iii) Wall building which takes place due to fracture fluid flow into the formation.

The contribution of the three mechanisms mentioned on fracture slurry leakoff rates are designated by C_v, C_c, and C_w, respectively. The combined effect of the three

coefficients define the leakoff coefficient. In practice, C_w is compared to the sum of C_v and C_c and the larger of the two quantities is taken as the fluid leakoff rate.

Cross-linked or straight gel fluids are used for hydraulic fracturing. For example, guar is either cross-linked with borate or used as straight gel. Fluid loss additives are added to the pad fluid to control fluid leakoff rates.

This experimental investigation was undertaken to quantify the effect of fluid loss additives on controlling fluid leakoff in fractured reservoirs. Slurries were prepared by mixing guar and polyacrylamide solutions with fluid loss additives. Due to equipment limitations, such as pressure rating of the plexiglass models, polyacrylamide was used to represent the viscoelatic nature of the cross-linked frac gels.

This research work consists of two main sets of experiments: flow experiments and fluid rheology experiments. Flow experiments focused on flow of slurries made up of guar and polyacrylamide solutions mixed with fluid loss additives such as silica flour, starch, oil soluble resin, 100 mesh sand and 20-40 mesh sand. The experiments were conducted using plexiglass models with leakoff sites of varying width, ranging from 0.01 inch to 0.08 inches. The results of these experiments show that several variables such as fluid velocity in the induced fracture, fluid rheology, leakoff site gap, solid concentration, particle size and size distribution affect slurry leakoff rate. Samples of these results are provided in Chapter IV in the flow experiment result section. The results indicate that there is a window where combination of these variables will result in formation of a sand node. And as a result, slurry leakoff rates will reduce considerably.

In this research, sand node is referred to as the accumulation of sand or additive particles at the leakoff site. The formation of a sand "body" or particles will effectively reduce the magnitude of the fluid leakoff.

The flow experiments are linked to fluid rheological properties. These properties reflect the fluid behavior under stress and indicate the adjustments polymer molecules make under these conditions. Such information is valuable when dimensionless groups such as Reynolds number and Weissenberg number are used to describe a fluid system during flow. Dimensionless groups take into account the effects of several properties simultaneously.

This dissertation is organized in eight chapters. Introduction to the problem and the research investigation is briefly covered in Chapter I. Chapter II covers literature review with topics on fluid rheology, fluid leakoff, particle settling, and particle migration. Description of laboratory equipment set up, the procedure for flow experiments with the data collection, and fluid rheological measurements are covered in Chapter III.

Chapter IV discusses the results of the flow experiments. In this chapter the flow experiments are subdivided into three categories of experiments: preliminary experiments, screening experiments, and flow experiments.

Fluid rheology data and the discussion are presented in Chapter V. The polymer rheology data include apparent viscosity, stress relaxation modulus G(t), storage modulus $G'(t)$, and loss modulus $G''(t)$.

In Chapter VI the results and observations from the flow and rheology experiments are linked. The discussion leads to an explanation of the behavior of the sand node formation and the mechanism of this process.

In Chapter VII, with the use of spreadsheet and given treatment and rock data, fracture dimensions are predicted employing the PKN model. The predictions are coupled with the laboratory findings as a predictive tool for planning and designing hydraulic fracturing treatment while accounting for possible natural fractures during the process. Chapter VIII concludes this research investigation with conclusions and recommendations.

Chapter II. Literature Review

There are several subject areas relevant to this investigation. This literature review is a brief review of research findings by other investigators. This section is organized in four main subjects: fluid rheology, fluid leakoff, particle settling and particle migration.

2.1 Fluid Rheology

Initially, lease crude oil was used as fracture fluid. Later, gelled fluid technology was implemented by using napalm, which led to the second generation of fracturing fluids. With the introduction of water base fluids, starch was used as a fracture fluid to increase viscosity and reduce pipe friction. However, starch was very shear and temperature dependent and moreover, very susceptible to salt concentration. With discovery of guar gum in the late 1950's, a more reliable gelling agent for water base fluids was introduced.[1] Guar gum is an extract from guar beans. It is a long chain polymer composed of mannose and galactose sugars.[2] With introduction of guar fluids, the study of their flow behavior and rheology was a necessity.

Rheology is the science of deformation and flow of matter. The two crucial tasks for a fracturing fluid are to maintain its integrity to the extent that it will carry the proppant load to the formation and secondly, break in a manner that the fracture faces could be cleaned from the gelatinous matter and flow back to the surface. Thus, it is

essential to understand fluid characteristics, specifically the apparent viscosity and the factors which influence this variable. It is also vital to understand fluid leak off and gel decomposition which affects clean up process.

2.1.1 Fundamentals

Rheology provides a means of measuring polymer fluid reactions to external stresses and strains. When stress is applied, polymer deforms and the molecule chains try to relieve themselves from the applied stress. This is called stress relaxation process. Rheology is a means to relate molecular structure to external factors such that fluid performance can be predicted.

Fluid resistance to flow is called fluid viscosity. There are two distinct types of liquid fluids, Newtonian and non-Newtonian. Newtonian fluids maintain constant viscosity when exposed to varying shear rates (i.e. water). In laminar flow, the behavior can be described by viscosity as follows:

$$\mu = \tau / \gamma' \qquad (2.1)$$

where μ = viscosity
τ = shear stress
γ' = shear rate

Non-Newtonian fluids are shear sensitive and exhibit viscosities which are shear dependent. The relationship between shear stress and shear rates are complex. Fracture fluid behavior is commonly represented by power law model as follows:

$$\tau_w = K' (\gamma')^{n'} \qquad (2.2)$$

where τ_w = shear stress at the wall
γ' = shear rate
K' = consistency index
n' = flow behavior index [3]

To describe a power law fluid one needs to determine n' and K'. By taking the logarithm of equation (2) and plotting shear stress τ_w as a function of the shear rate γ' the slope of the straight line will equal n' and K' will be the Y intercept. Other fluid models are used for other non-Newtonian fluids. For example, Ellis model is used for pseudoplastic fluids, Bingham plastic model is used for fluids with yield stress and linear viscosity behavior, and Herschel-Bulkley model describes the behavior of fluids having a yield stress with non-linear viscosity feature.[4]

Materials respond to an applied force by exhibiting elastic or viscous behavior or through a combination of both called viscoelastic behavior. Almost all fracture fluids exhibit viscoelastic behavior and their mechanical properties are time and temperature dependent.

A Hookean material under constant stress deforms immediately to a constant strain and recovers instantly to its original shape when stress is removed (steel spring). However, when stress is applied to a Newtonian fluid, it deforms continuously and does not recover its original form when stress is removed (i.e. water). A viscoelastic material

exhibits a combination of these two behaviors. There would be an incomplete and time dependent recovery after stress is relieved.

Base gel fluids (hydrated polymer fluids) are cross-linked with metal ions or transition metal ions to form more rigid and viscous fluids called cross-linked gel fluids. When placed in a cup and shear is applied, cross-linked gel fluid will climb up the cup. This is due to stresses generated in the fluid which are normal to the direction of shear. This behavior is called Weissenberg effect.

The viscoelastic behavior of cross-linked gels are studied under dynamically varying shear stress. The elastic behavior is described by storage modulus (G') and the viscous effects are measured by the loss modulus (G"). G' is attributed to the energy storage of the cross-linked gel whereas G" is related to energy dissipation through viscous effects under shear conditions. The sum of these two moduli will define dynamic shear modulus (G*).

$$G^* = G' + iG'' \qquad (2.3)$$

where G' = storage modulus
G" = loss modulus

G' and G" values are related to fracture fluid rheology. Friction pressures encountered during the fluid pumping is related to the G' values. G' is a measure of the energy the fluid will store when it is sheared. Analysis of data collected for two sets of cross-linked and non-cross-linked hydroxypropyl guar fracture fluids with identical polymer concentration for each set has shown that the ratio of G' values for cross-linked

fluids were greater than the ratio of G' values for the non-cross-linked fluids. Whereas, the ratio of G" for the cross-linked and non-cross-linked fluids stayed almost the same. The more viscoelastic the fluid is, the higher the G' value thus, the higher friction pressures. In the optimization process, it will be important to design cross-linked fluids such that the G' value will be reduced while the G" value will stay the same compared to the uncross-linked fluid.[3]

2.1.2 Apparent Viscosity Measurements and Instrumentation

Fracture fluid rheology is an important factor taken into account in a frac job. The apparent viscosity exhibited by the fluid under the prevailing reservoir conditions (i.e. temperature, shear rate, pH) will determine the success of the operation. Thus, it is important to ensure quality control on the job site such that injected fracture slurry meets the required gel rheology before and during the fracturing. One of the devices used for the on-site gel property measurements are rotational viscometers. Rotational viscometers measure fluid viscosity at a constant shear rate using either a rotating cup and stationary bob and/or a stationary cup and a rotating bob similar to the configuration for Fann and Brookfield viscometers, respectively.

Fluid apparent viscosity is obtained by measuring the shear stress induced in the fluid due to the torque on the bob, and the shear rate is obtained at each rotational speed. The drawbacks in these measurements are the constant shear rate, the unsheared fluid

remaining in the bottom of the cup, and the viscoelastic properties of the fluids which introduce inaccuracy when measurements are made at high shear rates.[4]

Fracture fluid rheology can yet be better characterized by "pipe viscometers." Pipe viscometers were introduced to simulate the actual fracture conditions in terms of temperature and shear rate. A polymer and cross-linker are mixed and pumped through a tubing. Gel fluid temperature is increased by heat transfer to the fluid system. This set-up simulates the temperature increase and the shear effects on gel fluid while being pumped through the tubing to the fracture. The pressure drop and flow rate measurements are collected and used to compute wall shear stress and rate of shear at the wall, respectively. The following equations can be used for such computations.

$$\tau_w = d * \Delta P_f / 4L \qquad (2.4)$$

$$\gamma'_w = 3(8q/\pi d^3)+(d\Delta P/4L)(\partial(8q/\pi d^3)/ \partial(d\Delta P/4L)) \qquad (2.5)$$

where τ_w = wall shear stress
d = diameter of the pipe
ΔP_f = frictional pressure drop
L = tube length
q = flow rate
γ'_w = rate of shear

The rate of shear at the tube is given by Rabinowitch-Mooney equation for a volumetric flow rate through the tubing.[5] The apparatus requires instrumentation which makes it inconvenient. For example, relatively long pipes (6 to 10 feet) are used for accurate pressure drop measurements. A pump is used to displace gel fluid through the system. Pipe viscometers tend to be bulky in size.

Helical Screw Rheometer (HSR) was constructed for its advantages over the pipe and rotational viscometers. HSR eliminates the complications of torque and flow rate measurements associated with rotational and pipe viscometers, respectively.[6] When operating a HSR, pressure differential and rotation rate data are collected. Rotation rate and pressure drop data are used to obtain the n' and K' values. Next, apparent viscosity of the gel fluid for a given shear rate can be computed.

2.1.3 Rheological Characterization of Slurries

Fracture fluids are proppant-laden gel solutions pumped into the fracture to keep the induced fracture open after pumping stops. Fracture geometry and extension during the treatment depends to a high degree on the rheological properties of the clean as well as proppant laden fluids.[6] It is of great importance to understand the rheological behavior of these fluids for successful frac job designs. However, there are difficulties in obtaining rheological measurements at existing fracture shear rates.

Early research results have shown that adding proppant to gel fluid would increase gel viscosity considerably. Other factors such as base gel concentration, proppant concentration, particle shape, size, density, temperature and shear rate affect fracture fluid viscosity. Correlations have been developed to estimate the increase in viscosity of a base gel fluid due to addition of proppant. By determining the consistency index K' and the flow behavior index n' for the proppant-laden base gel fluid, one can determine the apparent viscosity.[7]

Recently, a model called GEFFAR has been developed which can estimate apparent viscosity of gel fluid loaded with proppant. In this model, viscosity is a function of solids loading and shear rate.[8] The equation used is as follows:

$$\mu(C_v,\gamma') = \mu_o(1-C_n)^{-a} \tan^{-1}((\gamma'/\gamma_L)^{n_o-1}) / \tan^{-1}((\gamma'/\gamma_H)^{n_o-1}) \qquad (2.6)$$

where $\mu(Cv,\gamma')$ = viscosity
n_o = clean fluid power law flow behavior index
γ_L , γ_H = adjustable parameters to match onset of deviation of low and high shear viscosity from the calculated power law viscosity
C_v = volume fraction solids
C_{vmax} = maximum volume fraction solids

C_n = C_v / C_{vmax}
a = slurry viscosity increase exponent ($1.2 < a < 1.8$)

To estimate apparent viscosity of a proppant laden fracture fluid using GEFFAR, a set of laboratory data of apparent viscosity as a function of shear rate for a cross-linked fluid is needed. The software constructs a plot of apparent viscosity as a function of shear rate using power law and GEFFAR models and provides regressed values for n' and K' for the fluid. From the plot, one can input γ_L, zero shear viscosity, and a large value for γ_H (onset of high shear plateau is very large shear rates). By adjusting the n' and K' values, best fit of the data can be constructed by GEFFAR. Next, the effect of added proppant to the gel fluid can be estimated by the following equation:

$$\mu = \mu_o(1-C_v/C_{vmax})^{-1.8} \qquad (2.7)$$

where, μ = fracture slurry viscosity
μ_o = gel fluid viscosity
C_v = volume fraction solids
C_{vmax} = maximum volume fraction solids ($0.5 < C_{vmax} < 0.6$)

2.2 Fluid Leakoff

A successful hydraulic fracturing treatment design depends on accurate knowledge of fluid loss properties of the fracturing fluids. The rates at which fluids leak off through fracture walls can affect fracture geometry and have economic impact. Therefore, a sound understanding of fluid leakoff is beneficial for a successful fracturing operation.

Howard and Fast [9] gave a description of the fluid loss and provided basic equation relating fracture area to fluid and the treating parameters. Hall and Dollarhide[10] investigated the effects of fracturing fluid velocity on fluid loss agent performance. They placed a core in a holder while the injected fluid passed in the annular space between the core and the core holder. Fluid leakoff was collected through a bore opening inside the core. Excess fluid was collected through the discharge valve. They observed fluid loss increase as the fracture flow velocity increased. The spurt loss was inversely proportional to the concentration of the fluid loss agent .

Penny and Conway[11] investigated the effectiveness of various fluid loss additives in controlling fluid leakoff. They suggested the use of particulate additives to control spurt loss in high permeable streaks and use of liquid hydrocarbon to control the leakoff coefficient (C_w).

Hall and Houk[12] conducted laboratory tests to determine fluid leakoff in the naturally fractured Buda formation. Fractured core of 1 3/4 inch diameter and 4 3/4 inch length was placed in a cell, 60 lb/Mgal guar fluid was pumped at 110 and 50 cc/min. For

leakoff control, a combination of fluid loss agents such as silica flour, 100 mesh oil soluble resin, fine oil soluble resin, and 70-170 mesh sand was used. Their results from laboratory tests showed that mixtures of fine and coarse particles were most efficient systems for fluid loss control in natural fractures. The best system evaluated for the field application was a mixture of fine and 100 mesh oil soluble resins.

Woo and Cramer[13] conducted laboratory tests and field evaluation of several fluid loss additives for use in the Williston Basin. For the experiments, a tapered slot of stainless steel of 2.1 inch in diameter and 1/4 inch thickness was employed. The slot was placed in a fluid loss cell and heated to 200 °F with cross-linked 40 lb/Mgal HPG fluid. Oil soluble resins of 100 and 250 mesh, 100 mesh sand, silica flour, and polymer/inert solid mixture were used as fluid loss additives. They showed that a mixture of 100 mesh sand and 100 mesh oil soluble resin performed best followed by 100 mesh OSR, mixture of silica flour and 100 mesh sand, mixture of 100 mesh sand and 250 mesh OSR, respectively.

Gulbis[14] conducted leakoff experiments using cores placed in a core holder. Hydroxypropyl guar of 40 lb/Mgal was in-line mixed with borate and transition metal (TM) cross-linkers. Leakoff data was collected for both cross-linked and non-cross-linked fluids. Their result showed that for TM-XL systems, fluid loss rate became constant after 25 minutes, while the other two systems had a declining fluid loss behavior. They attributed this to the continued filter cake deposition and the change in filter cake permeability. They also showed that silica flour was very effective in fluid loss control in non-cross-linked fluids. They also found diesel to be an effective fluid loss agent.

Roodhart[15] investigated the effect of rock permeability and shear rate on the dynamic fluid leakoff coefficient and the effect of fluid flow on filter cake build up. Their core leakoff experiments were conducted using 0.48 % HEC solution with silica flour as a solid additive and cross-linked HPG gel with 5 % diesel as a liquid leakoff additive. The results showed that the cross-linked system had thicker cake which would reduce the thickness of a fracture, causing higher shear rates and lower apparent viscosities. This can lead to narrower and longer fractures. Flow past the filter cake limited filter cake thickness build up, and the leakoff rate became constant. They also showed that the spurt loss was proportional to the square root of the permeability and was independent of the type of the leakoff additive.

Zigrye et al.[16] tested the effect of several fluid loss additives on cross-linked guar and linear guar. Diesel, silica flour, and a combination of diesel and silica flour were used as fluid loss additives. Bandera cores were used for the experiments. They used a flow loop apparatus to condition the fluids to shear and temperature encountered in down hole conditions. Their test showed that fluid loss of cross-linked fracturing fluids is best controlled by diesel. For linear systems, fluid loss was best controlled by means of particulate additives.

Gruesbeck[17] investigated the transport of solid suspensions through perforations. Two transparent lucite tubes of 3 inch ID and 7 inch ID with multiple perforations were fitted to represent a wellbore. HEC-water solutions were used to prepare slurries. Brady sand, Ottawa sand, UCAR glass beads, and sintered bauxite were used. 40/60, 20/40,

15/18, 10/20, and 6/9 were used. They derived a differential equation which stated that the motion of a particle was governed by gravity and drag force. Their results showed a good agreement of theoretical and experimental data. They concluded that increase in particle concentration downstream of the perforations will cause particle bridging at the perforation entrance and lack of particle transportation through the perforations, resulting in formation of a sand bed in the casing. To prevent bridging, the ratio of perforation diameter to average particle diameter should at least be 6/1. To prevent a particle bank from forming in the casing, either the pumping rate or the viscosity of the injected liquid be adjusted.

2.3 Particle Settling

An essential component of a successful treatment is creating a conductive proppant layer in the fracture channel. The proppant distribution is influenced by the physical environment that the injected slurry encounters, such as the shear rate, fluid leakoff, sand loading, and slurry rheology which affects the proppant dynamic and static settling rates and consequently affect distribution of proppant in the fracture.

Particle transport in hydraulic fractures in part determines the geometry of the propped fracture. Settling rate determines the distribution of the particles in the fracture. Terminal settling rates are governed by the gravitational force, drag force, density of the fluid and the particle, and the diameter of the particles. Depending on the flow regime that the particle experiences, the settling velocity can be estimated. For a laminar, transition, and turbulent regions, the following equations apply:

$$V_o = g\,(\rho_p - \rho)\,d^2 / 18\mu \qquad \text{Stokes' law} \qquad (2.8)$$

$$V_o = 0.20[g(\rho_p - \rho)/\rho]^{.72}\,[d^{1.8}/(\mu/\rho)^{0.45} \qquad \text{Transition region} \qquad (2.9)$$

$$V_o = 1.74[g\,(\rho_p - \rho)/\rho\,]^{0.50}\,d^{0.5} \qquad \text{Newton's law} \qquad (2.10)$$

Where V_o = settling rate velocity
ρ = fluid density
ρ_p = particle density
μ = fluid viscosity
d = particle diameter
g = acceleration of gravity

Once in the fracture, the fluid and the particle experience laminar conditions. Stokes' law is the equation which is widely used for this type of analysis. Numerous experimental research studies have been conducted to investigate the proppant settling rate. Novotny[18] presented a method to predict the proppant transport in vertical fractures and its settling during the treatment, and the fracture closure. He conducted experiments using a concentric cylinder and measured fall rate of the proppant.

Hannah[19] et al. conducted experiments investigating proppant transport in fracturing gels. They measured the fall rate of proppant in non-Newtonian fracturing gels using a concentric cylinder similar to Novotny's apparatus. Experimental data did not agree with the theoretical predictions and the discrepancy was not discussed.

Clark and Harkin [20] designed a large (4 ft by 12 ft) transparent vertical fracture model to investigate the proppant carrying capability of Newtonian and non-Newtonian fluids. They investigated the effect of fluid properties, proppant size and concentration,

fracture width and fluid velocity. They were the first to report the clustering of the proppant during the experiments. They made the observation that the particles can agglomerate which leads to fall rate increases. They concluded that agglomeration was an important factor in proppant transport, and that when flow stops, the clusters settle and coalesce with other particles resulting in settling velocities many times greater than that of a single particle.

Shah[21] investigated proppant settling rates for non-Newtonian fluids under static and dynamic conditions. He devised a new approach for analysis of the prop settling data. He pumped HEC (20,35 lb/Mgal) and HPG (30,35,50, 80 lb/Mgal) solutions through a 7 ft long Plexiglas column for dynamic fall rate data. This was done by holding the particles in place by means of fine stainless steel wire, and measured flow rate at which the particles would stay stationary in the column. The same column was used to obtain static settling rate data. He proposed to plot the velocity data on log-log scale as a dimensionless group of $\sqrt{\ }(C_D^{2-n'} N'^{2}_{Rep})$ as a function of dimensionless particle Reynolds number, N'_{Rep}. This type of plot generated a family of curves which were only a function of fluid model parameter, n . His results indicated that the dynamic settling velocity data agreed reasonably well with the correlation developed from static velocity data.

Clark and Quadir [22] completed a critical review of particle settling equations proposed by other investigators. They reported that Swanson concluded that the use of

Stokes' equation was not sufficient because it did not account for the shear associated with the particle fall in power fluids. He devised an equation which was applicable for any shape particle over a wide range of particle Reynolds number. The equation derived by Swanson was:

$$V_o = V_N/\alpha \, [\, 1/ (1+\sqrt{48}\, \beta_P \, \mu/d\rho V_N)] \qquad (2.11)$$

Where $V_N = \sqrt{4gd(\rho_p-\rho)/3\rho}$ (2.12)

V_o = settling velocity
V_N = velocity
α = 1.277 boundary layer coefficient (for sand)
β_p = 2.800 boundary layer coefficient (for sand)
μ = fluid viscosity
d = particle diameter
ρ = fluid density
ρ_p = particle density
g = acceleration of gravity

Zigrand and Sylvester developed an explicit equation for the settling velocity given by:

$$V\psi = c- (c^2 - a^2)^{0.5} \qquad (2.13)$$

$$c = 1/2 \, (2a + b^2) \qquad (2.14)$$

$$a = 2.0/0.63(3^{0.5}) \, [g \, (\rho_p - \rho) \, (1- \varphi)/\rho(1-\varphi)^{1/3}]^{1/2} \qquad (2.15)$$

$$b = 4.8/0.63 \, [\mu e^{(5\varphi/3(1-\varphi)} /\rho d \,]^{1/2} \qquad (2.16)$$

where a = constant
b = constant
c = constant
ρ = fluid density
ρ_p = particle density
μ = fluid viscosity

V_ψ = velocity for prop fractional concentration
φ = volume/volume particle concentration
d = particle diameter

Daneshy published an expression for the settling velocity of spherical particles in a power law fluid as follows:

$$Vo = [g (\rho_p - \rho) d^{n+1} / 18K(3)^{n-1}]^{1/n} \quad (2.17)$$

Where K = fluid consistency index
n = fluid flow behavior index
ρ = fluid density
ρ_p = particle density

Harrington proposed the following equation for cross-linked fluids

$$V_o = \beta[g(\rho_p - \rho)d^2 / 18\mu a] \quad (2.18)$$

Where β = 0.22
μ = fluid viscosity
d = particle diameter
ρ = fluid density
ρ_p = particle density
g = acceleration of gravity

Their study of models indicated that equations 11, 13, and 17 produced similar results for calculated settling velocities, and the equation (18) gave inconsistent results for the same conditions used in this study. They also concluded that the assumption that the shear effects on the viscosity of the fluid do not affect the settling velocity of the suspended particles, is not completely valid and will produce optimistic estimates of the particle transport.

Roodhart[23] analyzed proppant settling data obtained by other investigators. He argued that the reason for the deviation of the data collected by previous investigators from Stokes' equation was due to neglect of fluid zero shear viscosity. He conducted experiments in a vertical slot flow model which consisted of two perplex plates separated by a removable spacer. Fluids could be pumped at rates of up to 0.23 bbl/min per foot of formation. He used the notion that the overall shear rate acting on a proppant particle is the vector sum of the shear rate due to proppant settling, and the shear rate imposed by the fluid motion at the location of the falling particle. He proposed using the following equations coupled with the Stokes' formulation to obtain settling velocities:

$$\gamma' = 1/\mu_\infty \{\tau - \tau_0 (1 - e^{-a\tau})\} \qquad (2.19)$$

where $a = (1 - \mu_\infty / \mu_o) / \mu_o$
μ_o = zero shear viscosity
μ_∞ = apparent viscosity
τ = shear stress
τ_o = apparent yield stress
γ' = shear rate

The three parameters are the two limiting viscosities (μ_o and μ_∞) and the apparent yield stress (τ_o). Using the above equation to compute apparent viscosity and Stokes' law, produced excellent results.

Research discussed so far only used a power law model with power law fluids. The studies were limited to viscous characteristics of the fluid and experiments were conducted at very slow motion in the Stokes' region. Acharya[24] conducted a study of particle transport in viscous and viscoelastic fracturing fluids. He investigated the

particle settling rates in low ($N_{Re} < 2$) and intermediate ($2 < N_{Re} < 500$) Reynolds numbers. He developed new correlation for proppant settling rate in inelastic and viscoelastic fracturing fluids for low and intermediate Reynolds numbers. He concluded that in low flow regions, the fluid elasticity did not affect proppant settling rates and a power law type rheological model for fluid viscosity was adequate for both inelastic and viscoelastic fracturing fluids. However, for intermediate Reynolds number region ($2 < N_{Re} < 500$), fluid elasticity enhanced particle settling and a power law model would not be adequate to describe the fluid behavior. His correlations for the low and intermediate regions were as follows:

$$V_{inelastic} = [g(\rho_p - \rho)d^{n+1}/18\,K\,F(n)]^{1/n} \quad \text{for low flow region} \qquad (2.20)$$

$$\text{Where, } F(n)=3^{3n-3/2}[33n^5-63n^4-11n^3+97n^2+16n / 4n^2(n+10)(n+2)(2n+1)] \qquad \text{.....(2.21)}$$

$$V_{inelastic} = \{3\rho/(4(\rho_p-\rho)g\,d_p)[(24F(n)/N_{Re}) + (F2(n)/_{Nre}) + F2(n)/N_{Re}\,F3(n)]\}^{-1/2}$$

for intermediate flow region (2.22)

$$\text{Where } F_2(n) = 10.5\,n - 3.5 \qquad (2.23)$$

$$F_3(n) = 0.32\,n - 0.13 \qquad (2.24)$$

d_p = particle diameter
ρ = fluid density
ρ_p = particle density
n = power law fluid index
K = consistency index of the power law fluid

V = velocity
g = acceleration of gravity

for viscoelastic fluids in intermediate flow region, the following equation can be used:

$$V_{VElastic} = V_{inelastic}\{1 - \alpha (N_{Re}.Wi)^{\beta}\}^{-1/2} \quad (2.25)$$

Where α = 0.18
β = 0.19
Wi = Weissenberg number
Re = particle Reynolds number

Particle settling in non-Newtonian fluids (polymer and cross-linked gels) was investigated by Jin and Penny[25]. They promoted the idea of using a dimensionless group in predicting the settling rates. Three dimensionless groups of Reynolds number, drag force, and viscoelastic number were developed. They conducted laboratory experiments using polymer and cross-linked gel systems. Physical parameters such as viscosity, drag force, friction factor, terminal velocity, shear rate, and relaxation time were either measured or computed. Xanthan, polyacrylamide, and HEC were the base gel fluids used. Borate cross-linked guar and HPG systems were evaluated at pH ranges of 8.5, 9.0, and 9.5 respectively. Algorithms were presented for particle settling prediction under both static and dynamic conditions. A plot of friction factor as a function of Reynolds number based on fluid viscous properties would lead to a particle settling rate computation.

Much of the research discussed so far was to obtain particle settling velocities which were due to gravitational force, fluid rheological properties, and shear effects. Cleary and Fonseca[2] conducted an experimental and numerical simulation to demonstrate the effect of slurry convective downward motion. They derived an equation showing that convention was scaled to fracture width while settling is scaled to proppant diameter. Experimentally, they showed that the heavy viscous fluid moves through a less viscous fluid. They called this observation "encapsulation". Their simulation results indicated that convection was the single most important cause of particle settling.

This concept was taken and investigated by Clark and Zhu[27] in an attempt to further investigate the convection phenomenon in an experimental apparatus. They used a slot model with an entrance/fracture-height ratio of 1:65, which qualified the model as a point source. Slot dimensions were 10.8 x 4.9 x 0.05 inches. For their experiments, HPG and glycerin were used as non-Newtonian and Newtonian fluids, respectively. Silica flour and salt were added as densifiers. Their Newtonian fluid results indicate that for a slight density difference between the displacing and the displaced fluid, the resulting flow pattern was slightly asymmetrical, whereas for high density differences, the entrance flow resembles a waterfall. The results of the non-Newtonian fluid experiments showed that the effects were similar except that the shape of the plume was more rounded and not elongated. When the displacing fluid density increased, the tendency to fall to the bottom of the model decreased. For data analysis, they developed two dimensionless groups, one

for each type of the fluids. The dimensionless group (N_c) was the ratio of the horizontal force to vertical force for Newtonian and non-Newtonian fluids. Conceptually, it is the ratio of the prevailing forces for the given flow conditions. If the ratio is less than one, then the vertical forces are favored and vice versa. Below is the equation for both fluid types:

$$N_c = 12\,\mu q / \Delta\rho g\, w^3 \quad (\text{for Newtonian}) \tag{2.26}$$

$$N'_c = 2\,(4 + 2/n)^n\; Kq^n / \Delta\rho g\, w^{(1+2n)} \quad (\text{for non-Newtonian}) \tag{2.27}$$

Where μ = fluid viscosity
q = flow rate
$\Delta\rho$ = density difference between the fluid and the particle
w = slot width
K = fluid consistency index
n = fluid flow behavior index
g = acceleration of gravity

The results obtained from these experiments showed convection in low viscosity fluids. Addition of a thickening agent to increase viscosity in non-Newtonian fluid decreases the convection effect.

Nolte[28] conducted a theoretical study of fluid flow considerations in hydraulic fracturing. On the particle migration aspect of the fluid flow, he argued that in viscoelastic fluids, particles would move toward the center due to a net force acting on the particle. He added that the force was analogous to the gravity force on the particle, and caused the particle to move towards the center. This would result in an increase of particle concentration near the center of the channel and cause formation of "sheet" flow.

For non-Newtonian fluids which are not viscoelastic, particles move toward the high shear region (the wall). Because fracturing fluids are both highly viscoelastic and non-Newtonian, the direction of migration may differ for different fluids and shear conditions.

The computer simulation of proppant transport in a hydraulic fracture is the topic of a published paper by Unwin and Hammond[29]. They developed a model which predicted the motion of a slurry in a narrow slot. They also obtained an estimate of the amount of gravity driven vertical motion of proppant that can occur within a fracture during placement. Their simulation showed that proppant settling and convection can occur on the time scale of a fracturing job. They indicated that convection was slightly stronger than settling. However, the settling was more enhanced when there was a sheet flow (particles migration toward the center) compared to particles uniformly distributed across the width.

Barree and Conway[30] developed a 3-D simulator called GOFFER which is capable of predicting proppant transport in fractures. The model was tested and verified against experimental observations in a 4 x 16 ft model. Their experimental results showed that convective flow occurs whenever there is bulk density gradient which exceed the viscous forces. The vertical velocities due to convection were hundreds of times greater than the single particle settling velocities. Finally, the proppant placement can be modified by varying injection rate and proppant scheduling. Their simulation results indicated that proppant-slurry transport can be predicted accurately by accounting for the

effects of single particle settling, convection, slurry rheology, and particle velocity profile.

2.4 Particle Migration

One interesting aspect of slurry flow is the particles migration across the conduit width during the flow. The direction of the migration is determined by the slurry rheology. Particle migration has been the topic of numerous research investigations and, currently, extensive research is underway to better understand this phenomenon.

Gauthier and Mason[31] conducted experiments to investigate particle migration in non-Newtonian media undergoing Couette flow. They used carboxyvinyl polymer as pseudoplastic, and polyacrylamide and polyisobutylene in decalin as viscoelastic suspending liquids. Polystyrene spheres and discs, aluminum particles, and polymethyl-methacrylate spheres were used as the suspended phase mixed with the polymer solutions. Experiments were conducted in vertical glass tubes of diameters ranging from 0.4 to 0.8 cm. The slurry was pumped at a constant rate by a withdrawal pump. The temperature was maintained at $22 \pm 0.5°C$.

Transational velocities were measured by taking cine films, and the particle behavior was observed by means of a travelling microscope mounted parallel to the tube. They observed that neutrally buoyant rigid particles suspended in pseudoplastic liquids

migrated across the planes of shear towards the region of higher velocity gradients (i.e. toward the walls). Conversely, particles moved toward the low velocity gradient (i.e. toward the center) in viscoelastic slurries. However, they did not have an explanation for the different behavior of the particle migration for the two rheologically different slurries.

Tehrani[32] investigated particle migration in tube flow using viscoelastic fluids used in hydraulic fracturing. Aqueous solutions of hydroxypropyl guar (HPG) were cross-linked with a borax and mixed with transparent acrylic particles of size 650-710 μm, which is close to the 20/40 mesh sand commonly used in hydraulic fracturing. Experiments were conducted in two vertical Perspex pipes (ID=6 mm, L=1.5 m), while continuous flow was provided by a peristaltic pump. He observed that particles move to the regions of low shear rates , i.e., the pipe axis, in shear-thinning weakly cross-linked fluids. The rate of migration increased for high Weissenberg number and larger shear rate gradients. On the contrary, strongly cross-linked fluids produced little or no particle migration. This behavior was due to the plug flow or wall slip which prevented migration. He concluded that the occurrence of migration was a function of the shear field strength and the balance between the elastic and viscous properties of the carrier fluid.

Chapter III. Experimental Design and Procedure

Following is a brief description of the laboratory apparatus and the procedures used for conducting flow experiments using the plexiglass models. Next, the flow system pressure behavior is explained. Finally, a description of the rheological measurements and relevant equipment is included.

3.1 Experimental Set Up

Figure 3.1 depicts the experimental apparatus. The laboratory apparatus consists of two 3-liter slurry reservoirs connected to a plexiglass model. The model is intended to represent in a qualitative way a natural fracture normal to the induced fracture. Slurry flows from one of the reservoirs to the other through the plexiglass model by means of air expansion which is supplied from a 5 gallon air bottle. A 25 psi Setra pressure transducer is used to monitor pressure in the air bottle. Slurry flow rate, slurry velocity and shear rate are computed using the recorded pressure data.

The plexiglass model is 12 inch long, 1 inch high, with a ¼ inch gap which represents the induced fracture. During an experiment slurry leaks through a slot of 1 inch length and a varying width ranging from 0.01 inches to 0.06 inches positioned in the center of the rectangular front face of the model. The slot configuration represents, in a very qualitative way, a natural fracture. The leakoff fluid is collected and weighed by a Sartorius balance. An average leakoff rate is calculated from the mass of collected fluid

The Data Acquisition Computer (DAC) processes signals from transducers as well as supplying power to the transducers.

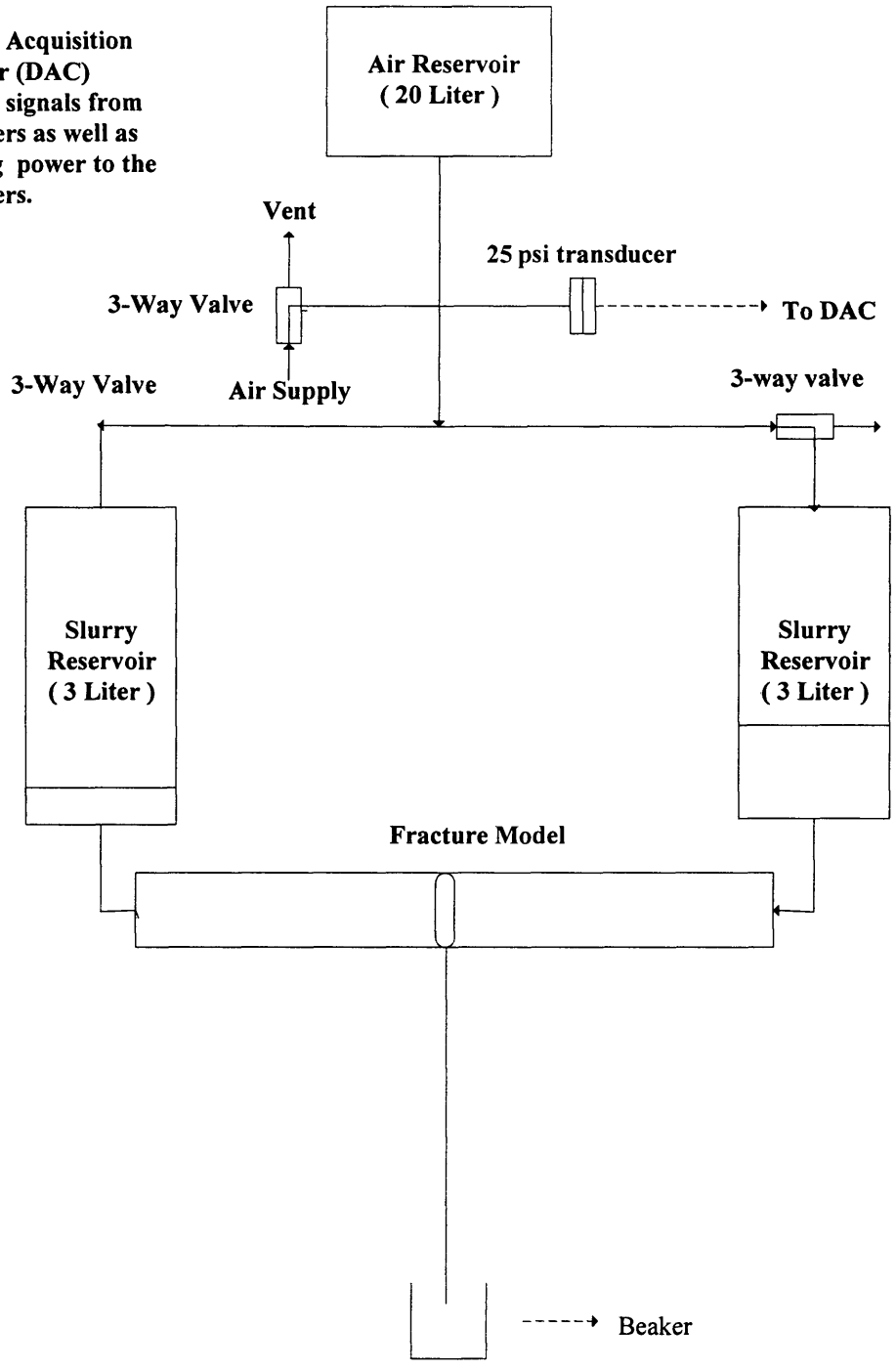

Fig 3.1 : Flow Diagram of Proppant Slurry Leak off

and the time duration of the experiment. Slurry flow in the model is videotaped for further analysis of the experiments.

Slurries were prepared by mixing guar and polyacrylamide solutions with fluid loss additives. For example, a 60 lb/Mgal guar would be mixed with 5 lb/gal 20-40 mesh sand to make up a slurry solution. Once the solution is prepared, one of the slurry reservoirs is filled. Next, the three-way valve placed at the top of the slurry reservoir is opened allowing the air in the bottle to flow into the slurry reservoir to displace the slurry. Flow of slurry solution into the model will result in fluid leakoff and flow downstream of the model. Pressure drop data will be a measure of the fluid flow in the model while the weight of the fluid collected will be a measure of the fluid leakoff. The fluid flow and the leakoff would be recorded by video camera for observations and analysis.

Once an experiment is completed, the model is disassembled and rinsed thoroughly with tap water and then air dried. Pressure data is used to calculate the incremental flow rates and average fluid velocity is obtained for each run. Average slurry leakoff rates are computed by taking the weight of the slurry leakoff divided by the duration of the experiment.

3.2 Pressure Drop Behavior In the Flow System

Initially the 3-liter cylinder is filled with slurry consisting of a 1000 cc polymer solution mixed with a predetermined amount of solid additives. Next, the air valve is

opened and flow is initiated. Figure 3.2 is a typical pressure drop behavior during slurry flow in the model. In this example, two runs are plotted. The initial air tank pressure is set at 3.0 and 2.2 psi, respectively. Once the valve is opened air fills the unfilled volume of the cylinder causing a sudden pressure drop due to air expansion in the unfilled portion of the cylinder. In this example, initial pressure declines to 2.9 and 2.1 for run 1 and run 2, respectively. From this point on tank pressure decline represents the slurry or fluid displacement in the cylinder through the plexiglass model. Pressure data is recorded for every 2 second time increment. For the purpose of calculations, pressure drop in every time increment is used to estimate incremental flow rate, velocity, and shear rate. Initial volume of tank is 5 gallons and air is treated as an ideal gas. It is apparent from the pressure behavior that slurry velocity changes during the experimentation. Thus, once velocity for each time step is computed, an average velocity for the entire experiment is calculated.

3.3 Rheological Measurements

Four fluid properties, viscosity, stress relaxation modulus, storage modulus, and loss modulus, were measured. Viscosity data were obtained using Fann-35 and Contraves viscometers. A Fann viscometer was used to obtain high shear rate data while the Contraves was used for the low shear data.

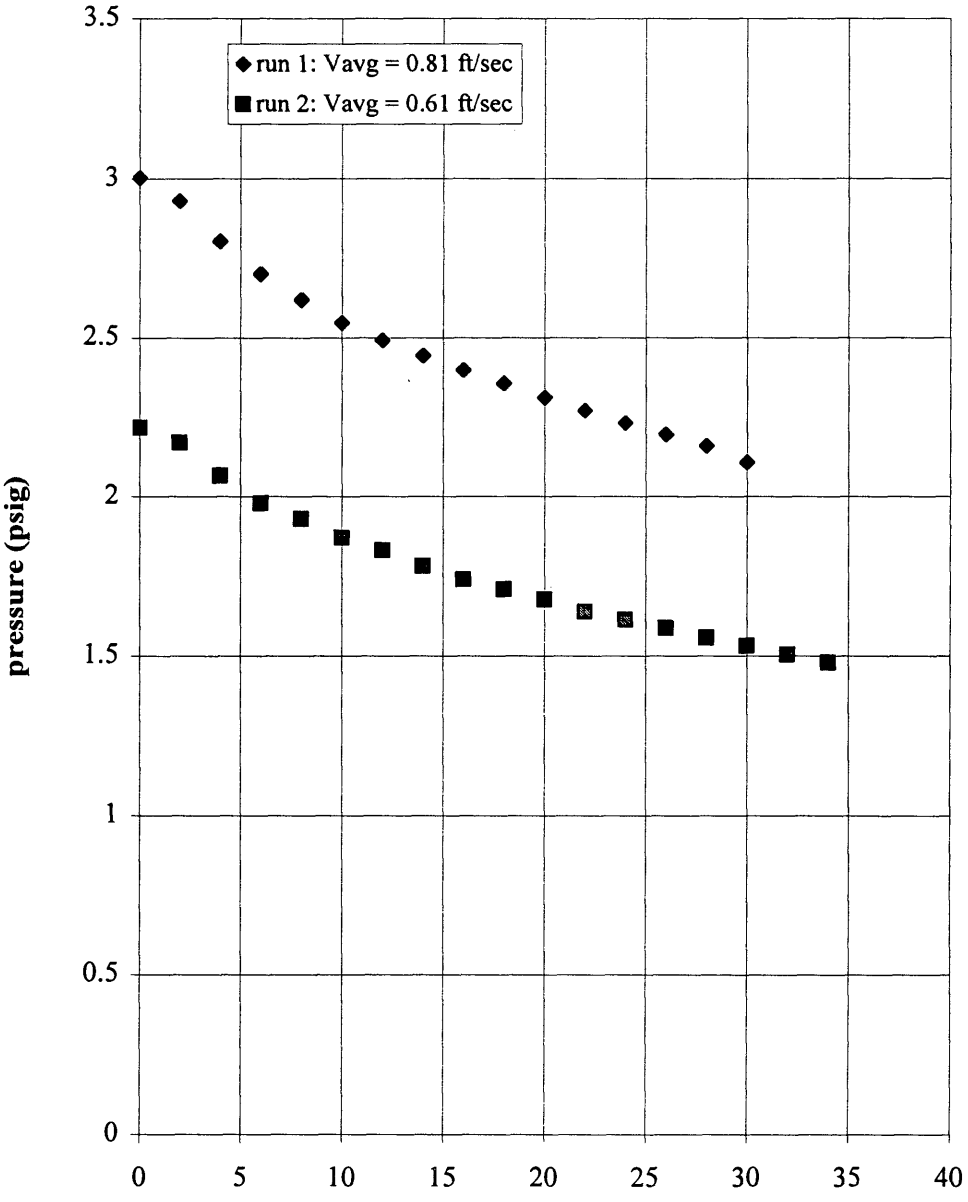

Fig 3.2: Pressure Behavior for Flow of 60 lb/Mgal Polyacrylamide Solution

Fann data was obtained by filling up the cup with the sample, and readings were taken at 3,6,100,200,300, and 600 rpm. Sample viscosity was then calculated using the appropriate factors provided by the user manual.

The Contraves viscometer has a similar set up (cup and bob) to measure the viscosity. When the cup is filled with the sample, bob is lowered into the cup and is centered gently by hand. Readings are taken by changing the rotary switch for speed steps (1 to 30). The speed rates correspond to shear rates of 0.00372 to 27.4 1/sec for a 1-1 cup and bob size, respectively. The measurements tend to be affected when high shear rates are applied or when polymer viscosity is so high that the reading is off scale. For the data collection, the measurements were discarded when the readings were not stable. Appropriate tables (provided by the Contraves viscometer manual) were consulted for viscosity calculations.

Stress relaxation modulus G(t) was obtained using Contraves viscometer. Initially, a sample was placed in the cup. A wire of a known diameter was placed between the key lever and the eccentric disc. Next, the wire was removed instantly while the digital readings were recorded by the computer. Recorded data represents the stress relaxation that the sample experiences after a step strain. The raw data were adjusted to the size of the initial step strain. The size of the strain was obtained by computing the cup movement due to removal of the wire. The ratio of the measurement to the strain size would be the stress relaxation modulus at the given time for the fluid.

Chapter IV. Flow Experiments

The experiments conducted in the plexiglass models are divided into three categories: preliminary experiments, screening experiments, and flow experiments. In the following sections the observations, results and conclusions drawn from each category will be discussed. The findings from each category were used to design and conduct the following category of experiments. The flow data is submitted in Appendix A.

4.1 Preliminary Experiments

The initial work concentrated on slurry flow using 60 and 80 lb/Mgal guar and polyacrylamide mixed with 5 lb/gal 20-40 mesh sand. Experiments were conducted using plexiglass models with a round 0.0625 inch diameter leakoff site. The results for the guar and polyacrylamide runs are plotted in Figures 4.1, 4.2, 4.3, and 4.4. Figure 4.1 is plot of leakoff rate as a function of slurry velocity for several batches of slurry runs. The results show that once slurry velocity reaches a low enough velocity (critical velocity) in this case 0.33 ft/sec, the particles in the slurry accumulate around the leakoff site and inhibit fluid leakoff. Similar flow behavior was observed for 80 lb/Mgal guar slurry, as depicted in Figure 4.2. These results indicate that velocity of 0.25 ft/sec was the critical velocity (v_c) for this slurry system, below which a sand node formed, and, as a result, fluid leakoff rate decreased.

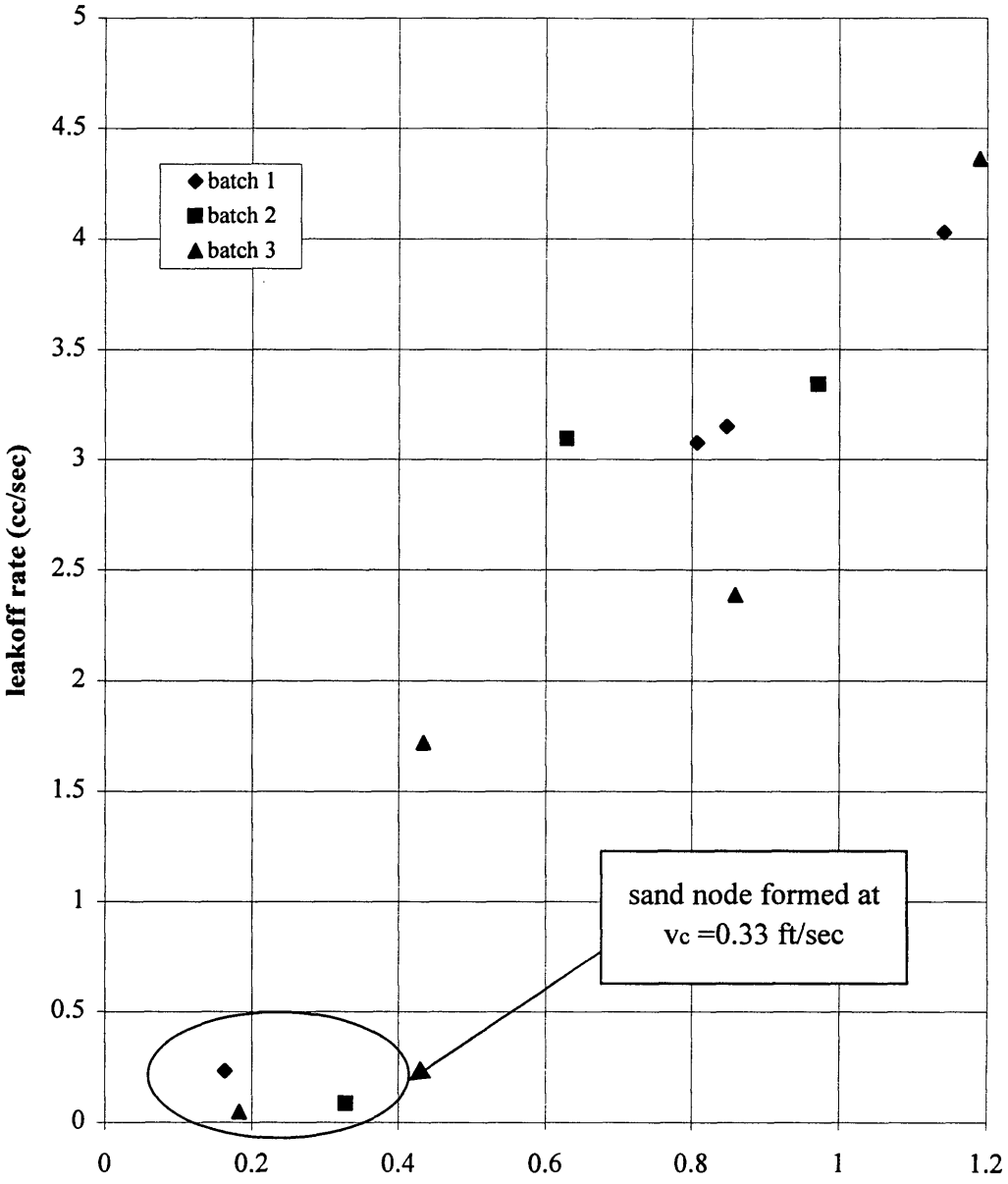

Fig 4.1 : Slurry Leakoff Rate for Several Batches of Guar Slurry (60 lb/Mgal guar and 5 lb/gal 20-40 sand)

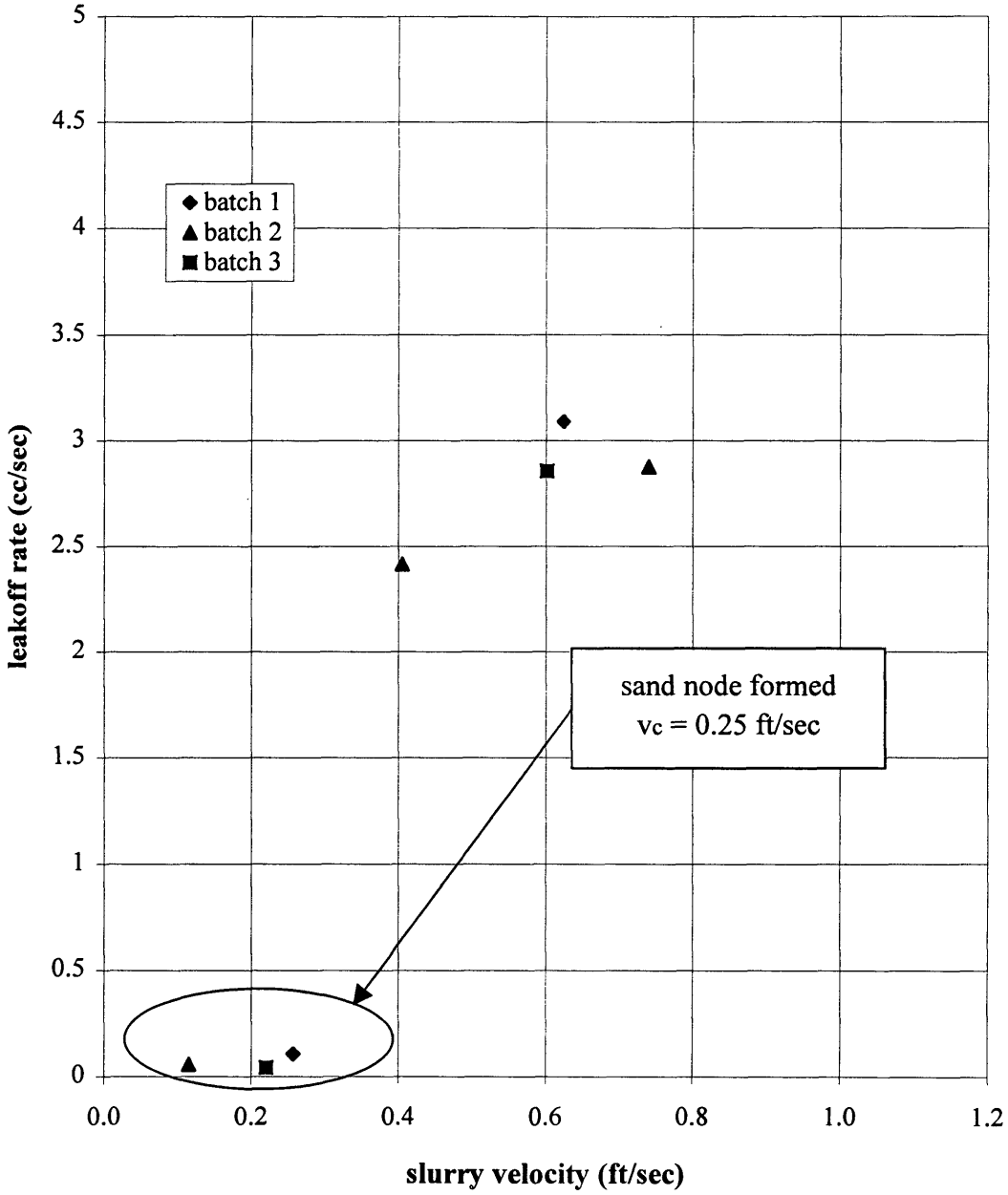

Fig 4.2: Slurry Leakoff Rate for Several Batches of Guar Slurry (80 lb/Mgal guar & 5 lb/gal 20-40 sand)

Polyacrylamide experiments were completed using 60 and 80 lb/Mgal of polyacrylamide solutions mixed with 5 lb/gal 20-40 mesh sand. Figure 4.3 is the plot of 60 lb/Mgal PHPA slurry. Data represent three sets of runs conducted using different polymer solution batches. The velocities are comparable to the guar slurry experiments conducted. However, sand node did not form in any of these experiments.

Figure 4.4 is similar experiments conducted using the 80 lb/Mgal PHPA slurry. When slurry velocity was reduced sand node did not form. Thus, slurry leakoff rates were not inhibited by the addition of the additive. However, the leakoff rates for the PHPA runs were about an order of magnitude smaller than guar experiments. These observations indicate that the polyacrylamide rheology had an effect on slurry leakoff rate.

4.2 Screening Experiments

The results and observations from preliminary experiments paved the way to conduct a new set of experiments using starch, silica flour, 100 mesh sand, and oil soluble resin as solid fluid loss additives. The initial flow experiments were conducted to make observations of the slurry flow in the plexiglass model. Once sand node formed in some of the experiments, then the geometry of the leakoff site for the plexiglass models were modified from a round 0.0625 inch diameter to a rectangle shape of 1 inch length and of 0.0833 and 0.0625 inch width. The rectangle shape better represented the shape of the natural fractures. Slurries of 60 and 80 lb/Mgal guar and polyacrylamide were

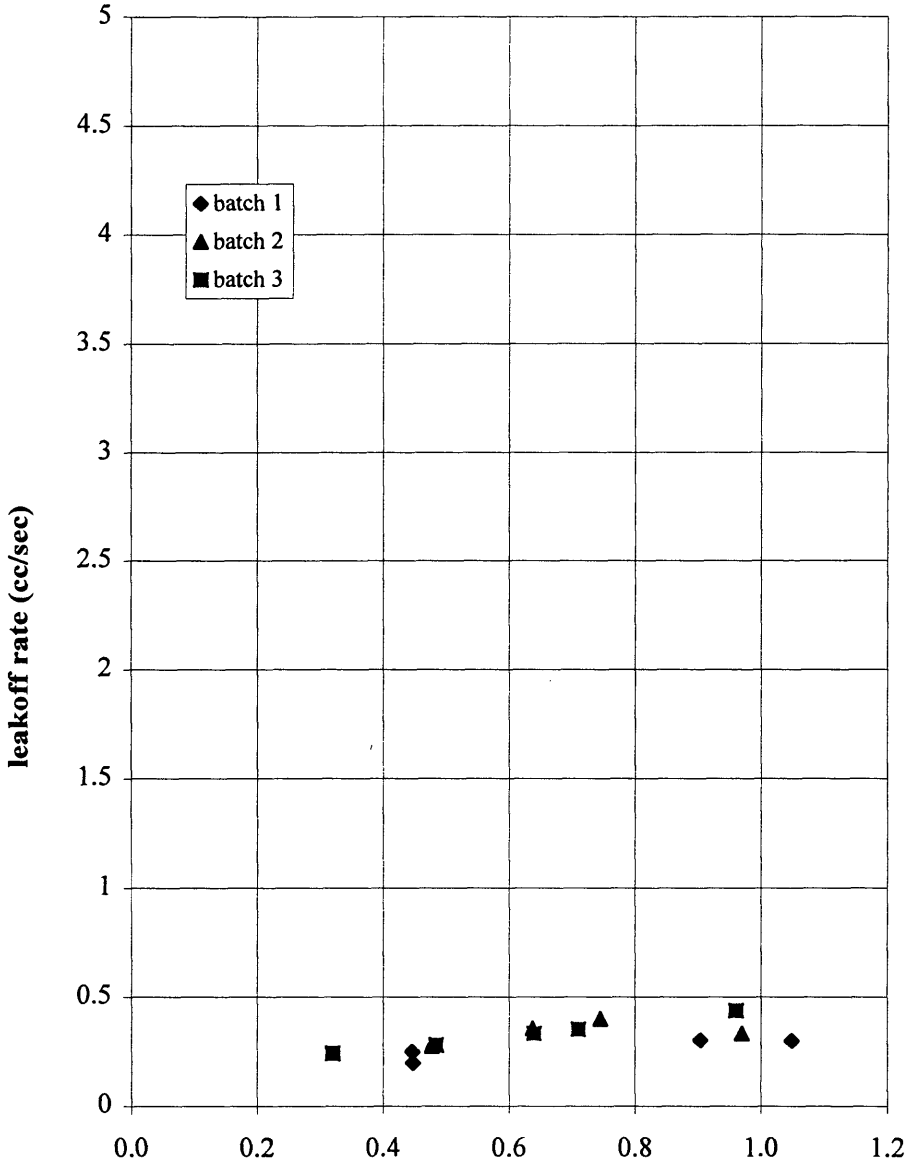

Fig 4.3: Slurry Leakoff Rate for Several Batches of PHPA Slurry (60 lb/Mgal PHPA &5 lb/gal 20-40 sand)- No sand node formed

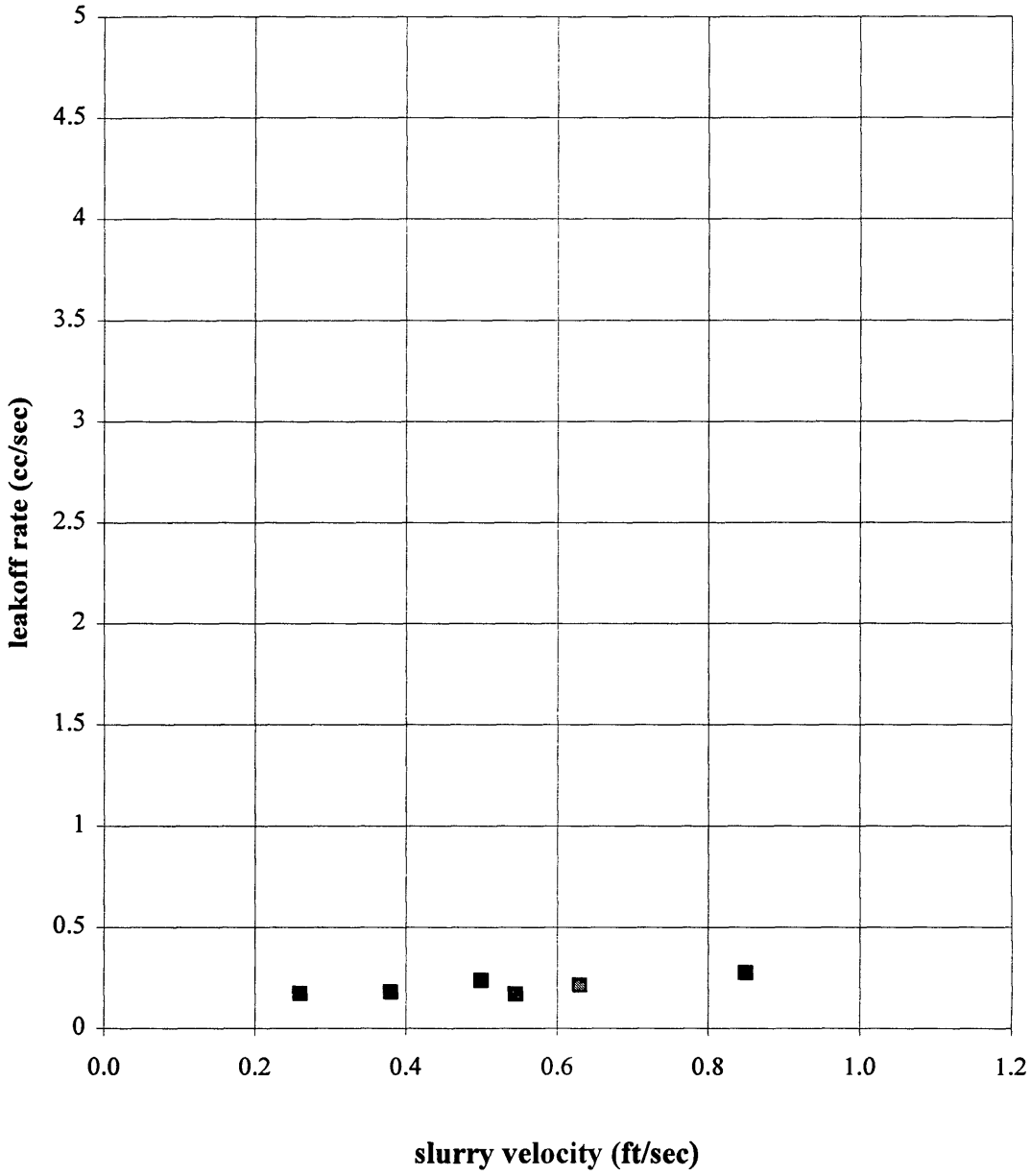

Fig 4.4: Slurry Leakoff Rate for Several Batches of PHPA Slurry (80 lb/Mgal PHPA &5 lb/gal 20-40 sand)-No sand node formed

Slurries of 60 and 80 lb/Mgal guar and polyacrylamide were prepared with 1/4, 1/2, and 1 lb/gal of the fluid loss additive. For the silica flour runs, 0.022, 1/4, and 1/2 lb/gal were used.

4.2.1 Polyacrylamide Experiments

Slurries were made by mixing polyacrylamide solution with fluid loss additives (silica flour, starch, 100 mesh sand, and oil soluble resin) at concentrations mentioned previously. Figures 4.5 and 4.6 are plots of leakoff rate as a function of shear rate for a 60 lb/Mgal polyacrylamide starch slurry. It is inconclusive from the data that increasing the additive concentration decreases leakoff rates due to viscosity increase. Leakoff rates are lower for models with smaller gap width which have smaller area for the slurry to flow and exit from the model.

From these experiments it was clear that for any kind of leakoff prevention in the models with leakoff sites that represent natural fractures, the additive particle size has to be in some way proportional to the gap width. Starch and silica flour would not be a practical approach for leakoff control in natural fractures; these additives acted as "viscosifiers". These experiments were conducted in models with a large slot width; however, it was clear that particle size and concentration will be a decisive factor in initiating a sand or particle formation.

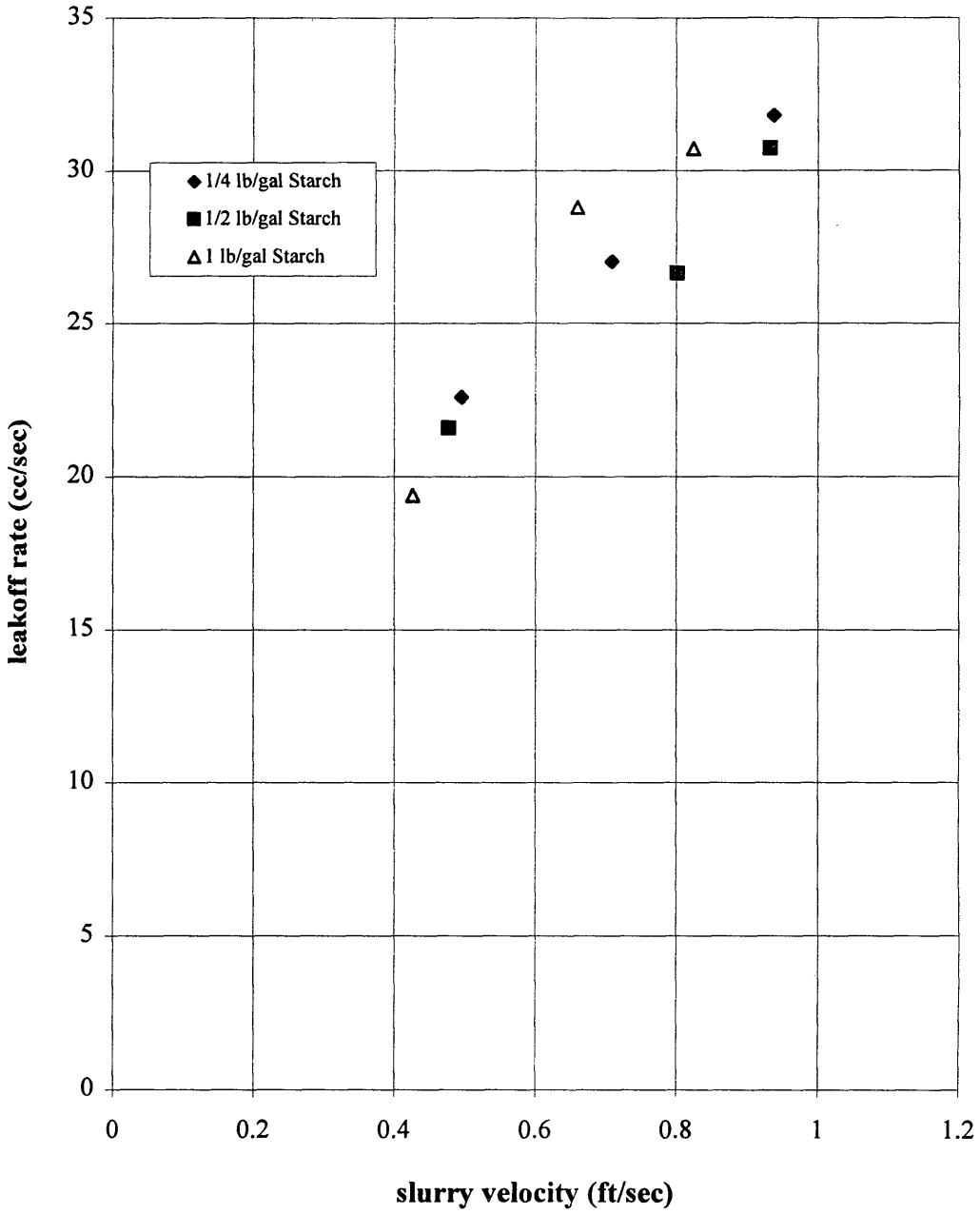

Fig 4.5: Leakoff Rate for 60 lb/Mgal PHPA-Starch Slurry (Slot Width 0.083 inch)

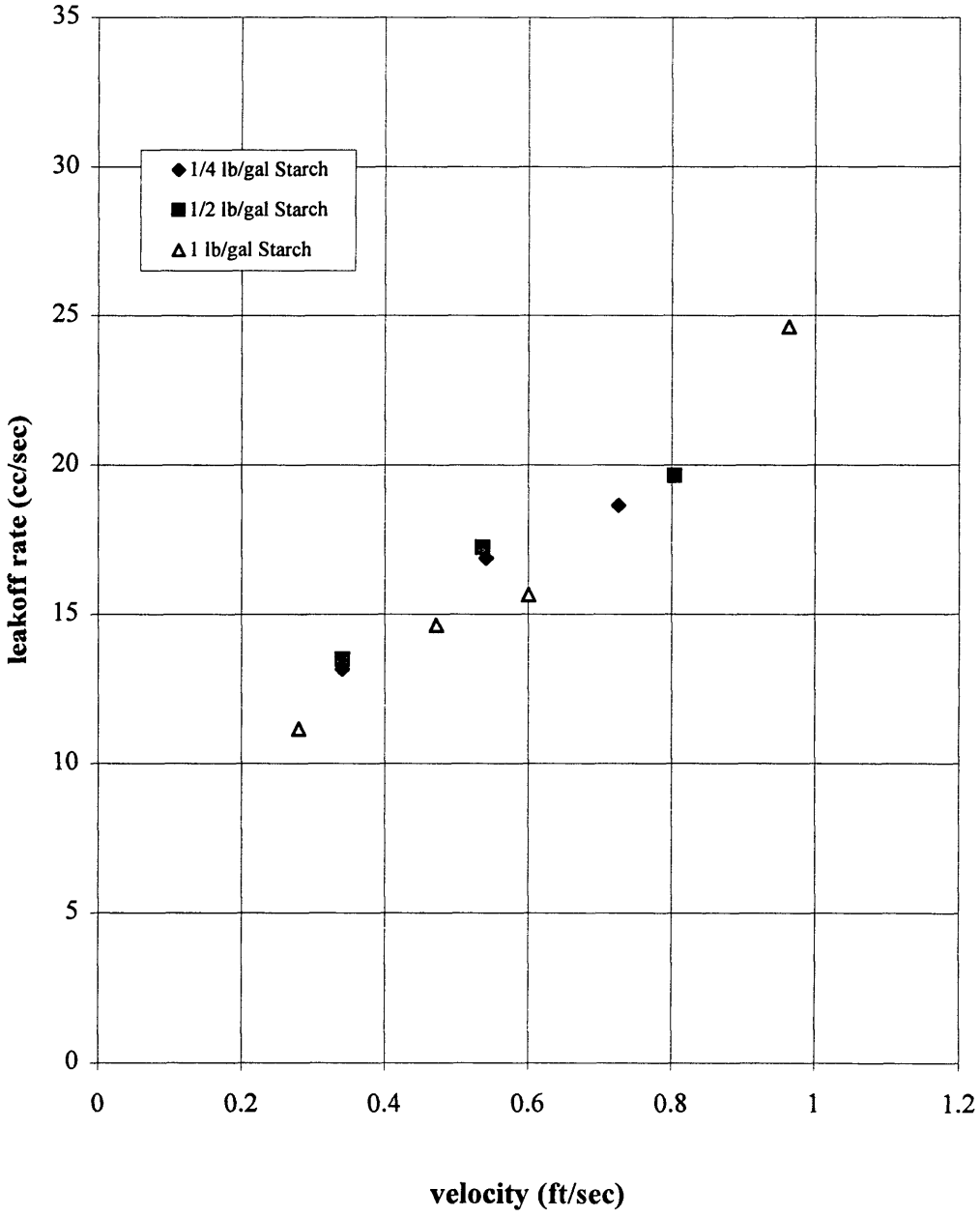

Fig 4.6: Leakoff Rate for 60 lb/Mgal PHPA-Starch Slurry (Slot Width 0.0625 inch)

Similar results were obtained for 80 lb/Mgal polyacrylamide slurry experiments. Figure 4.7 indicate that leakoff rates are only affected by the viscosity and the gap width, and the latter has a more pronounced effect, respectively.

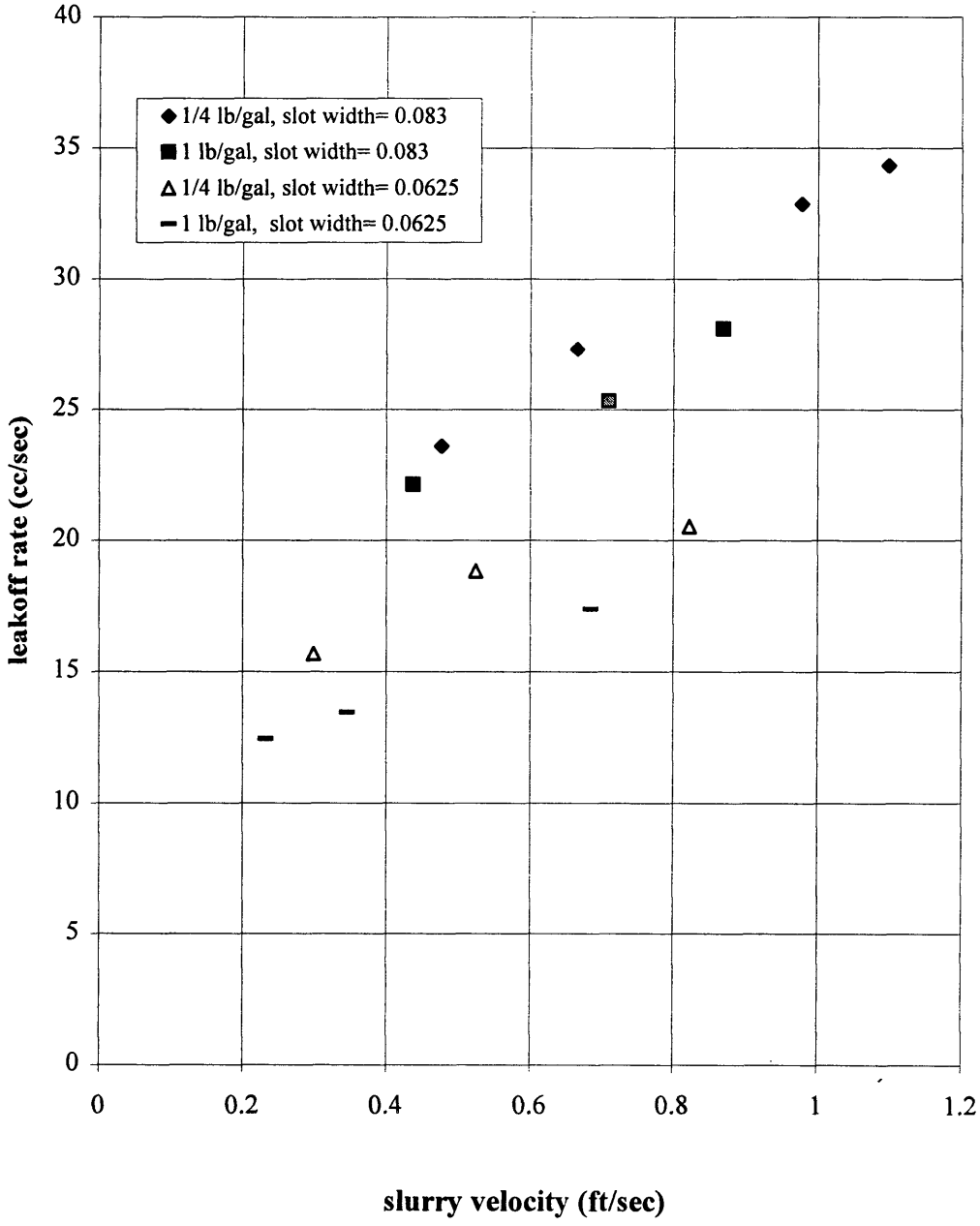

Fig 4.7: Leakoff Rate for 80 lb/Mgal PHPA-Starch Slurry

4.2.2 Guar Experiments

Guar slurries were made by mixing 60 lb/Mgal and 80 lb/Mgal guar solutions with silica flour, starch, 100 mesh sand, and oil soluble resin. The experiments were conducted using the 0.0833 " and 0.0625" slot width.

The results of the experiments for the 60 lb/Mgal and 80 lb/Mgal slurries are plotted in figures 4.8 through 4.11, respectively. The leakoff rates are plotted as a function of shear rate for each of the slurry.

Figures 4.8 and 4.9 are plots of fluid leakoff rate as a function of shear rate for 60 lb/Mgal guar mixed with starch for experiments conducted in models with slot width of 0.0833 inch and 0.0625 inch. It is apparent from the data that the higher the concentration of the additive, the lower the leakoff rate which shows the viscosity effect. Moreover, the size of the leakoff-site, in this case the width of the site influences the magnitude of the leakoff rate. These results are consistent with the PHPA experiments. However, the magnitude of the leakoff rates for the guar slurries are higher than the PHPA slurries which is due to the rheology of the base solution.

Figures 4.10 and 4.11 are results from 80 lb/Mgal guar slurries conducted in 0.0625 and 0.0833 inch slot models. The viscosity and area to flow effects are apparent from the data. Comparison of the similar data for different rheology (guar vs. polyacrylamide) shows that lower leakoff rates exit for PHPA slurries compared to guar.

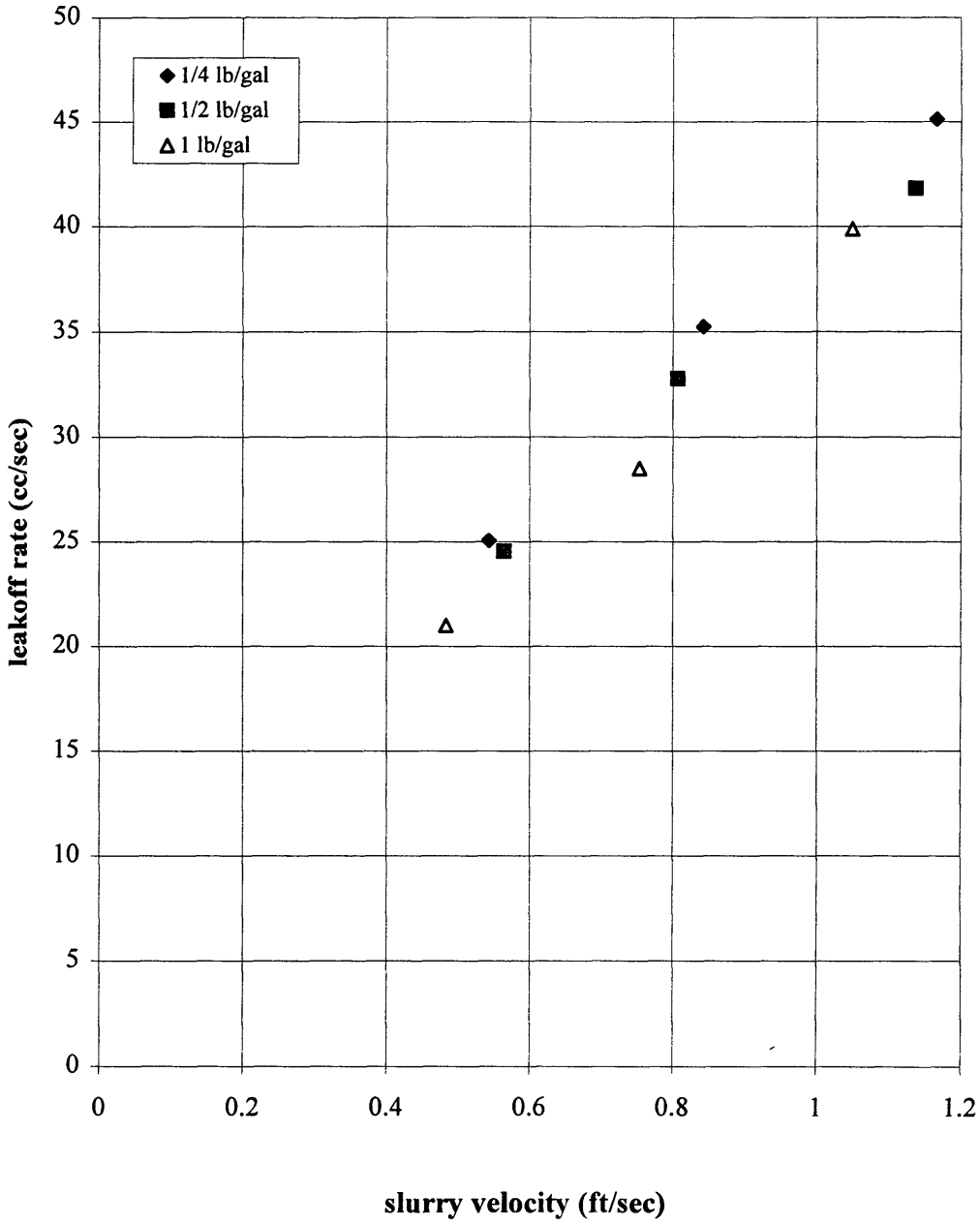

Fig 4.8: Leakoff Rate for 60 lb/Mgal Guar-Starch Slurries (Slot Width 0.083 inches)

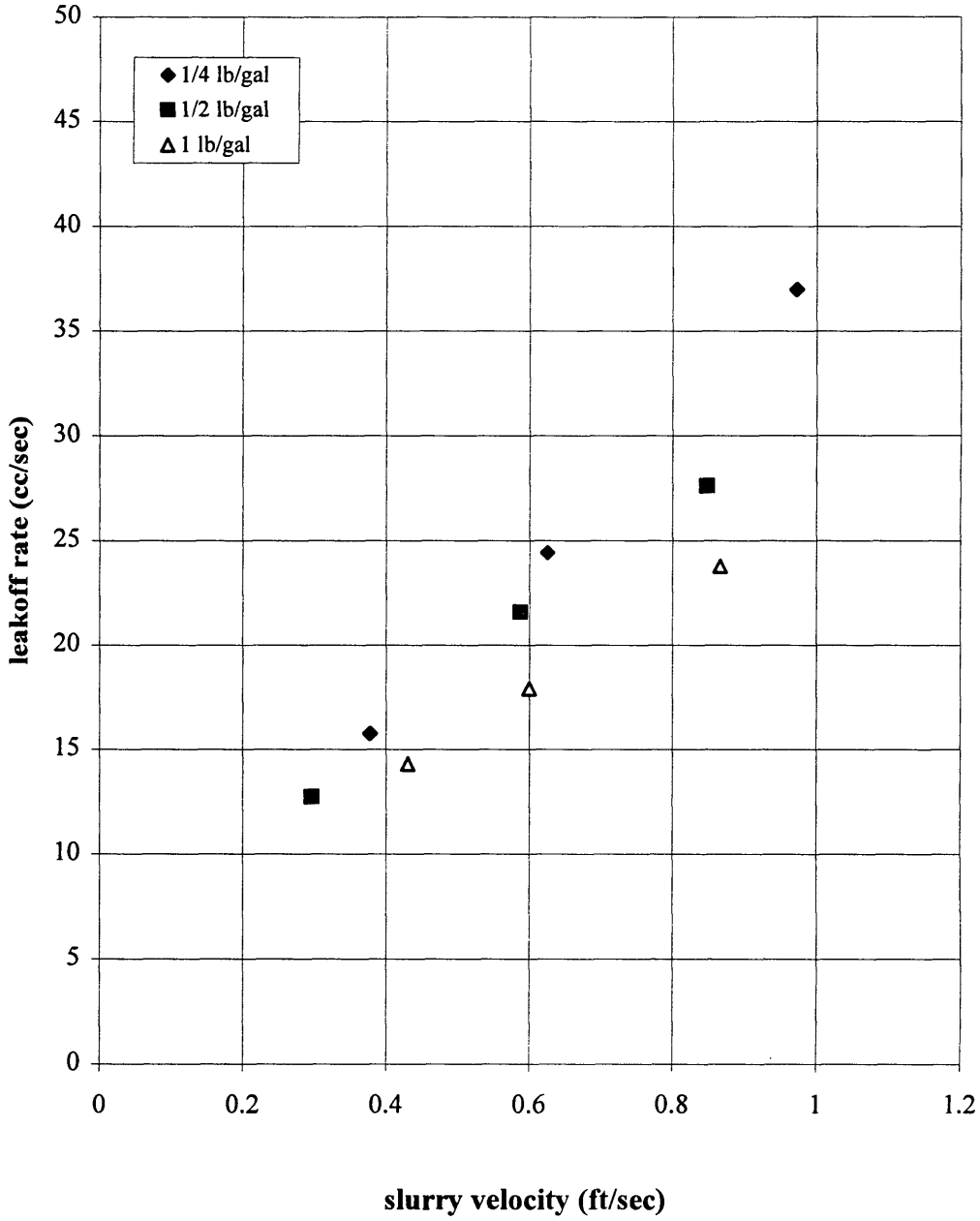

Fig 4.9: Leakoff Rate for 60 lb/Mgal Guar-Starch Slurries (Slot Width 0.0625 inches)

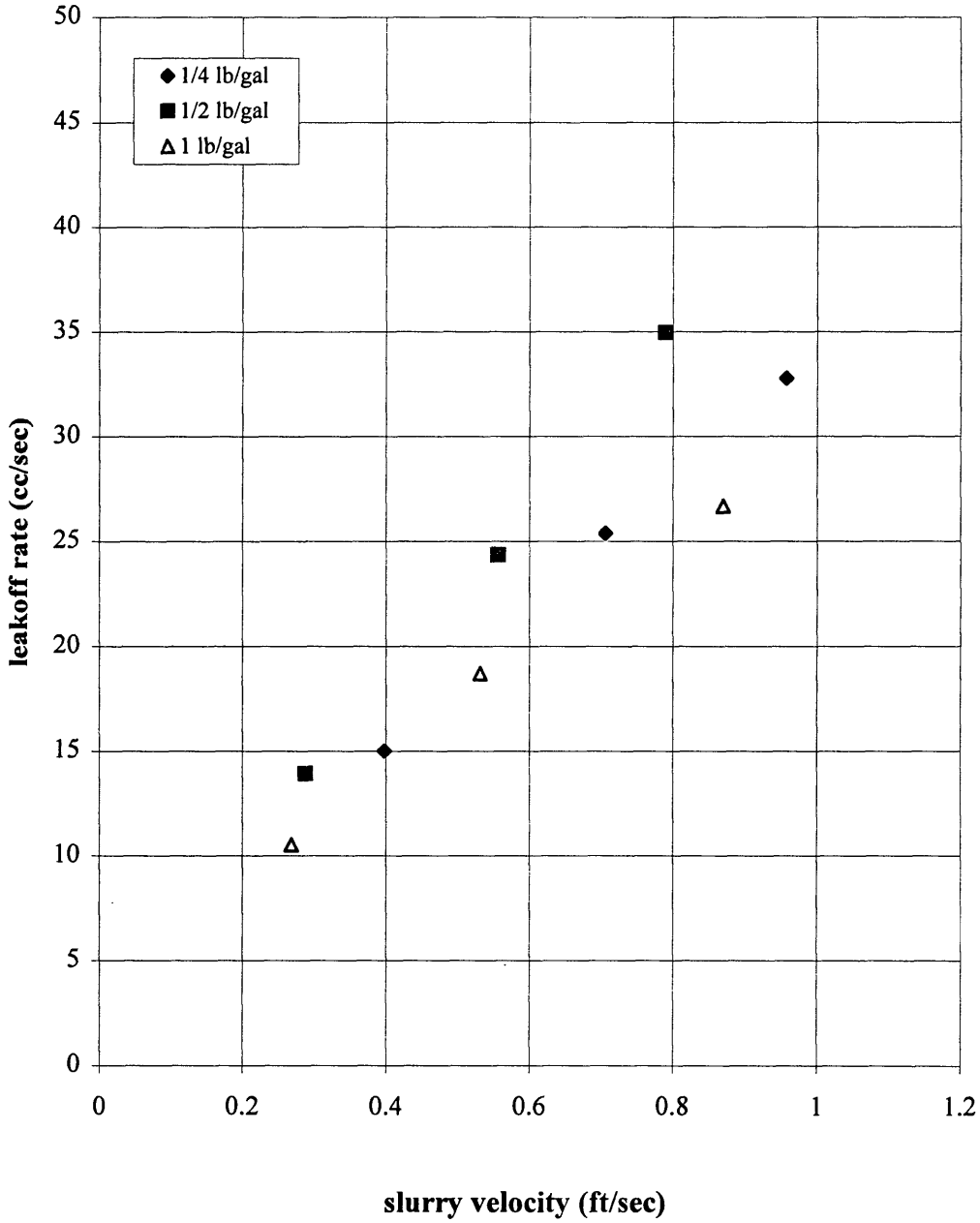

Fig 4.10: Leakoff Rate for 60 lb/Mgal Guar-Starch Slurries (Slot Width 0.083 inches)

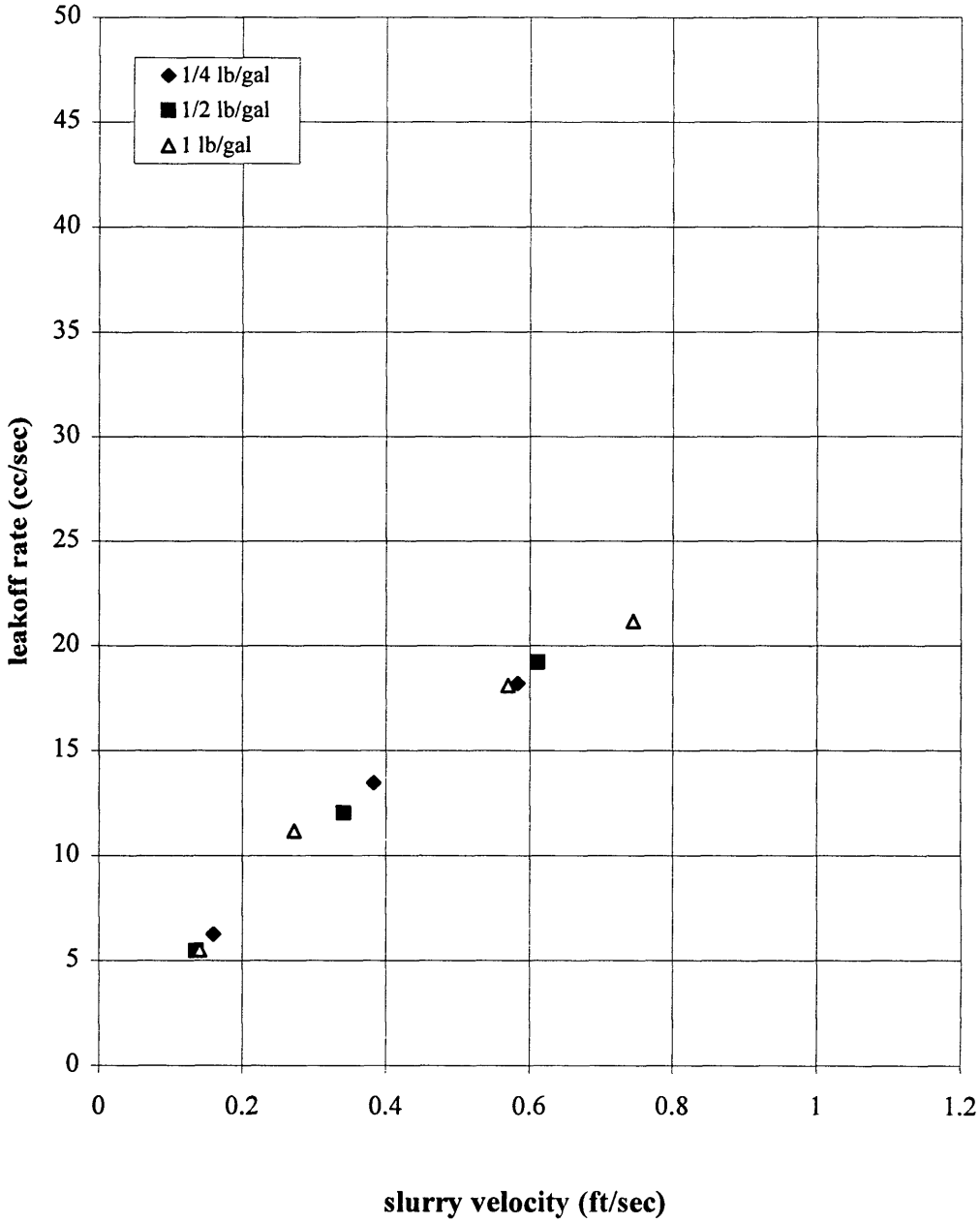

Fig 4.11: Leakoff Rate for 60 lb/Mgal Guar-Starch Slurries (Slot Width 0.0625 inches)

The results for the screening experiments indicate that effective leakoff control will not be accomplished using additives and/or due to slurry properties. It is essential to build a wall or cake at the leakoff site in order to inhibit slurry leakoff effectively.

To accomplish this task, existence of solid particles in the slurry is essential. Accumulation of particles at the leakoff site at a proper rheological and physical condition will facilitate sand node formation. As an example, parameters in this process are natural fracture width, particle size and concentration, and the slurry velocity in the induced fracture.

The results from the experiments have shown that the leakoff rates were affected by the size of the slot width, fluid velocity, and slurry viscosity. Therefore, the slot width of the models used were large relative to common natural fracture sizes; new models were built with slot width of 0.06, 0.05, 0.03, and 0.01 inches.

Eleven experiments were conducted using the new models. Figure 4.12 is plot of leakoff rate as a function of fluid velocity in 0.01 and 0.03 inch slot width models for 60 lb/Mgal guar mixed with 1 lb/gal starch. It is evident that the leakoff rates are noticeably affected by the model slot size. For example, the leakoff rates for the 0.01 inch and 0.03 inch slot sizes are 1.2 cc/sec and 11.2 cc/sec for approximately equivalent slurry velocities. The leakoff rates are a factor of about 10 larger for the 0.03 inch slot width compared to the 0.01 inch slot width.

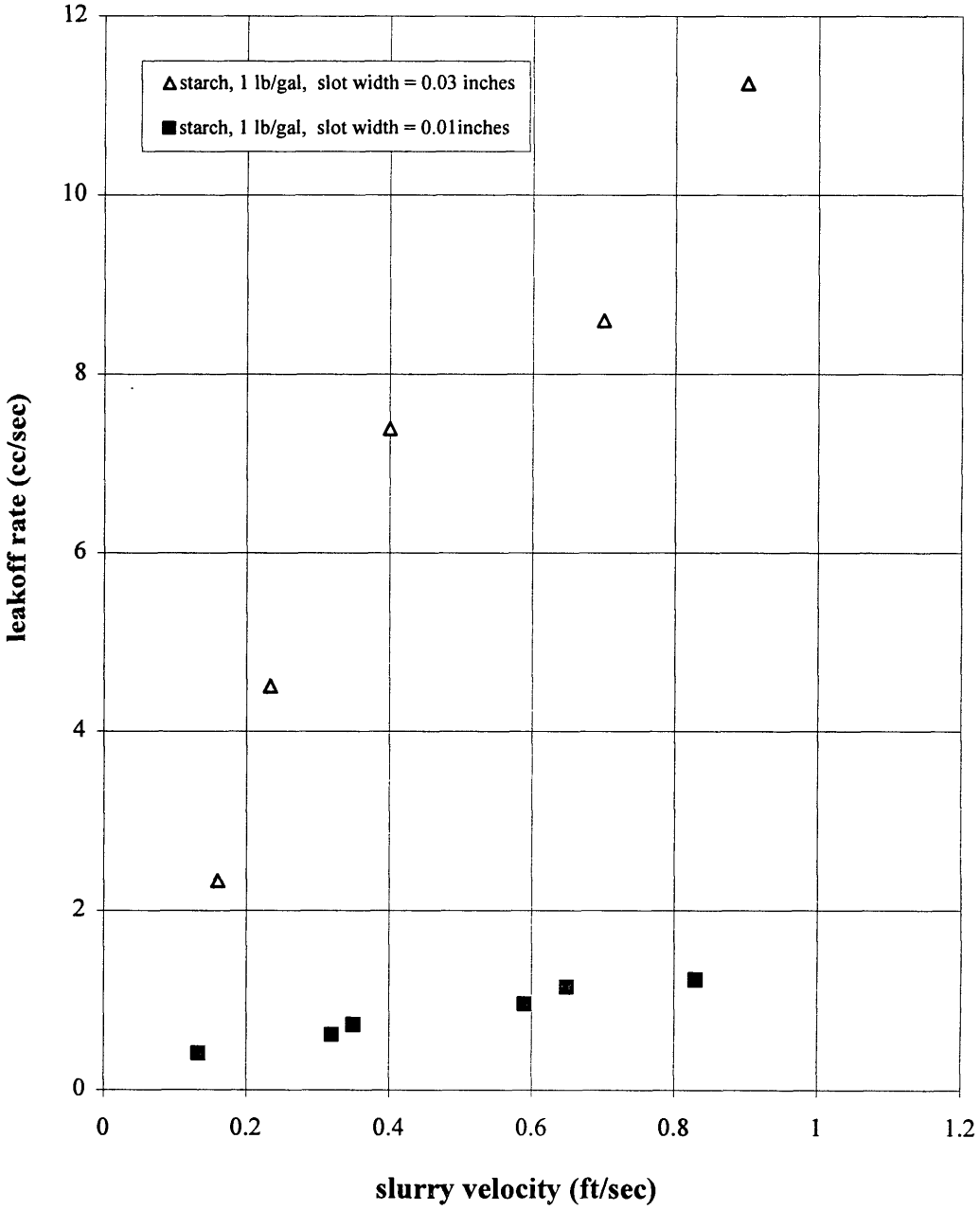

Fig 4.12: Slurry Leakoff Rate for Several Guar Slurries (60 lb/Mgal guar)

4.3 Flow Experiments

Results and observations from previous experiments set the course to further investigate slurry leakoff by varying polymer concentration, additive concentration, and more importantly the particle size distribution. Guar and polyacrylamide solutions were used as power law and viscoelastic fluids, respectively.

For guar polymer concentrations were 40, 60, and 80 lb/gal, while for polyacrylamide concentrations of 20, 40, 60, and 80 lb/Mgal were used. For these experiments plexiglass models with dimensions of 12 x 1 x 1/4 inches and leakoff site with rectangular slot geometry were used. Slot width ranged between 0.01 to 0.06 inches. 100 mesh and 20-40 mesh sand were used as solid fluid loss additives either individually or mixed at differing concentrations for some of the experiments. Higher additive concentrations were used when experiments were conducted in models with larger slot width and vice versa. The data for these experiments are listed in Table I. Column 1 lists the polymer type and its concentration while Column two indicates the additive type and the corresponding concentrations used for the experiments. Finally, Column 3 shows the size of the slot width that was used for the experiment. For example, the first row in Table I indicates that experiments were conducted using slurry solutions of 40 lb/Mgal guar solutions mixed with additive concentration of 1 lb/gal of 20-40 mesh sand, 1 lb/gal of 100 mesh sand , and 1 lb/gal of mixed 20-40 &100 mesh sand . These experiments

were conducted using models with slot width sizes of 0.01, 0.03, and 0.06 inches, respectively.

Table I: Specifics of the Flow Experiments

Column I	Column II	Column III
Polymer Solution Concentration (lb/Mgal)	**Additive Type & Concentration (mesh) & (lb/gal)**	**Slot Width (inches)**
Guar 40	20-40, 100, (20-40 &100);1 lb/gal	0.01,0.03,0.06
Guar 60	20-40; 1/4, 1, 5 lb/gal	0.01,0.03,0.06
Guar 60	20-40, 100, (20-40&100); 1/4, 5 lb/gal	0.01,0.03,0.06
Guar 60	NDB; 3 lb/gal	0.01,0.03
Guar 80	20-40; 5 lb/gal	0.05
Guar 80	NDB; 1.85 lb/gal	0.05
Polyacrylamide 20	20-40; 3 lb/gal	0.03,0.06
Polyacrylamide 40	NDB; 3 lb/gal	0.01,0.03
Polyacrylamide 60	20-40; 5 lb/gal	0.05,0.06
Polyacrylamide 80	20-40; 5 lb/gal	0.05,0.06

One of the main objectives of these experiments was to investigate the conditions under which a sand node would form for a given experiment. Another objective was to investigate the effect of particle size distribution on the leakoff rates.

4.3.1 Guar Experiments

Guar solutions of 40, 60, and 80 lb/Mgal were mixed with 100 mesh and 20-40 mesh sand at concentrations ranging from 1/4 up to 5 lb/gal. Following is a brief description of the results of these experiments. In general, it was observed that slurries made up with additives with particle size distribution were more effective in controlling fluid leakoff rates. The relevant data is provided in appendix A.

4.3.1.1 40 lb/Mgal Guar & 20-40 & 100 mesh Sand

Experiments were conducted with slurries of 40 lb/Mgal guar solution mixed with 1 lb/gal 20-40 mesh sand, 1 lb/gal 100 mesh sand using models with slot width of 0.01 and 0.03 inches. The results are plotted in Figures 4.13 and 4.14. Figure 4.13 shows that leakoff rates are higher through the 0.03 inch slot compared to the 0.01 inch slot for the slurry of 1 lb/gal 20-40 mesh sand. The leakoff rate is affected by the width or the area to flow and also by the relative size of the width compared to the particle size. The 20-40 mesh sand particles (D_p = 0.42 mm – 0.84mm) will be captured or filtered out at the 0.01 inch slot size and thus block the site and influence the slurry leakoff rate. A similar trend is observed in Figure 4.14, where a slurry of 100 mesh sand is used. The 100 mesh sand particles of 0.15 mm in diameter easily flowed out of the leakoff site therefore, the area to flow controlled the rate of the slurry leakoff. The comparison of these two plots indicate that slurry leakoff rates are higher for the 100 mesh sand slurry and that the

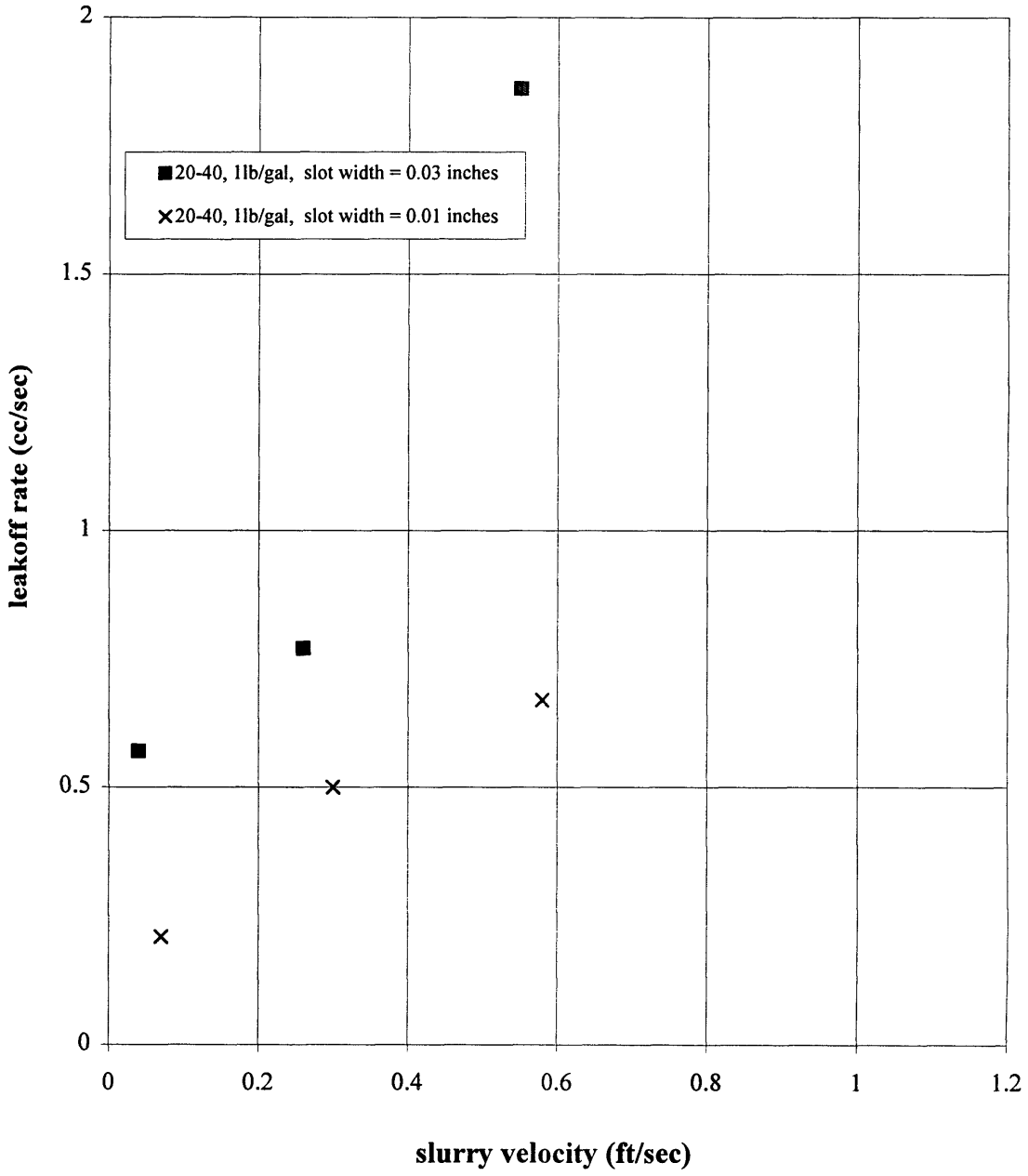

Fig 4.13: Leakoff Rate for Several Guar Slurries (40 lb/Mgal guar)

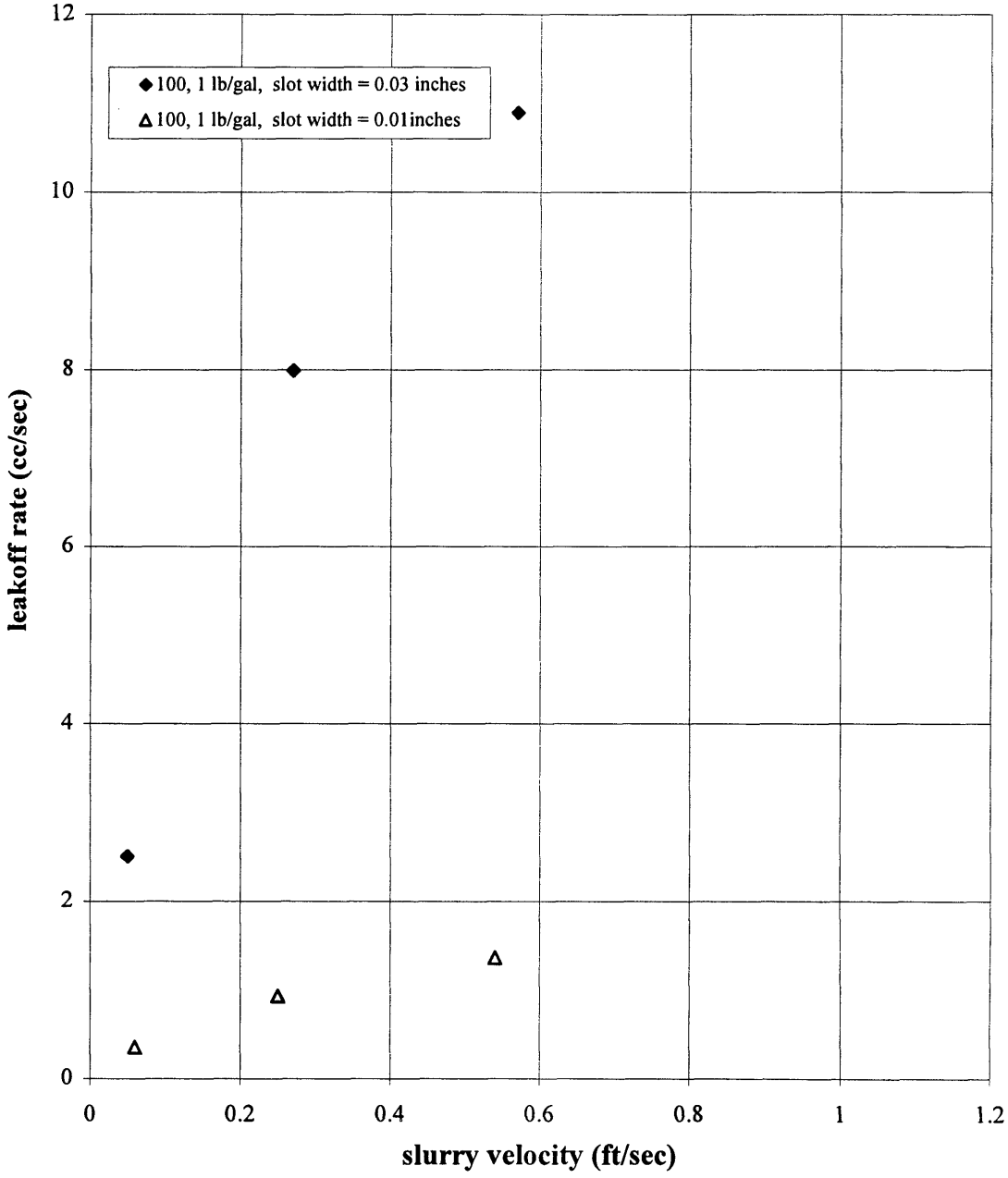

Fig 4.14: Leakoff Rate for Several Guar Slurries (40 lb/Mgal Guar)

leakoff site width strongly affects the leakoff rate. For example, the leakoff rate at about 0.60 ft/sec is about 1.9 cc/sec for the 20-40 mesh additive, compared to 11 cc/sec for the 100 mesh additive for the 0.03 inch slot models.

Eighteen experiments were conducted using 1 lb/gal 25 wt%, 50 wt%, and 75 wt% 20-40 mesh and 100 mesh sand using the 0.03" and 0.01'' plexiglass models (see Figures 4.15 and 4.16). In all of these experiment no sand node formed. The results show that the slurry leak-off rates were not affected by the particle distribution size which was due to discharge of the particles through the leakoff site. However, the magnitude of the leakoff rates were affected for the experiments conducted in the 0.01 inch slot model. For example, the leakoff rate in the .03 inch model is about 3.4 gr/cc and 4.1 gr/cc for average slurry velocity of 0.55 ft/sec and 0.8 ft/sec in the 0.03 inch slot model, respectively. However, for similar flow rates through the 0.01 inch model, the leakoff rates are a factor of 5 smaller, respectively. This reduction is partly due to the width effect and the particle size distribution effect.

The comparison of leakoff data for the 20-40 mesh slurry data in the 0.01 inch model with the mixed additive slurry data for the same slot width indicates that the leakoff rates are lower for the mixed additive data. The 50 wt% mixture seems to be an optimum mixing combination for these experiments. Due to settling problem, no further experiments were conducted by increasing additive concentration.

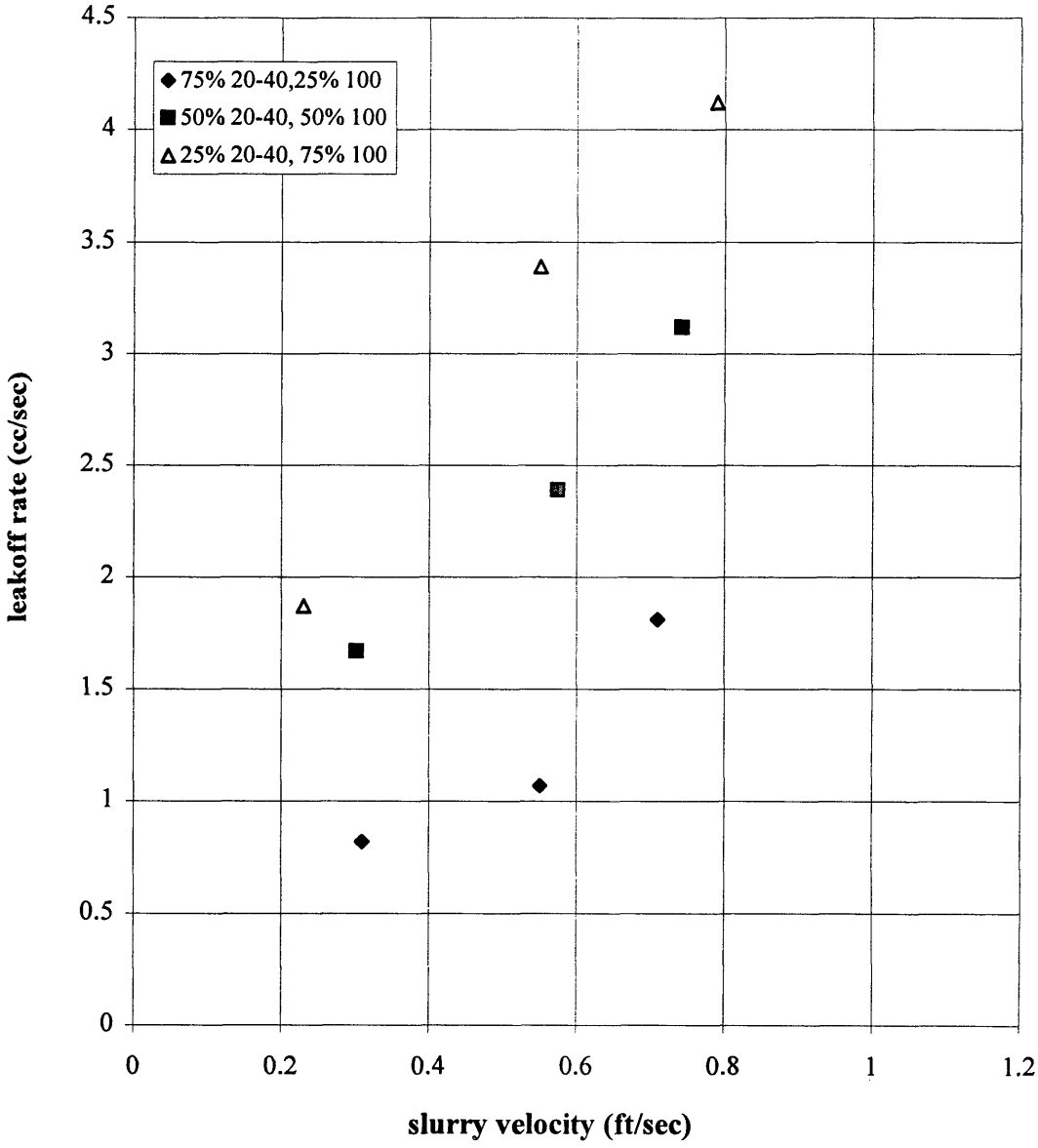

Fig 4.15: Slurry Leakoff Rate for Several Guar Slurries (40 lb/Mgal Guar, 1 lb/gal additive, 0.03")

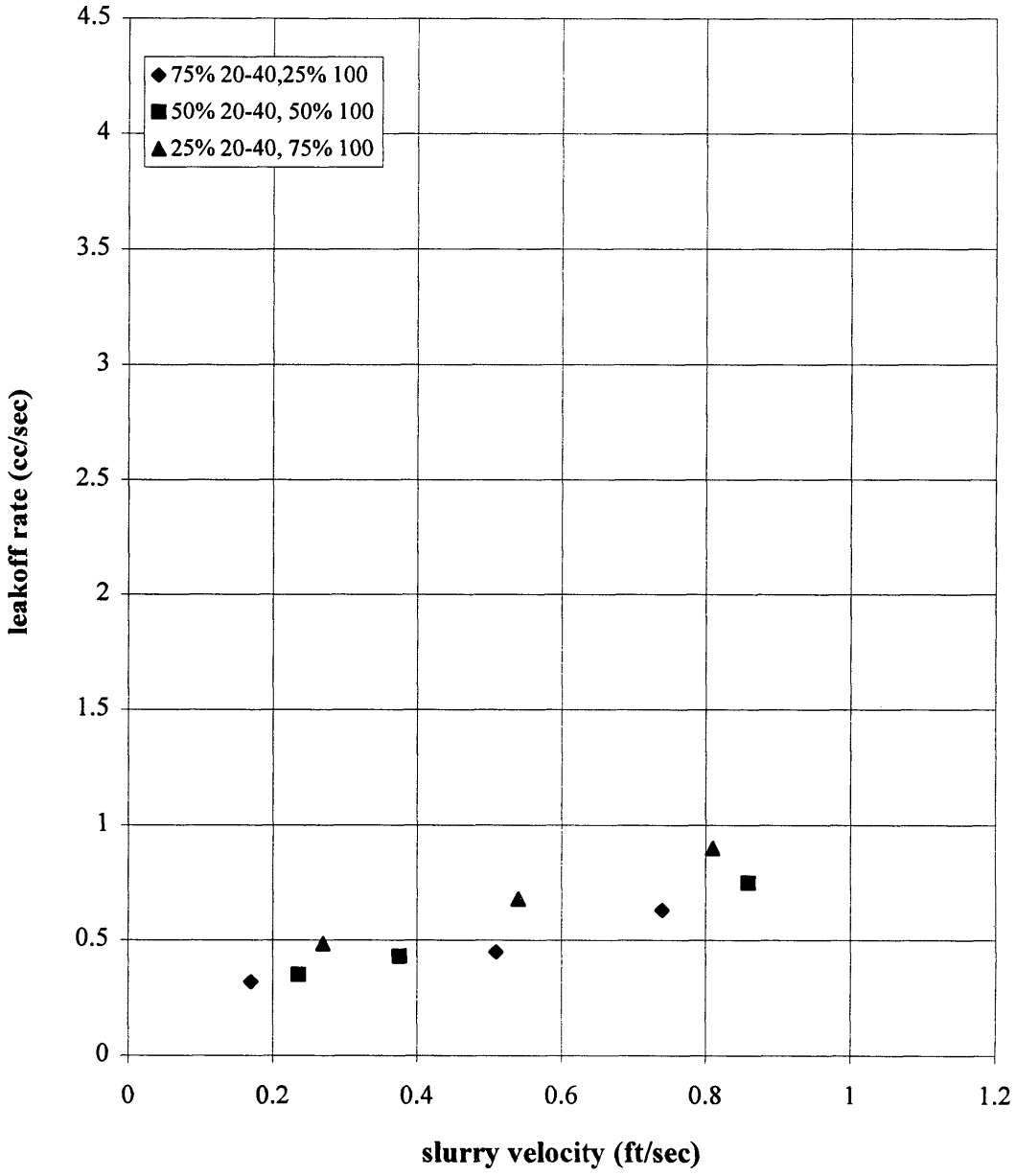

Fig 4.16: Slurry Leakoff Rate for Several Guar Slurries (40 lb/Mgal Guar, 1 lb/gal additive, 0.01")

4.3.1.2 60 lb/Mgal Guar & 20-40 mesh Sand

Slurries of 60 lb/Mgal guar with additive concentrations of 1/4, 1, and 3 lb/gal were used for experiments conducted in 0.01 inch, 0.03 inch, and 0.06 inch models. The results are plotted in Figures 4.17, 4.18, and 4.19, respectively.

Figure 4.17 shows a series of experiments conducted in a 0.01 inch slot model where slurries with additive concentration of 1/4 lb/gal of 20-40 mesh, 100 mesh, and the mixture is used. The 100 mesh sand slurry has the highest leakoff rate because the particles pass through the slot opening. The 20-40 mesh has lower leakoff rate relative to the 100 mesh slurry due to entrapment of the particles at the leakoff site. The mixed additive has a similar behavior; however, the slope of the data seems to be slightly steeper relative to the 20-40 mesh slurry. This might be due to discharge of the 100 mesh sand particles from the leakoff site, thus affecting the leakoff rates. Figure 4.18 depicts the experiments conducted in 0.06 inch model using 1 lb/gal 20-40 mesh and mixed additive. The slurry leaks off through the leakoff site. It is evident that the additive concentration is very low, and thus slurry is discharged without having any impact on the fluid flow behavior. Subsequently, the additive concentration was increased to 3 lb/gal. The results are plotted in Figure 4.19. It was concluded that there should be sufficient amount of additive in order to block the leakoff site.

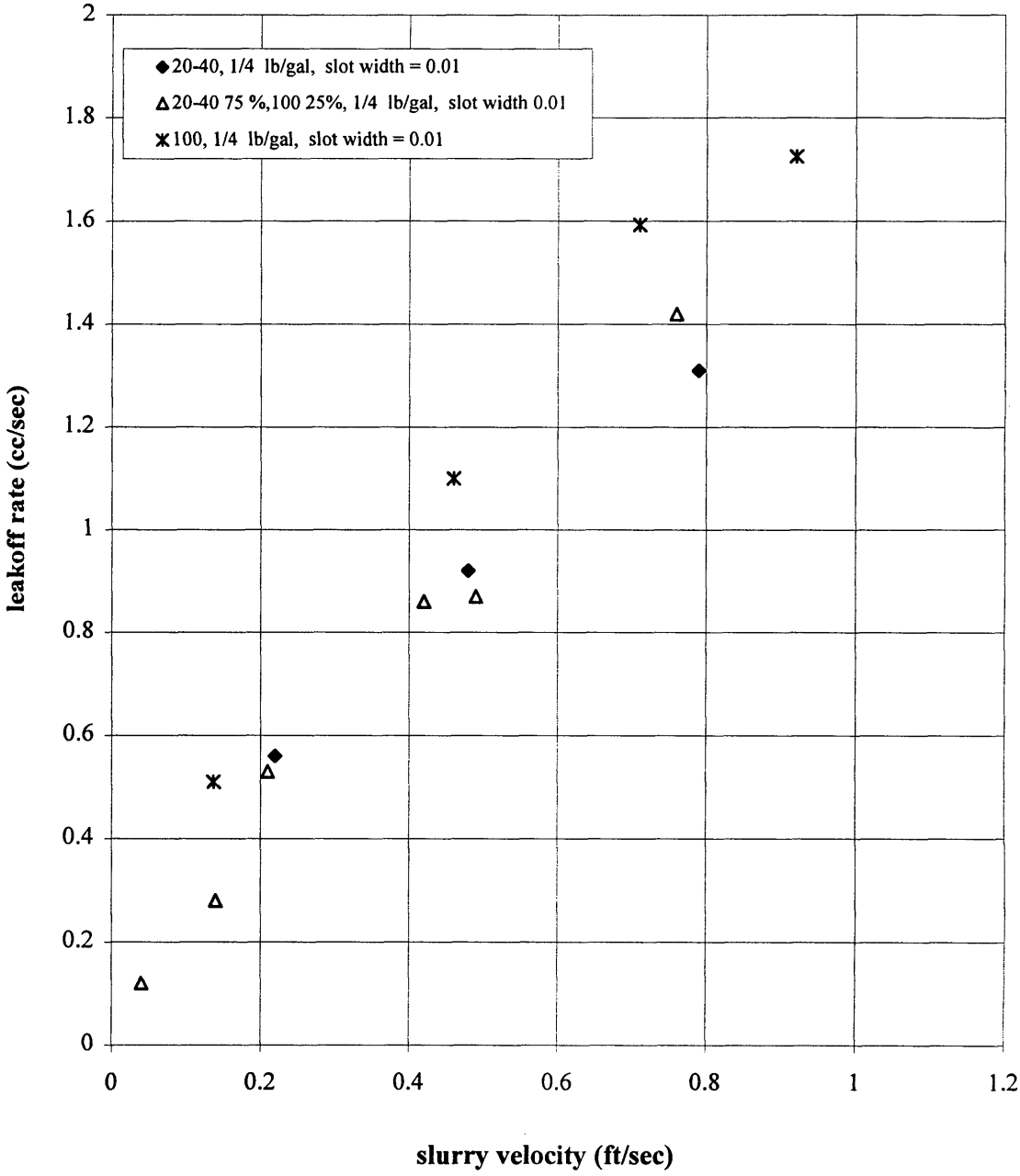

Fig 4.17: Slurry Leakoff Rate for Guar Slurries (60 lb/M gal Guar)

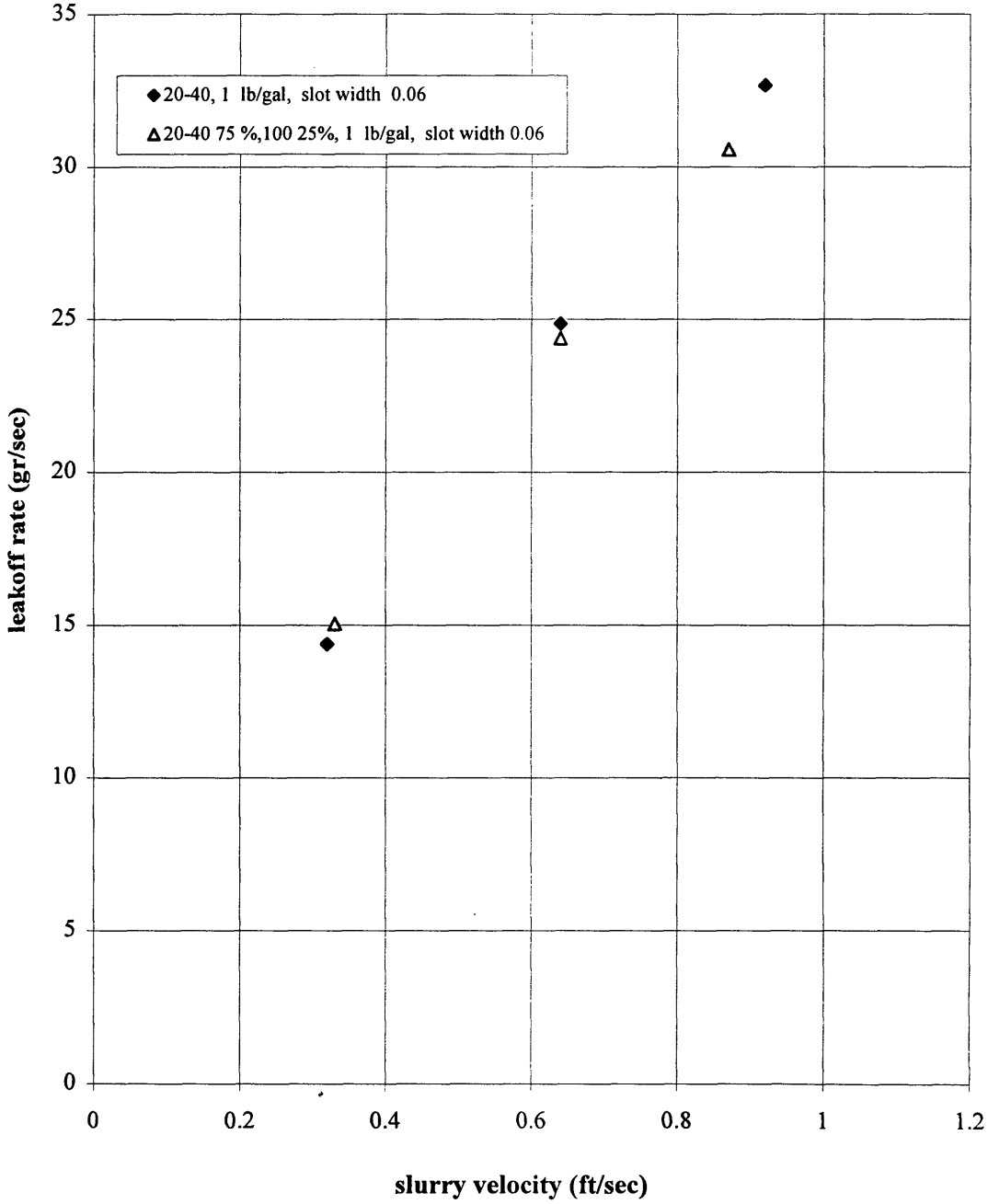

Fig 4.18: Slurry Leakoff Rate for Guar Slurries (60 lb/Mgal Guar)

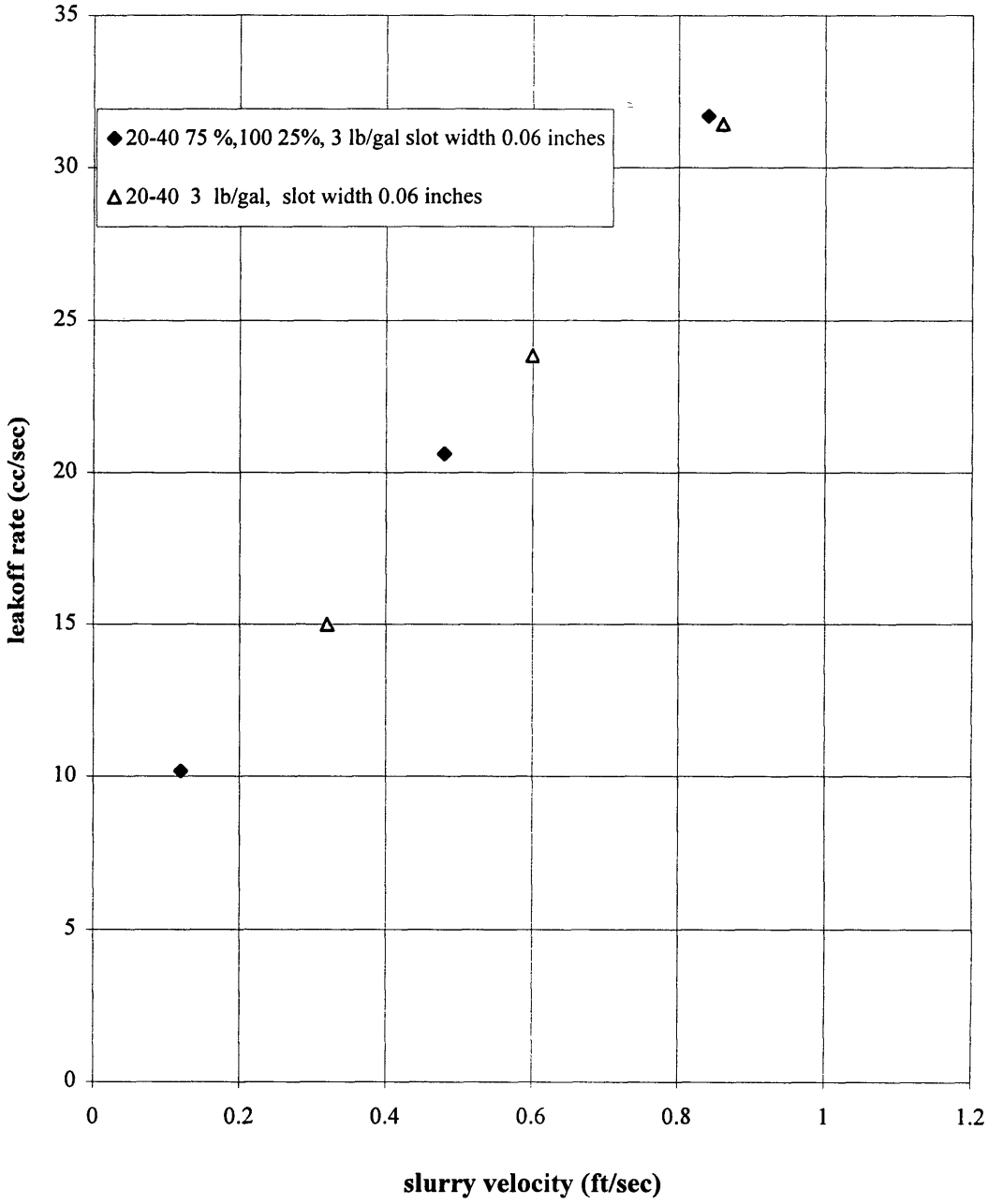

Fig 4.19: Slurry Leakoff Rate for Guar Slurries (60 lb/Mgal Guar)

4.3.1.3 60 lb/Mgal Guar & NDB (Neutral Density Beads)

The results of the above experiments led to a set of experiments which was conducted using models with slot width of 0.01 and 0.03 inches. There was a change of the additive from sand to neutral density beads (NDB). The use of neutral density beads with density of approximately 1 gr/cc would enhance particle suspension at low flow rates. Neutral density beads have a particle diameter range of 0.01-0.025 inches, which approximated the 20-40 mesh sand particle diameter size range. The slot width was larger or equal to the particle diameter in the 0.03 and 0.01 inch slot, which eliminated filtration of the particles at the leakoff site. Figure 4.20 shows that as the slurry velocity decreased in the model a sand node formed which significantly decreased slurry leakoff. The leakoff rates are higher for the 0.03 inch slot compared to the 0.01 inch, due to the width difference of the two sites.

4.3.1.4 80 lb/Mgal Guar & 20-40 mesh Sand

The investigation thus far showed that it was possible to form a sand node by varying the important parameters such as the slurry makeup and the model specifications. To further investigate our findings, an increase of the particle concentration and larger slot width was desired. Use of a more viscous slurry was necessary to eliminate particle settling while rheology effect on node formation could further be investigated. Therefore, 80 lb/Mgal was mixed with 5 lb/gal 20-40 mesh sand and experiments were conducted in

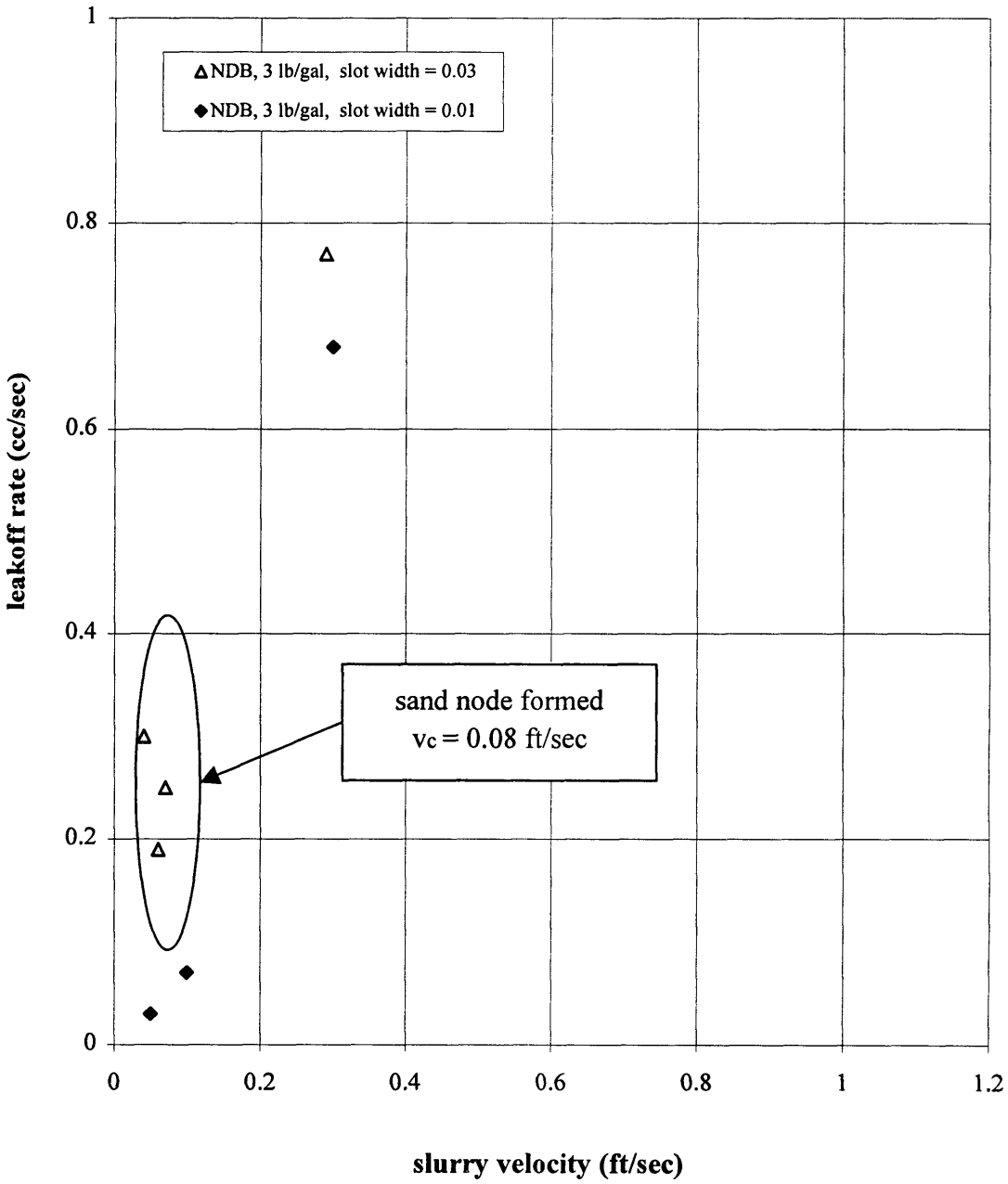

Fig 4.20: Slurry Leakoff Rate for Several Guar Slurries (60 lb/Mgal guar)

a plexiglass model of 0.05" slot width. The results are plotted in Figure 4.21. The results show that a sand node formed at the leakoff site for velocities less than 0.25 ft/sec.

A set of experiments were also conducted using 1.85 lb/gal NDB (equivalent volume fraction for 5 lb/gal 20-40 mesh sand), which resulted in similar observations. Sand node formed at velocities of less than 0.2 ft/sec. However, the leakoff rates were higher compared to 20-40 mesh sand. This difference could be due to the difference between the surfaces of the sand and neutral density beads. The sand particles seem to "glue" to each other when in contact with each other and thus allow less discharge while the surface of the neutral density beads are more "slippery" such that slurry seeps out and discharges through the slot more freely.

The results obtained from the guar experiments indicate that slurry leakoff is inhibited by formation of the sand node at the leakoff site. The leakoff rates can be further reduced favorably by use of additives particle size distribution. It was also observed that sand concentration and the leakoff site size (slot width) influence sand node formation at the leakoff site.

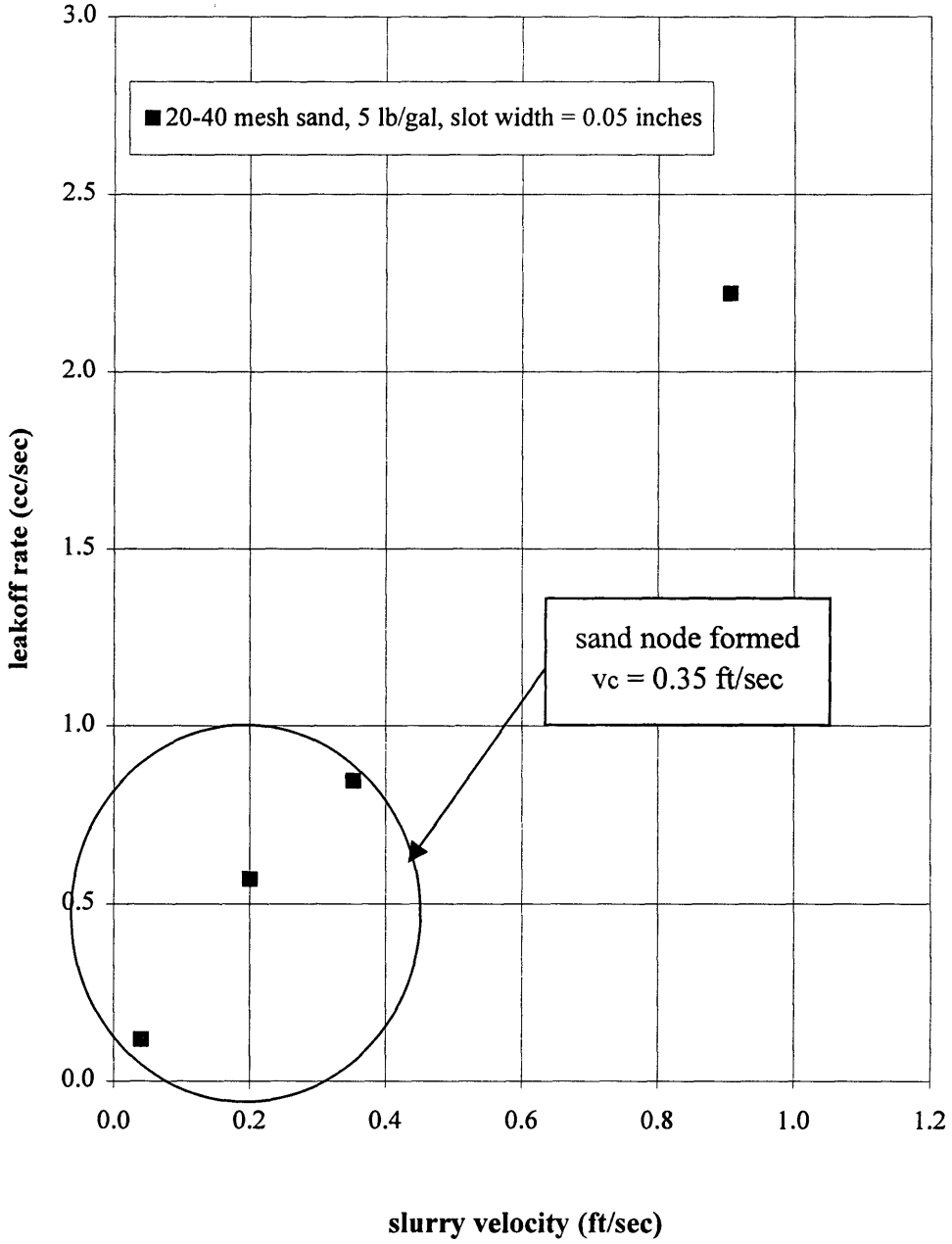

Fig 4.21: Slurry Leakoff rate For 80 lb/Mgal Guar Slurry

4.3.2 Polyacrylamide Experiments

The intent of this set of experiments was to investigate the effect of polymer rheology on the slurry leakoff prevention. Polyacrylamide is a viscoelastic fluid which has different rheological properties compared to power law fluid such as guar. The experiments were conducted with the identical additive type and concentrations in the similar plexiglass models. However, by adjusting polymer concentration, slurry rheological properties were altered which enabled us to compare the results of these flow experiments to the guar runs.

4.3.2.1 20 lb/Mgal Polyacrylamide & 20-40 mesh Sand

Previously, flow experiments were conducted using 60 and 80 lb/Mgal polyacrylamide slurry of 5 lb/gal 20-40 mesh sand in a plexiglass model with a round leakoff site of 1/16". It was observed that a sand node did not form at the leakoff site for the range of velocities for the flow experiments. This behavior was due to the fluid rheology. Therefore, polymer concentration was reduced to 20 lb/Mgal and the viscoelasticity of the solution was reduced.

Figure 4.22 depicts the results of flow experiments conducted in plexiglass models of 0.06 inch and 0.03 inch slot width using a 20 lb/Mgal polyacrylamide and 3 lb/gal 20-40 mesh sand. Sand nodes formed for velocities of less than 0.18 ft/sec.

Figure 4.23 shows the results of experiments completed using slurry with 5 lb/gal sand concentration conducted in plexiglass models with slot width of 0.05 and 0.06 inch.

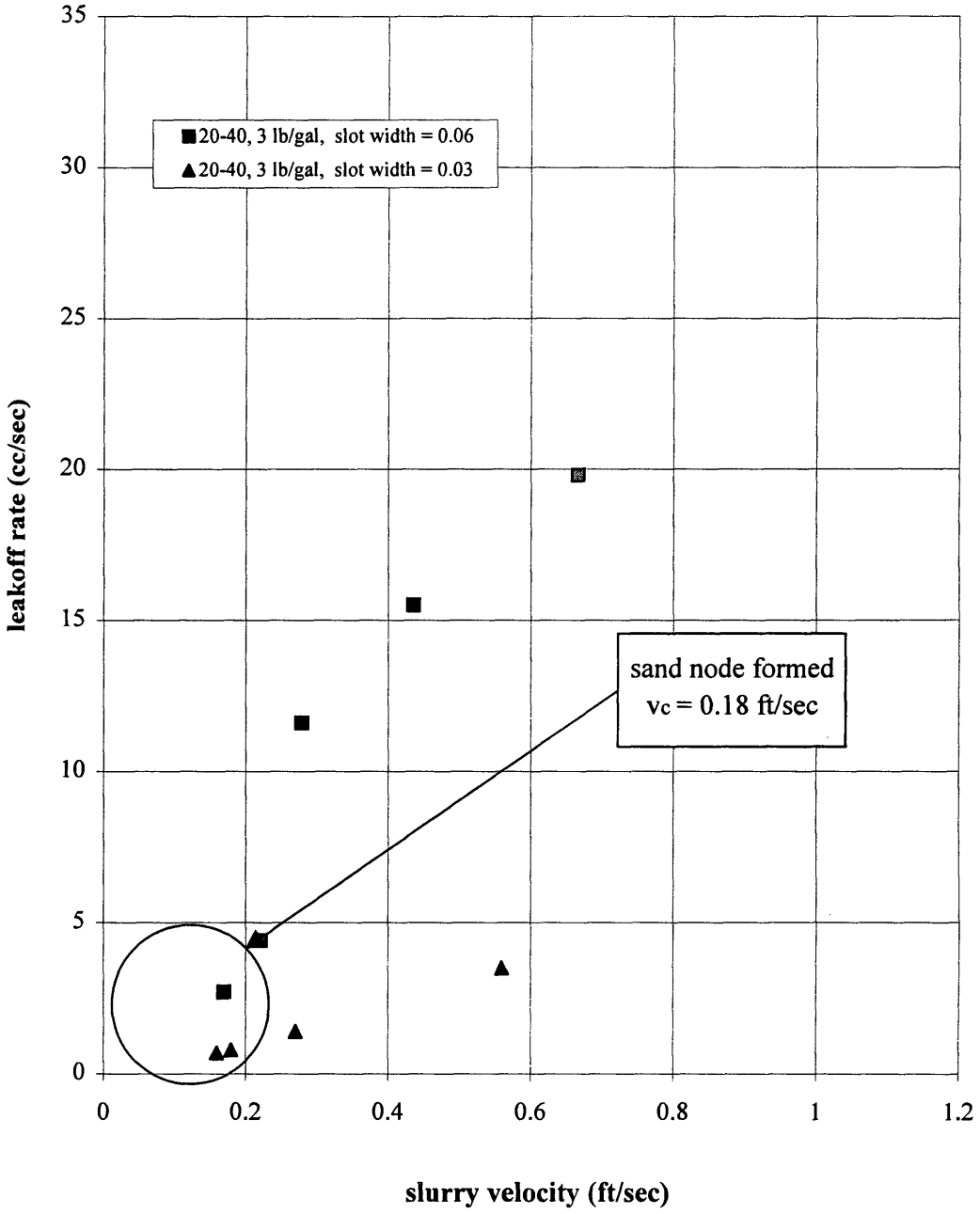

Fig 4.22: Slurry Leakoff Rate For 20 lb/Mgal PHPA

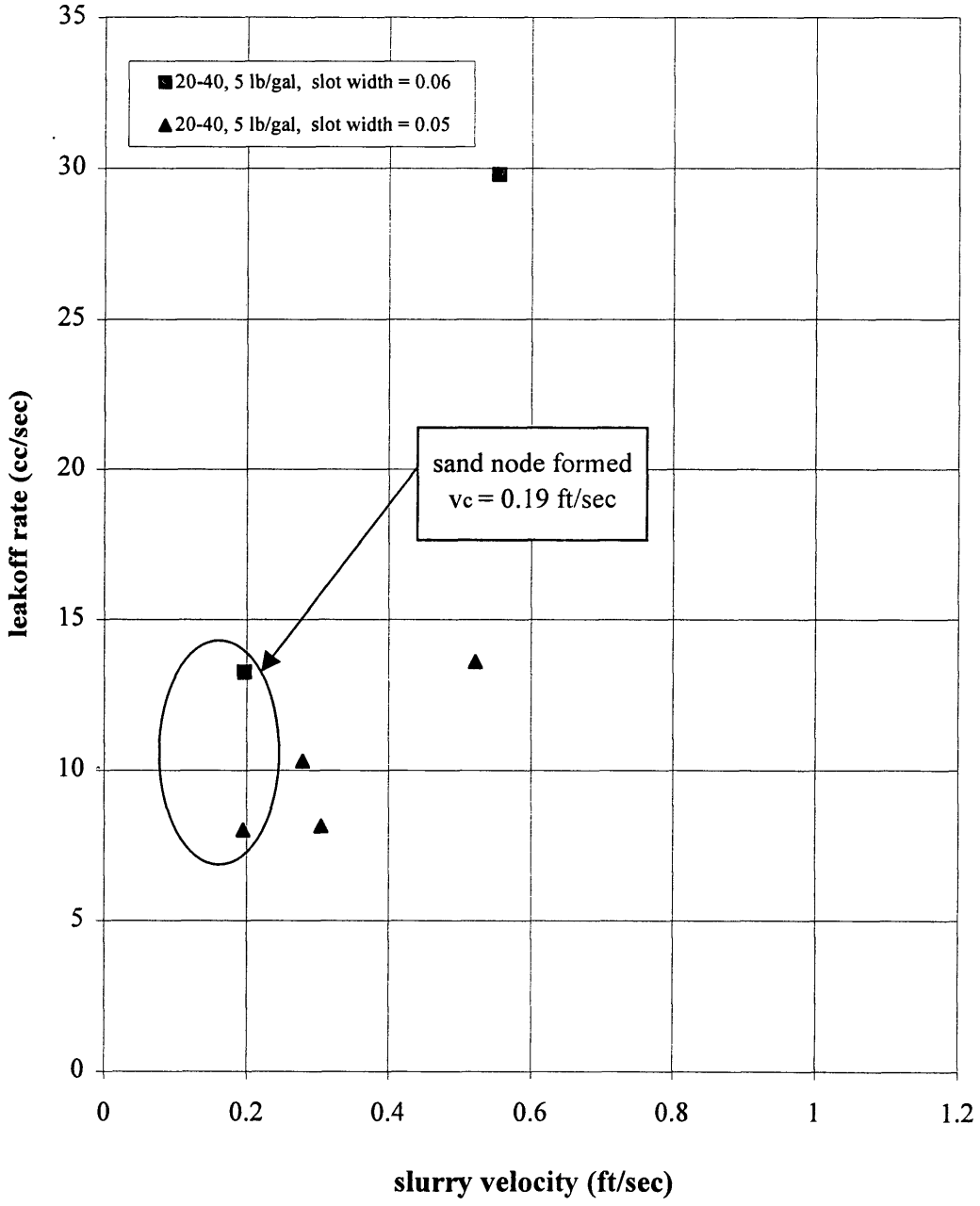

Fig 4.23: Slurry Leakoff Rate For 20 lb/Mgal PHPA

The results show that slurry leakoff was inhibited when the velocity reached 0.19 ft/sec. The results of these experiments are similar with respect to critical velocity; however, when the velocity decreased substantially there was substantial sand settling at the end of the run. This effect did not fundamentally alter the outcome of the experiment though it affects the accuracy of the experimentation. The significance of these experiments lies in the fact that with these observations it is possible experimentally to change the critical parameters such as fluid rheology for any slurry system and form a sand node to control fluid leakoff effectively.

4.3.2.2 40 lb/Mgal Polyacrylamide & Neutral Density Beads (NDB)

Figure 4.24 is a plot of flow experiments conducted using the 40 lb/Mgal polyacrylamide slurry with the equivalent volume fraction of 5 lb/gal sand concentration. This set of experiments were conducted in plexiglass models of 0.03 inch and 0.01 inch slot width. The results show that slurry leakoff decreased once node formed. The corresponding velocity was about 0.08 ft/sec. This velocity is lower than the critical velocity obtained for the 20 lb/Mgal PHPA slurry. This could be due to higher viscoelasticity of the 40 lb/Mgal solution relative to the 20 lb/Mgal polymer solution; thus node forms at lower shear rate, which is consistent with our previous observations and conclusions.

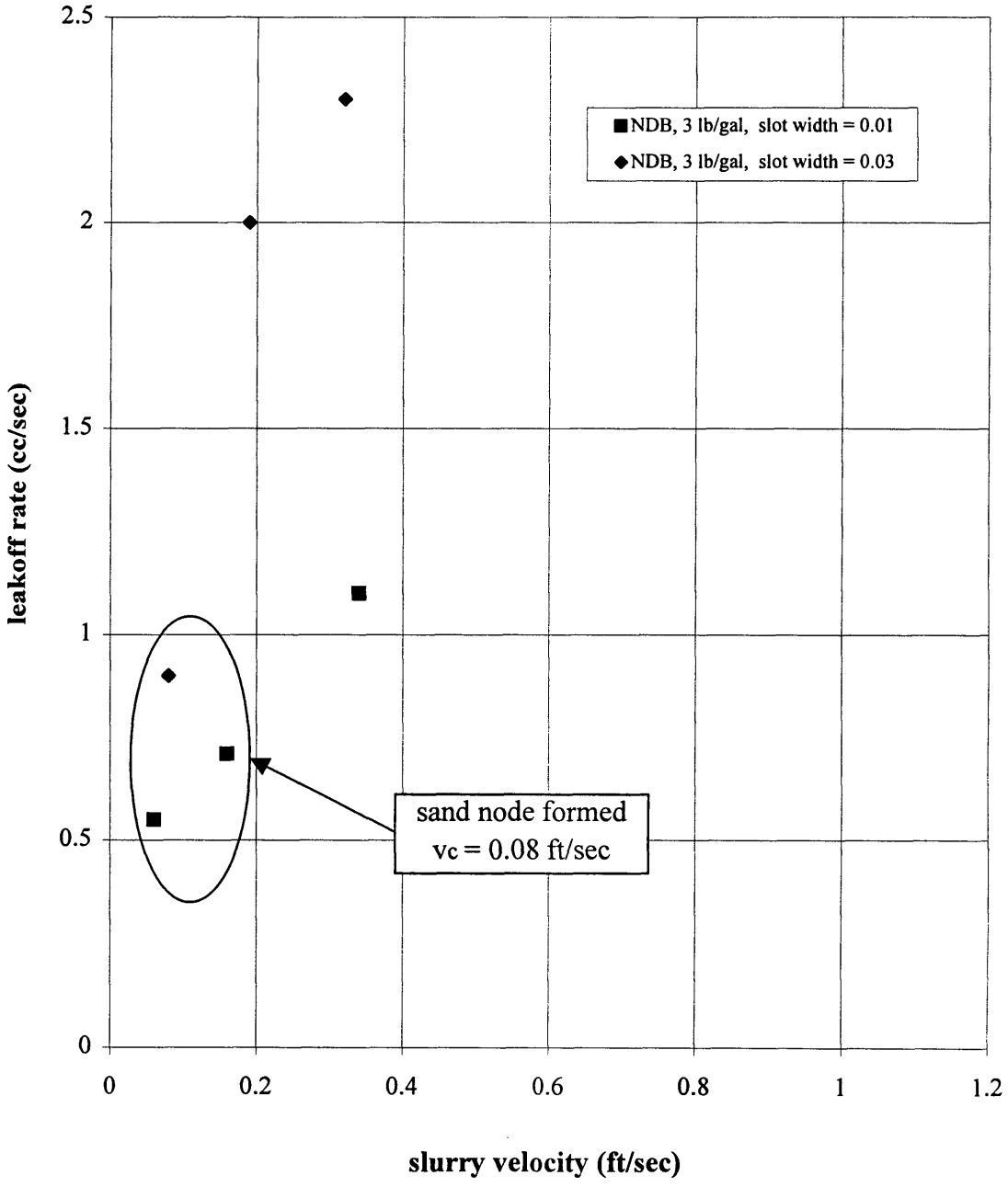

Fig 4.24: Slurry Leakoff Rate For 40 lb/Mgal PHPA

4.3.2.3 60 lb/Mgal Polyacrylamide & 20-40 mesh Sand

The results from the 20 lb/Mgal and 40 lb/Mgal slurry experiments showed that by reduction of the shear rate it was possible to create a sand/particle node at the leakoff site. Experiments with 60 lb/Mgal polyacrylamide slurry of 5 lb/gal of 20-40 mesh sand were conducted in order to explore the effect of the increased viscoelasticity of the slurry due to increased polymer loading. Previous experiments conducted in the models with round leakoff site with diameter of 1/16 inch had not resulted in any kind of leakoff control. Thus, more experiments were conducted in plexiglass models with slot width of 0.06 inches.

Figure 4.25 is the plot of slurry leakoff as a function of slurry velocity. Sand node did not form for any of these experiments, even though some runs were conducted at unrealistically very low velocities. Reduction of the flow/shear rate to a very low level will reduce the viscoelasticity of the slurry and thus enhance the possibility of the sand node formation; however, with these unrealistically low velocities the integrity of the slurry would be preserved.

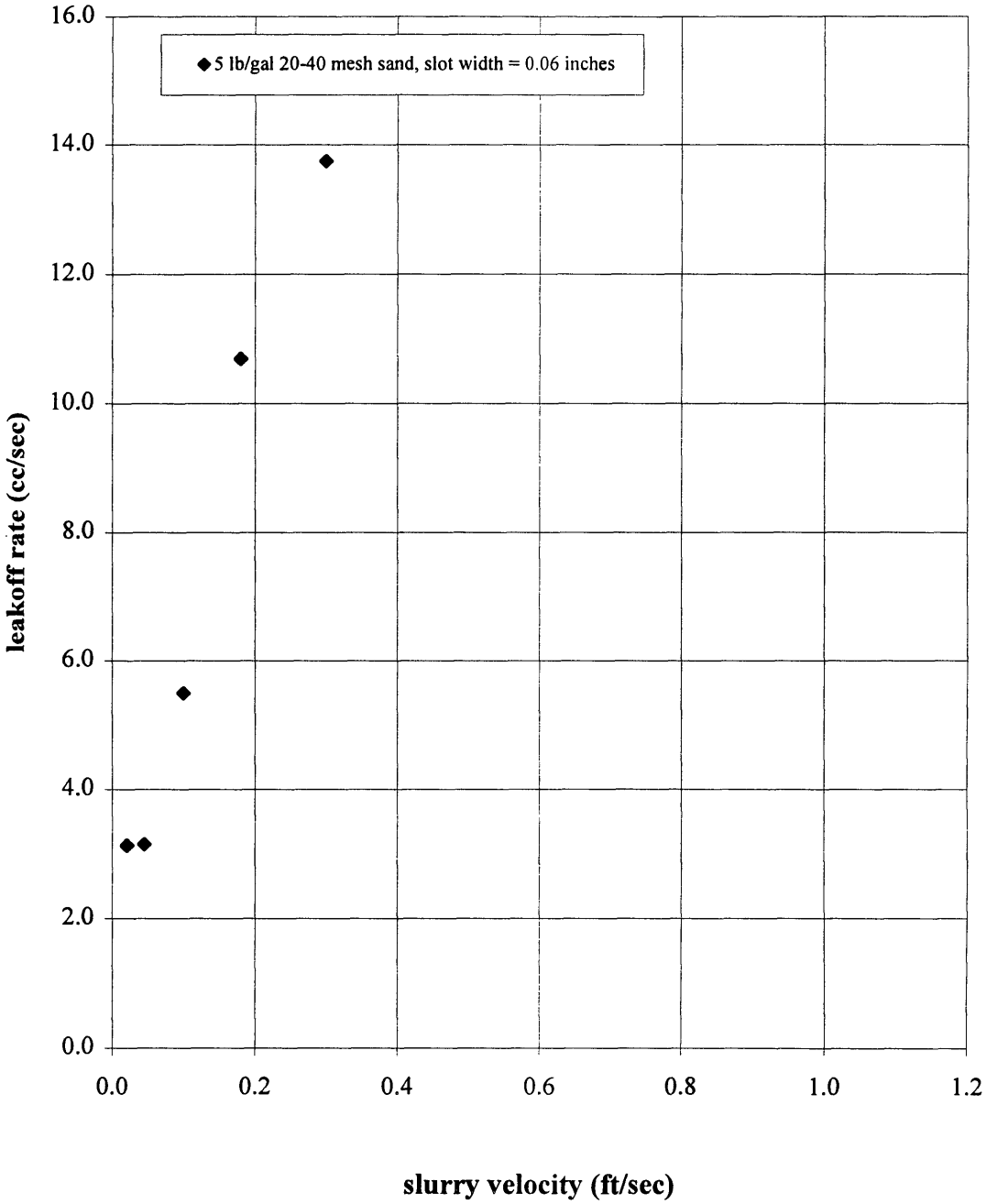

Fig 4.25: Slurry Leakoff Rate For 60 lb/Mgal PHPA
No sand node formed

4.3.2.4 80 lb/Mgal Polyacrylamide & 20-40 mesh Sand

Two sets of experiments were conducted using 5 lb/gal 20-40 mesh sand in 0.06 inch and 0.05 inch slot plexiglass models. The results are plotted in Figure 4.26. Both sets of the experiments were conducted at very low flow rates in order to decrease the magnitude of the first normal stresses, which mainly represent the viscoelasticity of the polymer solution.

Reduction of the shear rate would have reduced the viscoelasticity of the fluid, thus giving rise to the possibility of the node formation. However, due to the high viscoelastic nature of the 80 lb/Mgal PHPA solution, at these shear rates it is not possible to initiate node formation. At the very low flow rates, specifically, toward the end of the experiments, particles tend to settle at which point the accuracy of the results are compromised. However, the very low rates are not feasible to be of practical value for it can not be implemented in the field. This situation does not contribute to a solution of the problem and limits further investigation.

4.3.3 Summary

The three types of slurry experiments performed have focused on variation of several parameters which affect fluid leakoff rates. The variations, though helpful in identifying the relative effects and their importance, point out the significance of the fluid rheology and fluid characteristics. It is true that the physical set up, such as the model width and leakoff site dimensions and relative location of the leakoff site with respect to the model width (i.e. scaling effect) affect sand node build-up and its characteristics;

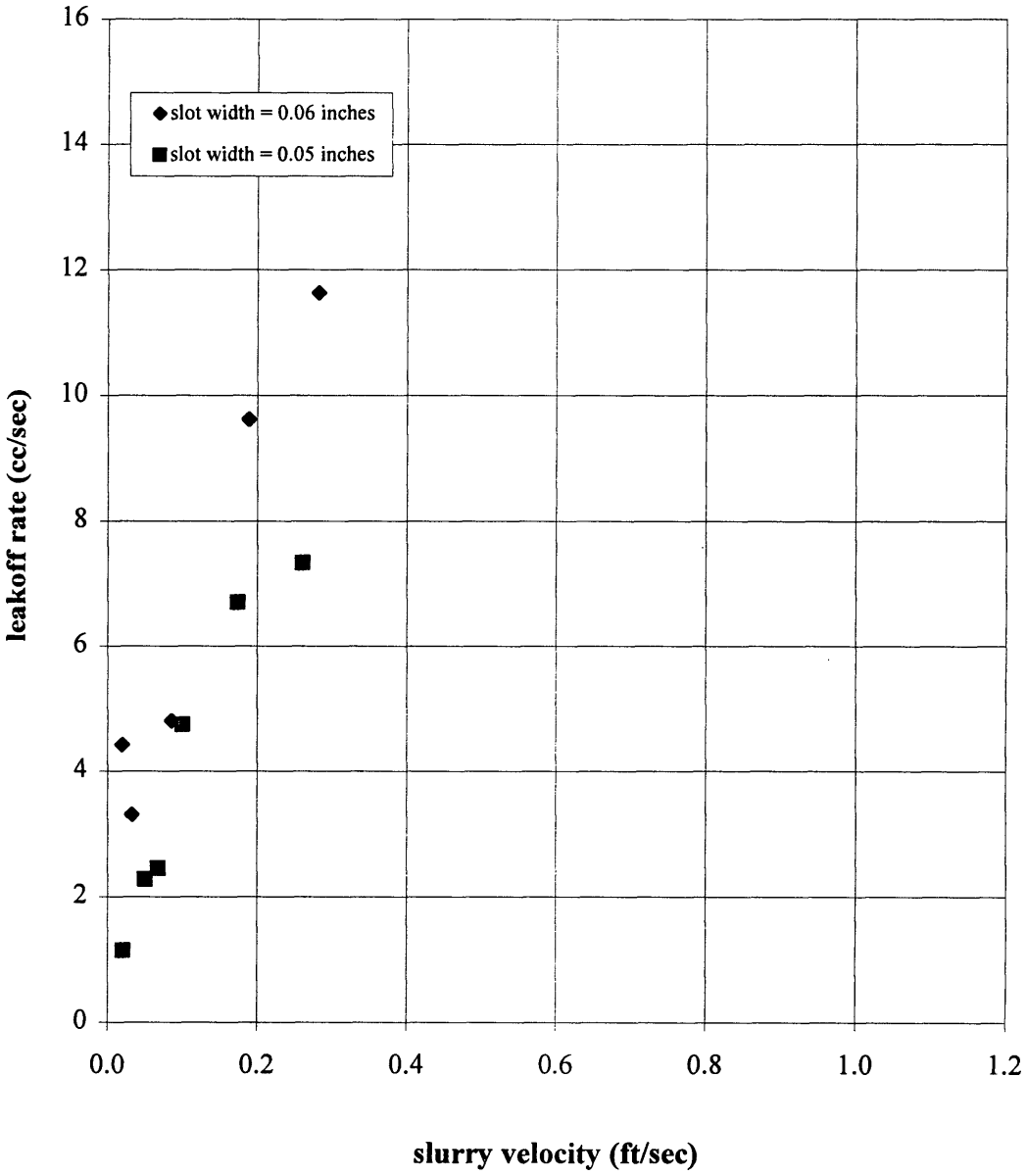

Fig 4.26: Slurry Leakoff Rate for Several Polyacrylamide Slurries (PHPA 80 lb/Mgal & 5 lb/gal 20-40 mesh sand)-No sand node formed

however, the fluid properties play an important role to bring about node formation which inhibits fluid leakoff. Through the completion of these experiments, it has been shown that fluid rheology, shear rate, additive concentration, size, and distribution and the slot width are important parameters determining the magnitude of the slurry leakoff rates.

Selection of particle size should be in accordance with the natural fracture width, otherwise it will not play a constructive role. Fluid apparent viscosity should accommodate a well suspended system otherwise settling will cause failure. Particle distribution size and concentration will help reduce leakoff rates by sealing sand node. Depending on the sand node permeability, sand out may be prevented.

Low fluid velocity in the induced fracture brings about node formation. It links all of the variables involved. However, fluid rheology stands at the top of the hierarchy of the variable importance. This is the variable which determines whether node will form or not.

Chapter 5. Results of Rheological Evaluations

5.1 Introduction

In this chapter essentials of polymer rheology, linear viscoelastic and nonlinear viscoelastic behavior of polymer solutions are summarized. The discussion on linear and nonlinear fluid behavior is accompanied by guar and polyacrylamide rheology data. The intent in this chapter is to familiarize the reader with the general concepts relating to polymeric fluid behavior. The rheology data (i.e. apparent viscosity, relaxation modulus G(t), longest time constant λ, average time constant λ_{avg}, storage modulus G′(t), and shear modulus G″(t)) are used to characterize the polymer solutions used for the flow experiments. The relationship of the rheological data to the flow experiments are presented and discussed in Chapter 6.

5.2 Polymer Rheology

In this research, dependence of the polymeric fluid rheology on the shear rate was studied. Rheology is the study of fluid deformation with stress. A fluid changes shape or deforms when it flows (i.e. in a slot). Figure 5.1 depicts two parallel plates filled with polymer fluid initially at rest. The space between the plates is denoted by Δy and the displacement is denoted by Δx.

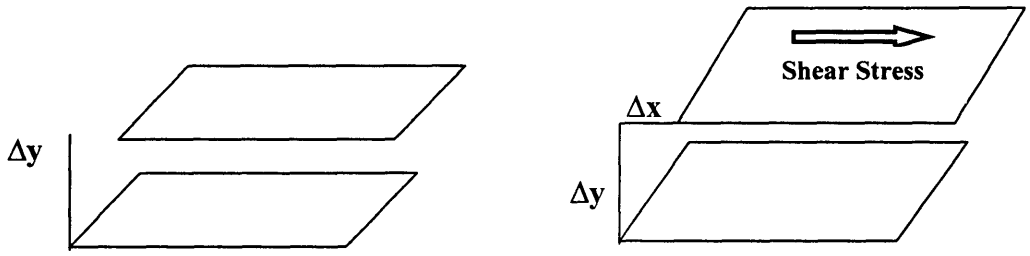

Figure 5.1: Deformation due to Shear Stress

Once a shear stress is applied to the top plate, there will be a displacement of the fluid in between the plates resulting in liquid deformation. Shear strain ε (dimensionless) is the ratio of the displacement over the spacing ($\Delta x/\Delta y$).

Figure 5.2 shows the velocity profile across the width of the plates when fluid flows due to the applied shear stress. Velocity is maximum in the center and reduces as a function of the position relative to the plate width. Velocity reaches zero at the boundaries.

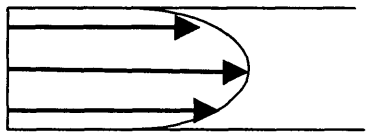

Figure 5.2: Velocity Distribution in Parallel Plates

The deformation rate or the shear rate γ'(1/sec) is defined as the rate of change of the shear strain with time. It may be calculated by taking the ratio of change in velocity over the spacing Δy. The fluid resistance to flow defined as the polymer solution viscosity μ(cp) may be obtained by taking the ratio of the shear stress τ(dynes/cm^2) over the shear rate γ'(1/sec).

The polymeric solution rheological properties depend on shear rate. In other words, the changes in the magnitude of the shear rate alter the rheological behavior of polymer solutions. Two distinct regions of linear and nonlinear viscoelastic behavior are identified where polymer solutions exhibit different physical behavior. We will discuss these two regions in the next two sections.

5.3 Linear Viscoelastic Region

This is a region of small shear rate and small strain in which shear rate change does not alter the measurement of fluid properties. For example, for a guar solution of 40 lb/Mgal, change of shear rate from 0.1 1/sec to 0.5 1/sec will yield viscosity of 600 cp (see Figure 5.3). However, viscosity decreases as the shear rate increases thereafter.

Similar behavior is observed when a polymer solution is subjected to a sudden strain (step strain). When stress is monitored as a function of time, it will exhibit an exponential decay behavior. Figure 5.4 depicts such behavior when G(t) the shear modulus decreases as a function of time in a linear viscoelastic region.

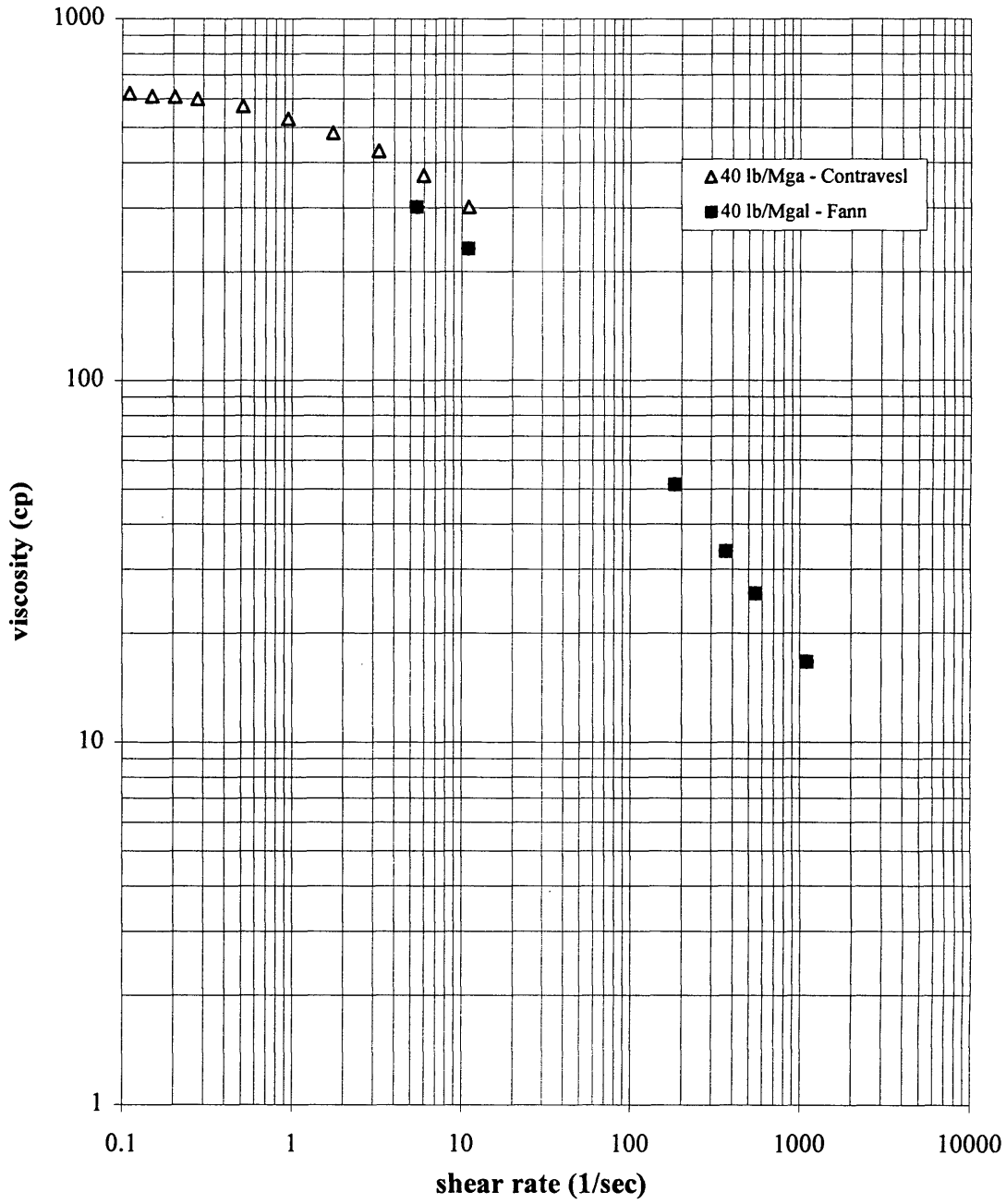

Fig 5.3: Guar Viscosity as a Function of Shear Rate (Fann & Contraves Measurements)

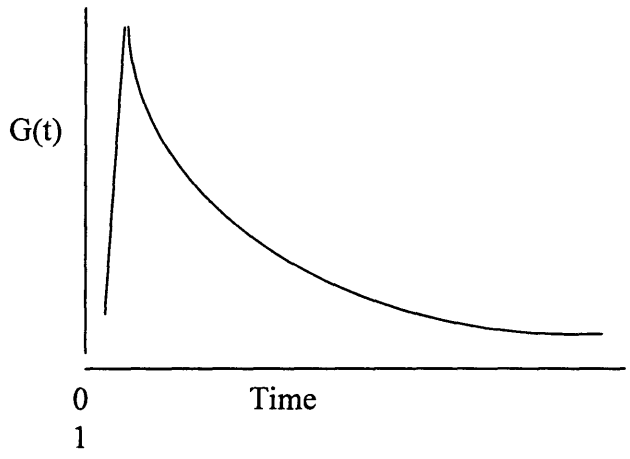

Figure 5.4: Shear Modulus Decay for a Step Strain Experiment

One may repeat this type of experiment by increasing the magnitude of the step strain until the relaxation modulus changes. The size of the step strain should be selected such that the shear modulus G(t) for the different step strains would not change. Within linear viscoelastic region, the relaxation modulus G(t) is constant; however, it changes when the size of the strain increases. Figure 5.5 is a plot of the relaxation modulus as a function of time for several step strain sizes for 60 lb/Mgal guar solution.. The relaxation modulus G(t) is constant for the step strain size up to 1.22, after which the shear modulus G(t) decreases due to a change of the step strain size. This variation is indicative of the nonlinear viscoelastic region.

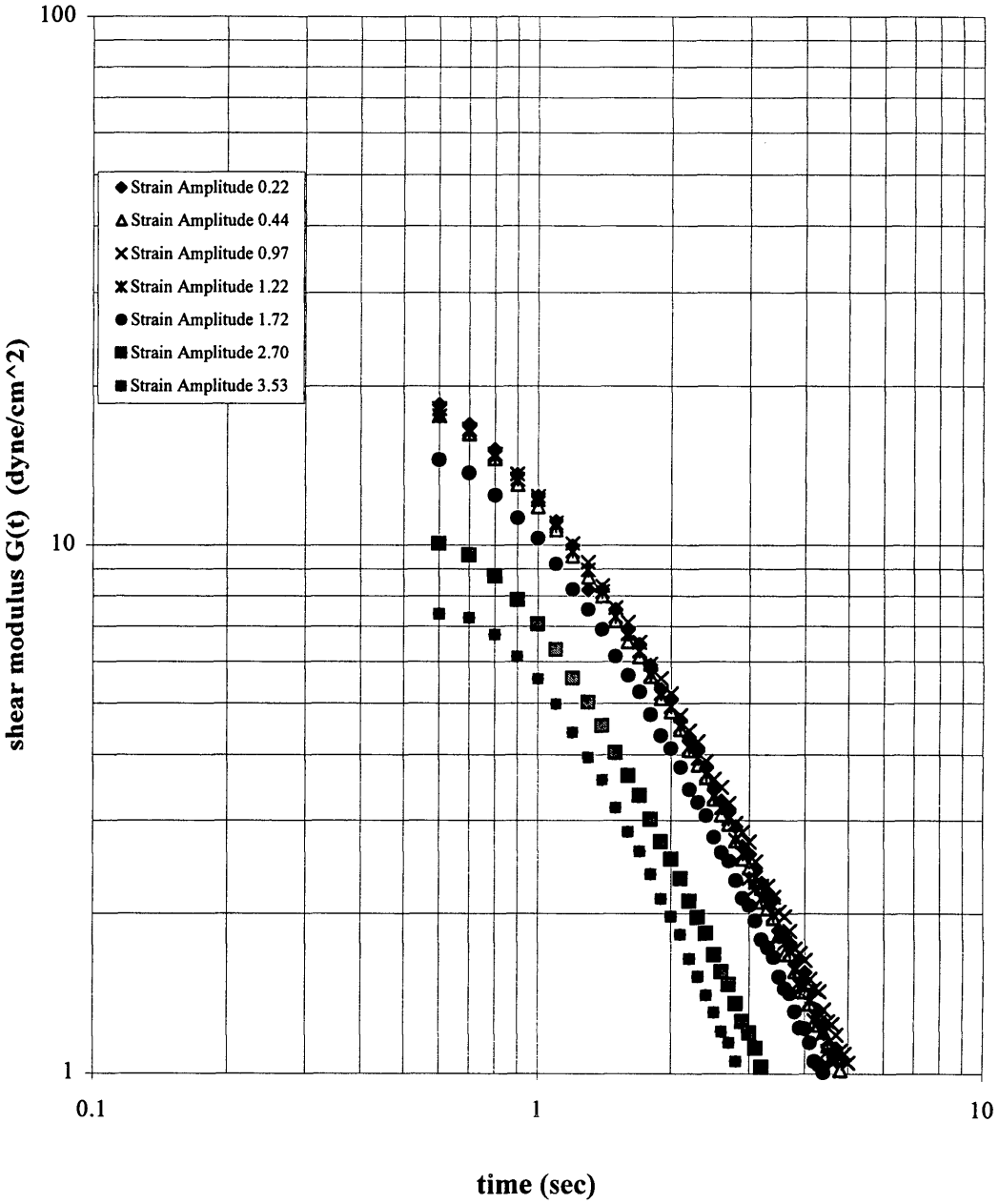

Fig 5.5: Stress Relaxation Modulus G(t) for Several Strain Steps (60 lb/Mgal Guar solution)

The exponential decay of the shear modulus for a polymer solution is characteristic behavior of the particular polymer solution for the given polymer concentration. Figure 5.6 is the plot of the relaxation modulus G(t) as a function of time for 80 lb/Mgal guar and 80 lb/Mgal polyacrylamide solutions under a strain amplitude of 0.42. It is apparent that the relaxation modulus G(t) for guar flattens at a higher rate compared to polyacrylamide and reaches equilibrium sooner than the polyacrylamide solution. The slope of the decay curve at long times is a measure of the longest time constant λ when plotted in a semi-log plot. The relaxation modulus data may also be used to obtain an average time constant as follows:

$$\lambda_{avg} = \int_0^\infty tG(t)dt \,/\, \int_0^\infty G(t)dt \qquad (5.1)$$

The average time constant for a polymer solution is the integral of the product of time and the relaxation modulus over the integral of the relaxation modulus G(t). The zero shear viscosity can be estimated using the shear modulus. This viscosity refers to the low shear rate region where it registers a constant value (refer to Fig 5.3). The zero shear viscosity is computed from the following expression:

$$\eta_0 = \int_0^\infty G(t)dt \qquad (5.2)$$

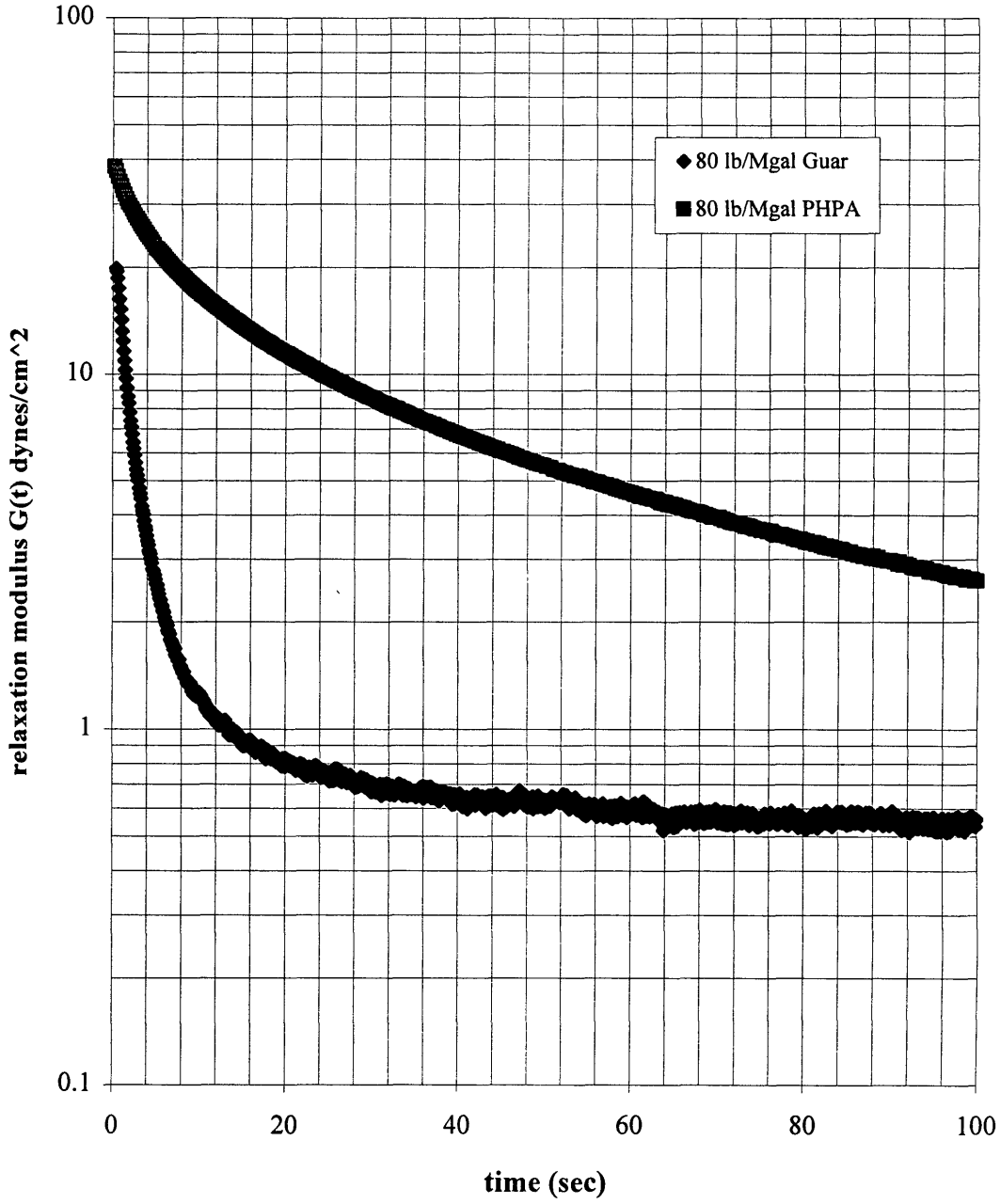

Fig 5.6: Relaxation Modulus Behavior as a Function of Time

The longest time constant, the average time constant, and the zero shear viscosity for guar and polyacrylamide solutions at different polymer concentrations were estimated from the G(t) data and are listed in Table II.

Table II: Characteristic Time and Viscosity for Guar & Polyacrylamide Solutions

Polymer type	Polymer concentration lb/Mgal	λ second	λ_{avg} second	μ_o cp
Guar	40	26	11	760
Guar	60	36	23	10,400
Guar	80	126	70	15,000
Polyacrylamide	20	25	25	6,600
Polyacrylamide	60	205	89	86,210
Polyacrylamide	80	278	116	120,750

The average time constant (λ_{avg}) for the guar solutions ranges from 11 to 70 seconds for concentrations of 40 to 80 lb/Mgal. For polyacrylamide λ_{avg} ranges between 25 to 116 seconds, for concentrations of 20 to 80 lb/Mgal. The time constants, λ and λ_{avg} for the polyacrylamide solutions, are greater than the time constant for guar. This is due to the fact that it takes longer time for a polyacrylamide solution to reach equilibrium compared to a guar solution for a given strain. It is also apparent from the data that the characteristic time increases with the increase of polymer loading. Once the shear rate

increases, then the rheological properties show shear rate dependence. This introduces the nonlinear viscoelastic region. The implications of shear dependent properties are discussed in the next section.

5.4 Nonlinear Viscoelastic Region

In this section we will discuss the effects of the shear rate on viscosity and the normal forces in the linear viscoelastic region. With increase of shear rate, fluid viscosity decreases and normal stresses become significant.

Figure 5.7 ideally depicts polymer solution viscosity as a function of shear rate. Initially, the viscosity stays constant with increase of the shear rate. This viscosity represents the zero shear viscosity μ_o. However, beyond this region the increase of shear rate leads to a decrease in viscosity. This region is called the "power law region."

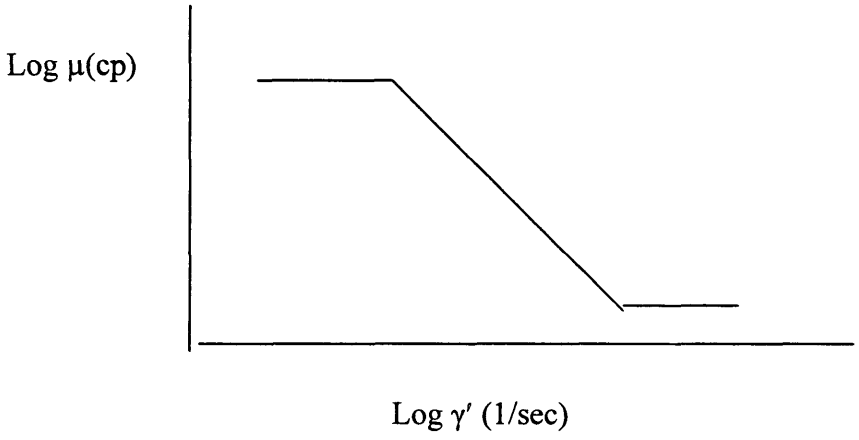

Figure 5.7: Viscosity Behavior of Polymeric Solutions

At higher shear rates there would be another plateau region where viscosity stays constant. For this investigation, the shear rate region between 10 1/sec and 100 1/sec was considered because this shear rate range generally exists in the induced fractures during hydraulic fracturing.

Figures 5.8 and 5.9 are plots of viscosity as a function of shear rate for several concentrations of polyacrylamide and guar solutions. The plots are constructed using collected data from Fann and Contraves viscometers. Fann viscometer data are for a shear rate ranges of 5.1 1/sec to 1120 1/sec, and Contraves viscometer data is for low shear rates of 0.05 1/sec to 10 1/sec. Figure 5.8 contains polyacrylamide viscosity data for concentrations of 20, 40, 60, and 80 lb/Mgal. At low shear rates, the zero shear viscosity range from about 15,000 to 90,000 cp for 20 lb/Mgal and 80 lb/Mgal polyacrylamide solutions, respectively. The increase in the shear rate causes a decrease in the viscosity. Meanwhile, there is a reasonable correlation between the Fann and Contraves measurements. Figure 5.9 is the viscosity data for guar solutions of 30, 40, 60, and 80 lb/Mgal concentrations. The zero shear viscosities range between about 200 cp to 30,000 cp, respectively. In contrast to polyacrylamide solutions, guar reaches its zero shear viscosity at relatively higher shear rates, which would indicate a smaller time constant for guar solutions compared to polyacrylamide. There is a good correlation between the two sets of the data collected by the two viscometers.

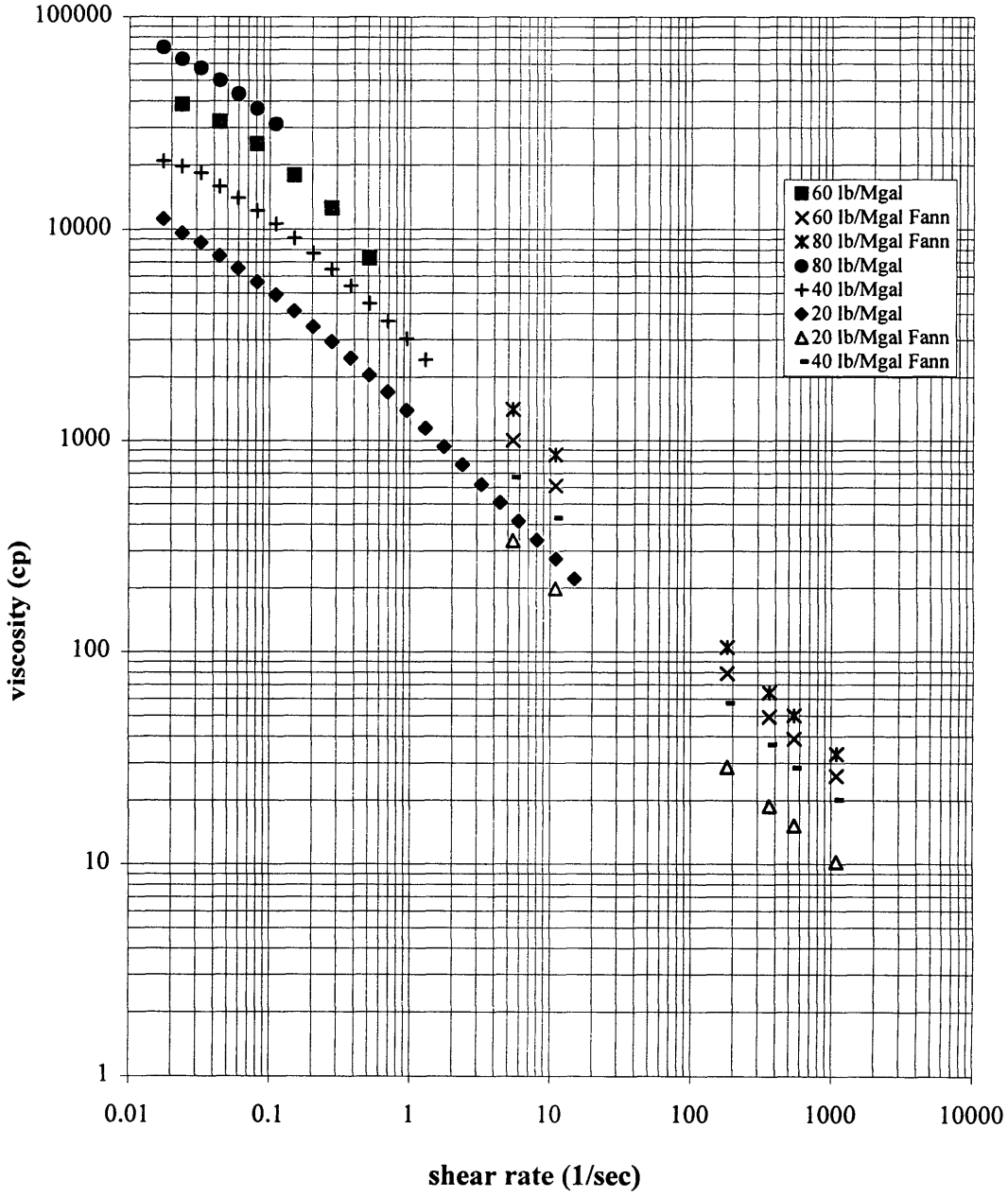

Fig 5.8: PolyacrylamideViscosity as a Function of Shear Rate (Fann & Contraves Measurements)

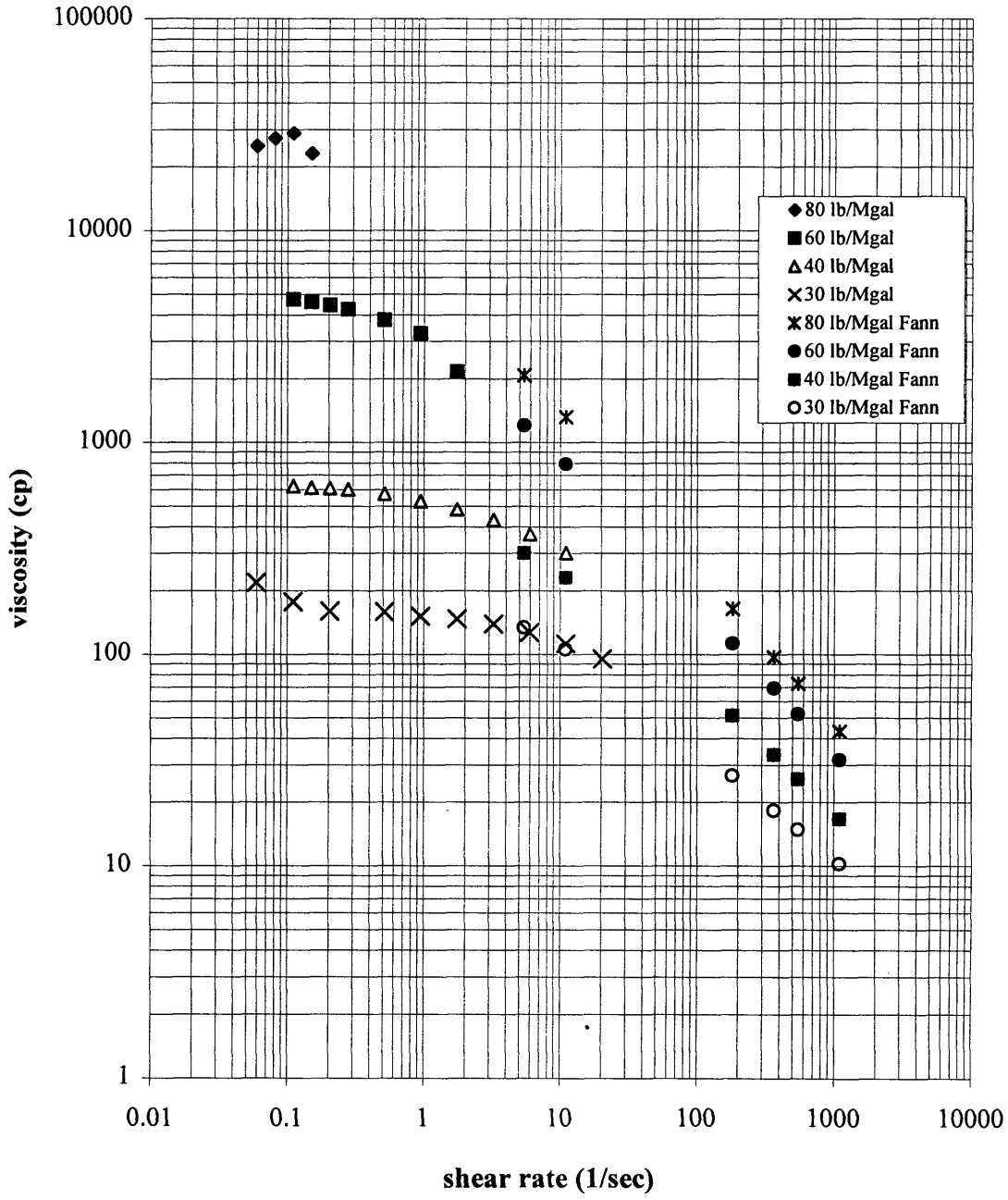

Fig 5.9: Guar Viscosity as a Function of Shear Rate (Fann &Contraves Measurements)

An increase in shear rate enhances the normal forces in the viscoelastic fluids. Figure 5.10 represents a small cubical element of a liquid at some instant and the forces acting upon it. Assume that the direction of forces are specified in 1, 2, and 3 directions. The normal forces are specified by the P_{11}, P_{22}, and P_{33}, and the shear component is denoted by P_{21}.

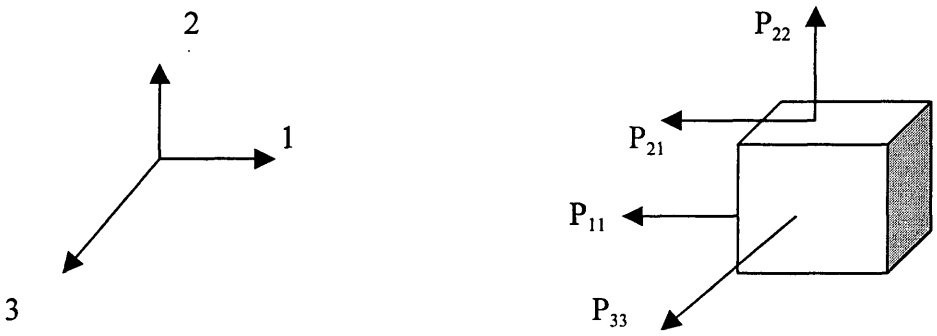

Figure 5.10: Stress Components in Shear Flow

The first normal stress difference (P_{11}-P_{22}) is denoted by $N_1(\gamma')$ and second normal stress difference (P_{22}–P_{33}) by N2(γ'), respectively. The first normal stress difference $N_1(\gamma')$ is larger in magnitude compared to the second normal stress difference N2(γ'). The magnitude of the normal stress difference increases with shear rate increase

A viscoelastic liquid can be specified by three shear rate functions, namely, shear stress function and two normal stress difference functions. They are denoted as follows:

$$\tau(\gamma')=\mu\,\gamma' \qquad (5.3)$$

where $\tau(\gamma')$ is the shear stress, μ is the apparent viscosity, and γ' is the shear rate. The first and second normal stress differences are as represented as follows:

$$N_1(\gamma') = \Psi_1(\gamma')\,\gamma'^2 \quad (5.4)$$

$$N_2(\gamma') = \Psi_2(\gamma')\,\gamma'^2 \quad (5.5)$$

Where $\Psi_1(\gamma')$ and $\Psi_2(\gamma')$ are the first and second normal stress difference coefficients. To characterize the polymer solutions, the storage modulus G'(t) data and the loss modulus G''(t) data were collected and used to calculate Weissenberg numbers (We) using equation 5.6 for the polymer solutions.

$$We = \Psi_1 * \gamma' / \eta \quad (5.6)$$

where We = Wissenberg number
Ψ_1 = first normal stress difference coefficient
γ' = shear rate
η = complex viscosity

First normal stress coefficient (Ψ_1) can be calculated from Laun's rule[34] using equation 5.7.

$$\Psi_1(\gamma') = 2\,\eta''/\omega\,[1+(\eta''/\eta')^2]^{0.7} \quad (5.7)$$

Where η'' = imaginary part of the complex viscosity
η' = real part of the complex viscosity
ω = frequency

The polymer solution viscosity η, can also be computed using equation 5.8 which is called Cox-Merz rule.

$$\eta = \eta'\,[1+(\eta''/\eta')^2]^{0.5} \quad (5.8)$$

η'' = G'/ ω
η' = G''/ ω

G′(t) and G″(t) data are used to compute the first normal stress coefficients Ψ_1 (Laun's Rule)[34], complex viscosity η (Cox-Merz rule)[34] and thus Weissenberg numbers for the corresponding shear rate range of up to 100 rad/sec was calculated. The assumption in use of both equations 5.7 and 5.8 is that the frequency and shear rate are interchangeable. By regression, Weissenberg values are estimated for the flow experiments.

Figure 5.11 depicts the G′(t) and G″(t) data for 60 lb/Mgal polyacrylamide solution. It is a log-log plot of G′(t) and G″(t) as a function of frequency. At a shear rate of about 0.1 rad/sec, G′(t) and G″(t) are about 8 and 10 dynes/cm^2. The two curves crossover at the frequency of 0.16 rad/sec and reach 42 and 100 dynes/cm^2 , respectively.

Figure 5.12 is a similar plot for the rheological properties of 60 lb/Mgal guar solution. It is a log-log plot of G′(t) and G″(t) as a function of frequency. At shear rate of about 0.1 rad/sec, G′(t) and G″(t) are about 0.07 and 0.44 dynes/cm^2. The two curves cross over at shear rate of 15.85 rad/sec and reach 9.7 and 14 dynes/cm^2. Weissenberg numbers are computed using G′(t) and G″(t) data and by regression Weissenberg values for the flow experiments are estimated.

Figures 5.13 and 5.14 depict the comparison of the rheological properties of the two polymer solutions. Figure 5.13 shows the behavior of the storage modulus G′(t) and Figure 5.14 shows the loss modulus G″(t) for the 60 lb/Mgal polyacrylamide and guar solutions.

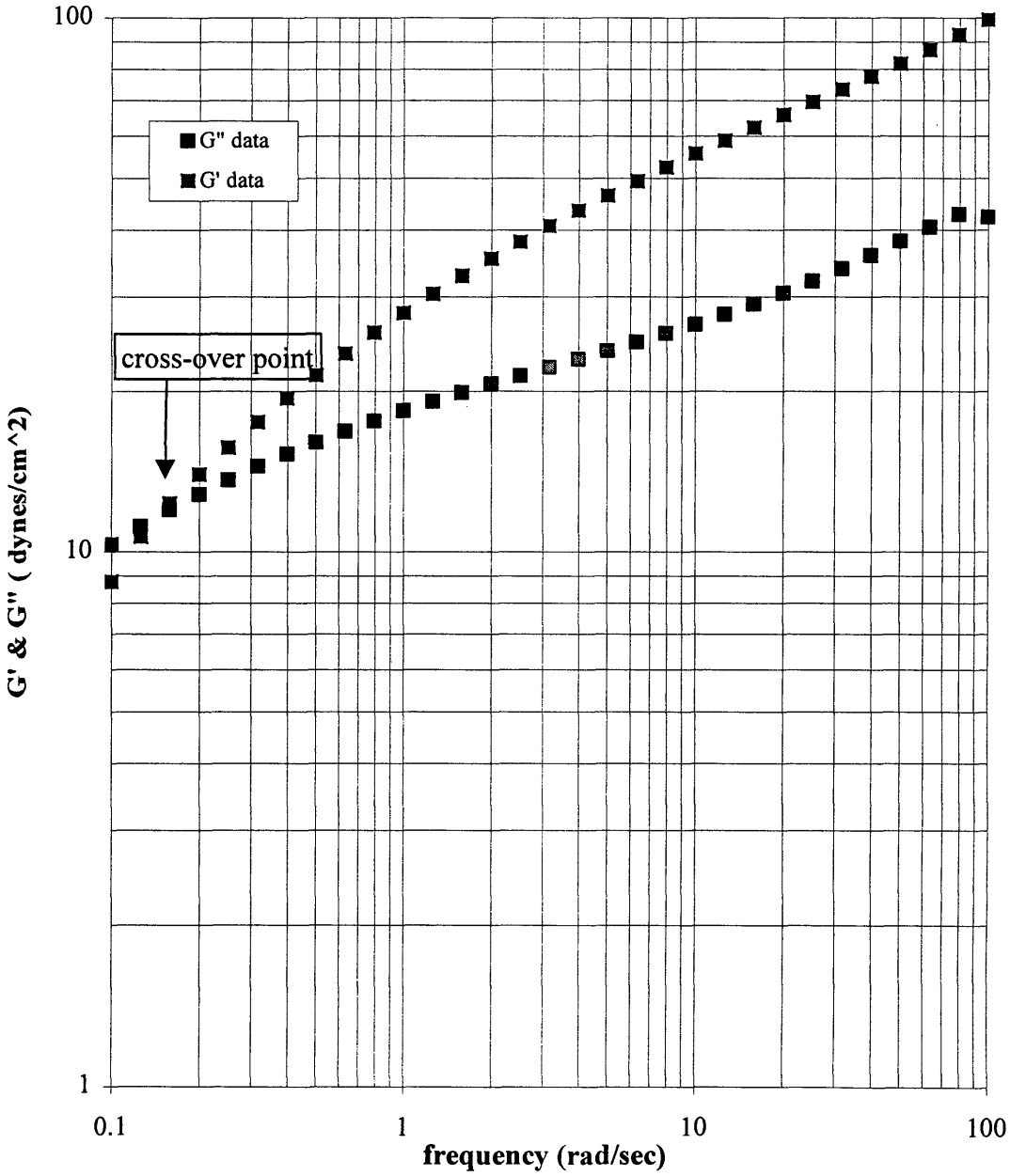

Fig 5.11: Rheological Properties of Polyacrylamide Solution (60 lb/Mgal)

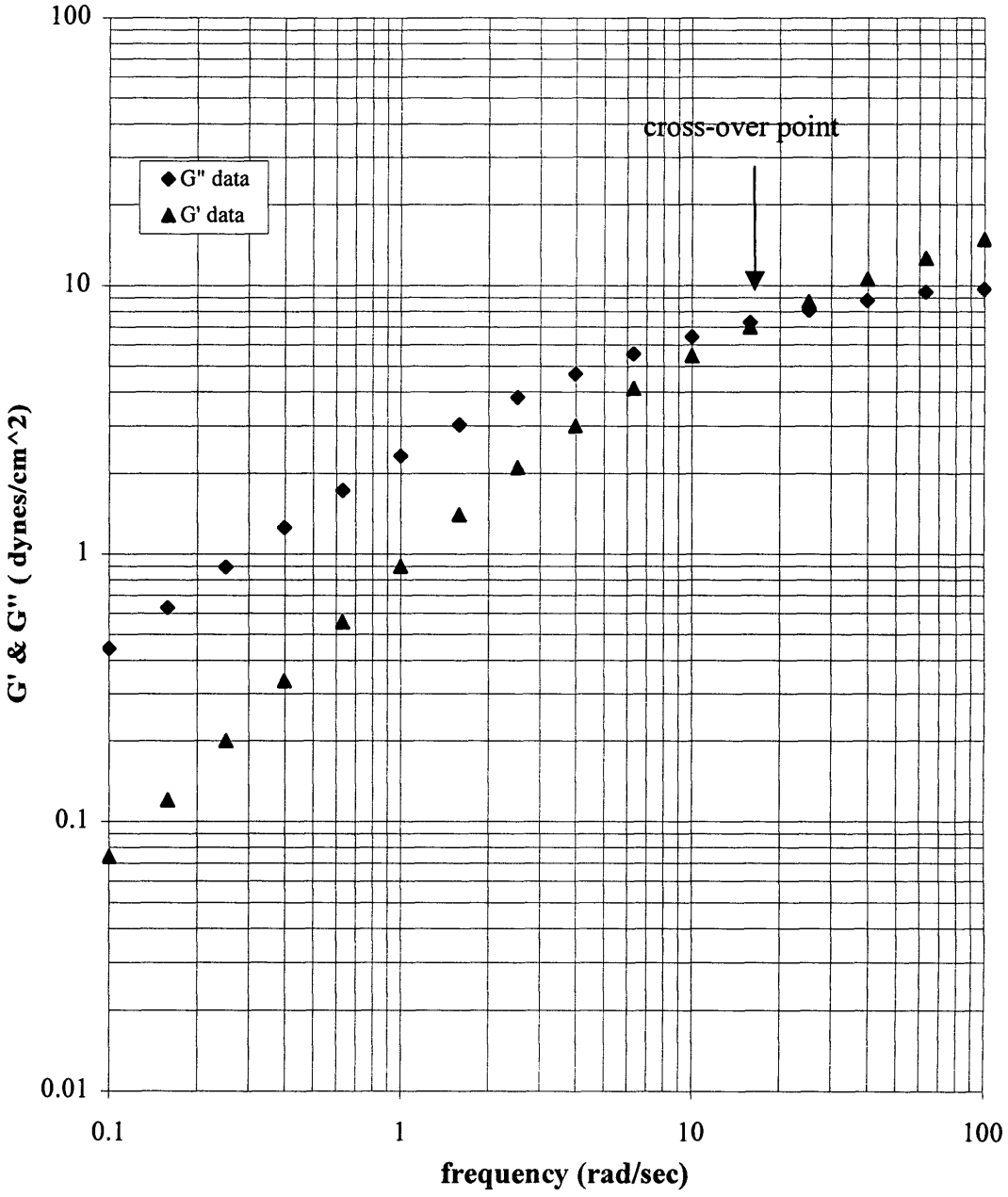

Fig 5.12: Rheological Properties of Guar Solutions (60 lb/Mgal)

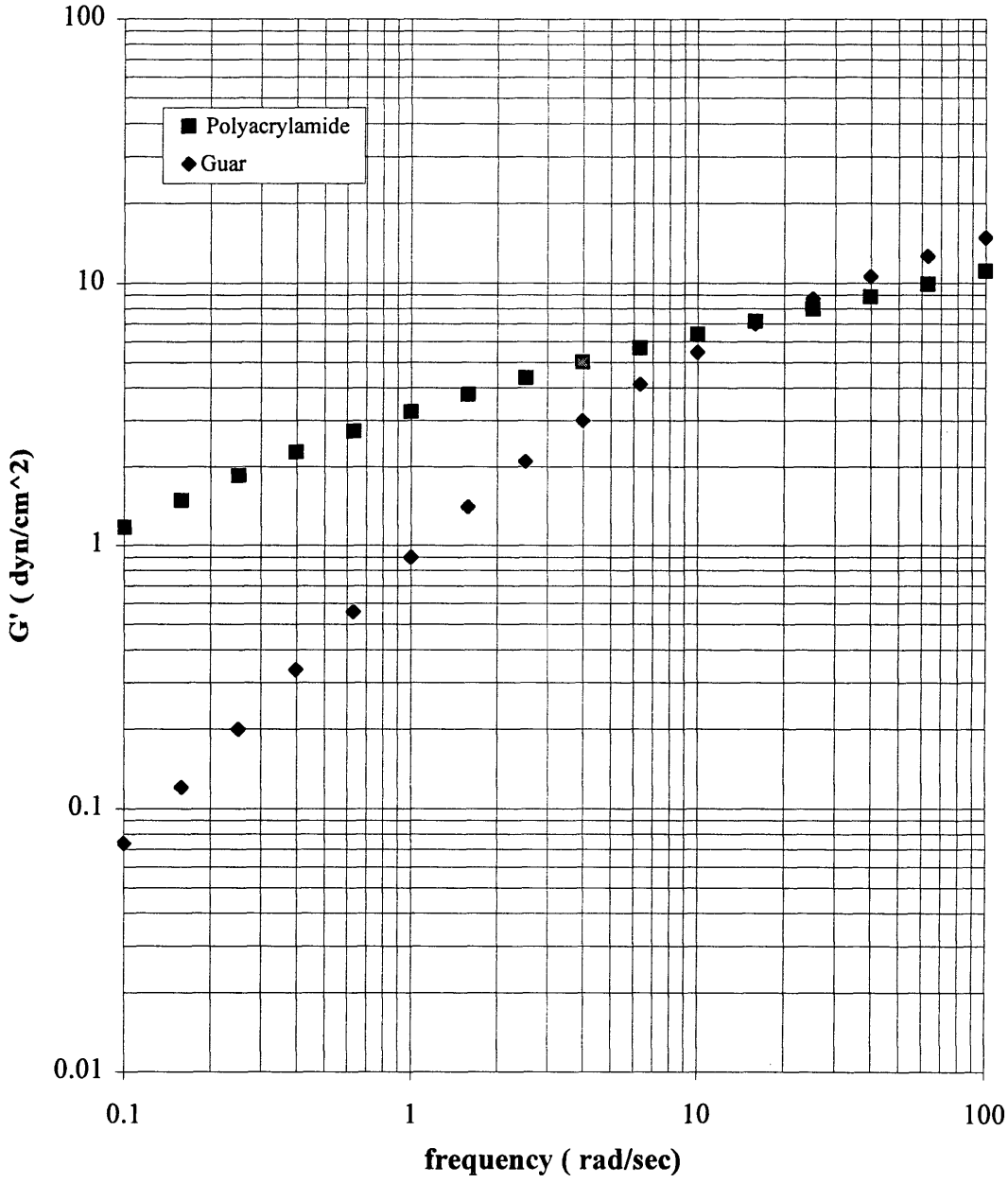

Fig 5.13: Rheological Properties for Polymer Solutions (60 lb/Mgal)

It is evident from figure 5.13 that polyacrylamide exhibits higher G′(t) or normal stresses when shear rates increase. At 0.1 rad/sec G′(t) is 1.2 dynes.cm^2 and 0.074 dynes/cm^2 and at 100 rad/sec it reaches 14.85 and 11.1 dynes/cm^2. The two curves cross over at 15.85 rad/sec with G′(t) value of about 7 dynes/cm^2. In other words, the guar solution has to experience higher shear rates of about 16 rad/sec before it will exhibit similar storage modulus compared to polyacrylamide solution. However, once the shear rate increases, they exhibit similar and closer magnitudes.

Similarly, Figure 5.14 depicts the behavior of the G″(t), the loss modulus for the two polymer solutions. The initial values at shear rates of 0.1 rad/sec are 0.44 and 1.26 dynes/cm^2 for guar and polyacrylamide solutions, respectively.

The two curves cross over at the shear rate of 1 rad/cm^2 and reach a value of 2.32 dynes/cm^2. Thereafter, the G″(t) values for the guar solution increase substantially and reach 9.72 dynes/cm^2, while polyacrylamide exhibits 4.91 dynes/cm^2, respectively.

It is evident from Figure 5.11 through Figure 5.14 that polyacrylamide solutions exhibit more viscoelastic property compared to guar solutions for the range of the shear rates encountered during the flow experiments. Thus normal stresses are more significant and play a more dominant role for polyacrylamide slurries compared to the guar slurries. However, guar solutions exhibit higher G″(t) values which in some way represent higher viscosity at higher shear rates especially for the shear rate range of the flow experiments.

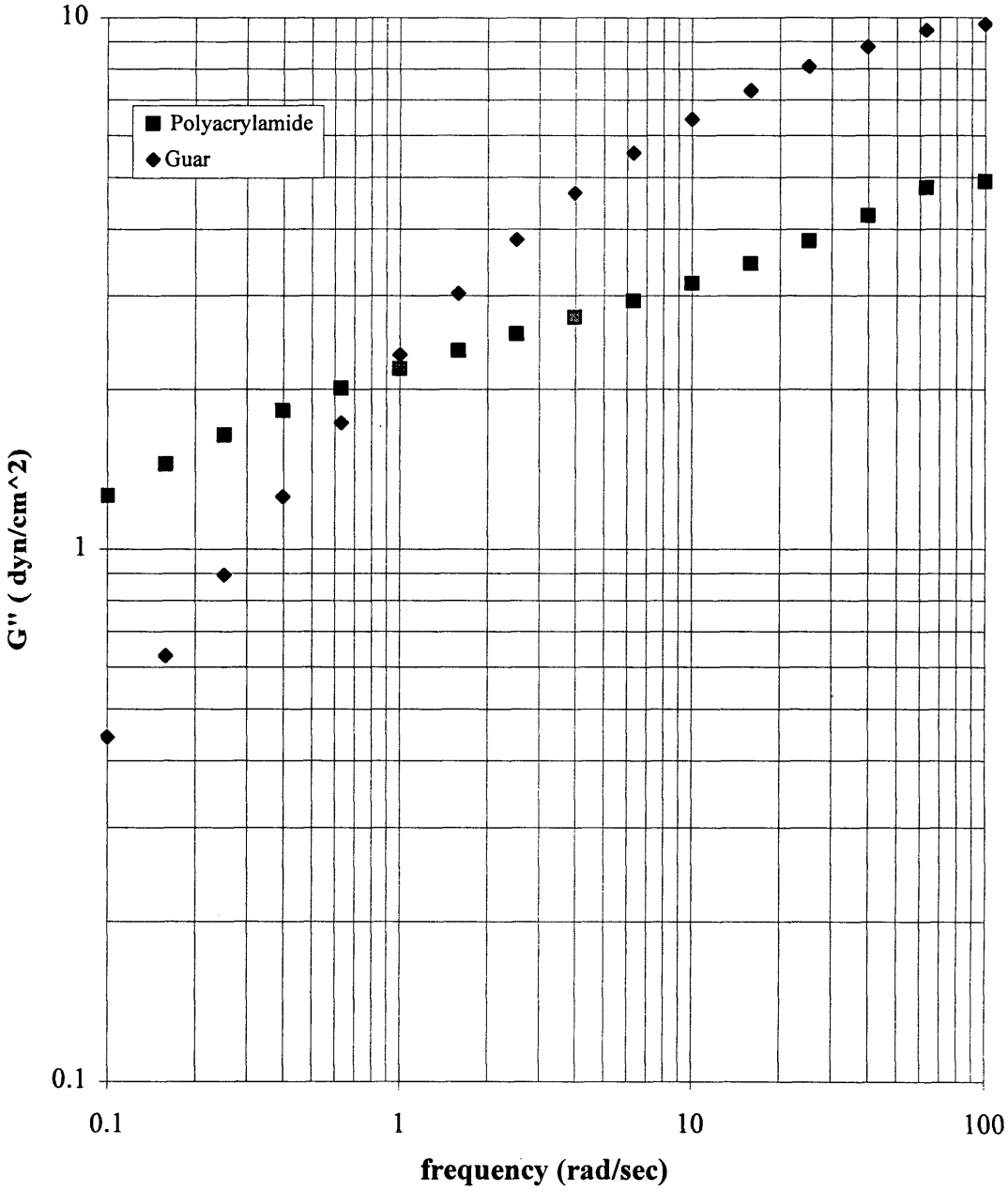

Fig 5.14: Rheological Properties for Polymer Solutions (60 lb/Mgal)

Similar data was collected for the remaining solutions. The data is provided in Appendix B. Upon completion of the fluid characterization, the rheological data were used to analyze the results of the flow experiments. The analysis of the results are discussed in Chapter 6.

Chapter 6. Analysis of the Results of the Flow Experiments

In this chapter the results of the flow experiments are explained in light of the results obtained from polymer rheological characterization experiments discussed in Chapter 5. For the purpose of the analysis the Weissenberg number and Reynolds number of the flow experiments are used

This chapter is organized by discussing the factors which affect sand node formation at the leakoff site. Next, the use of the dimensionless groups to quantitatively characterize the sand node build-up is discussed. Finally, an explanation for the mechanism of the sand node formation is included.

6.1 Factors Affecting Sand Node Formation

Sand node formation at the leakoff site was the main feature observed during some of the flow experiments. Three factors that influence node formation identified during flow experiments are slurry velocity, slurry rheology, and proppant concentration. The effects of these factors will be discussed in the following sections.

6.1.1 Slurry Velocity Effects

Slurry velocity affects node formation in two ways. First at high flow rates, the inertia prevents proppant accumulation at the leakoff site such that a portion of the

injected slurry flows down stream and the remaining portion exits through the leakoff site. At high velocities node formation is inhibited. Second, the low velocities create an opportunity for the particles to interact and accumulate at the leakoff site which leads to node formation.

During the flow experiments, it was observed that there was a "critical" velocity at or below which a sand node may form depending on the slurry rheological properties. For example, during a series of flow experiments conducted in a plexiglass model with a round leakoff, when the velocity of 80 lb/Mgal guar slurry decreased from 0.75 ft/sec to 0.25 ft/sec a sand node formed. Further reduction of the velocity for a series of successive runs resulted in similar behavior and results. The velocity of 0.25 ft/sec is referred to as the critical velocity for this particular slurry system. Similar experiments were conducted for 60 lb/Mgal guar slurries for which sand node formed at the critical velocity of 0.37 ft/sec. After completion of these experiments, it was concluded that the slurry velocity was an important factor for sand node formation.

6.1.2 Rheology Effects

The effects of fluid rheology on node development may be explained by the viscoelastic property of the flowing slurry. Polymer solutions, such as polyacrylamide, exhibit high viscoelastic properties (rod climbing behavior), while guar solutions show low viscoelasticity for a given shear rate (~ shear rate range of 5 1/sec to 50 1/sec).

Viscoelastic behavior of the polymer solutions are highly influenced by the applied shear rates. During a slurry flow, shear rate invokes the normal forces and consequently influences sand node formation. This effect can be characterized by Weissenberg number and Reynolds number which capture the fluid properties and flow conditions. As a result, the experimental observations are correlated quantitatively and analysis of these results help explain the node formation phenomenon for the flow experiments.

The following section is organized by discussing the effects of the fluid viscoelastic properties and shear rate on the outcome of the flow experiments, followed by the analysis of the Weissenberg and Reynolds data computed for the flow experiments.

6.1.3 Fluid Viscoelasticity and Shear Rate Effects

Initially, flow experiments were conducted using guar and polyacrylamide slurries with identical polymer concentrations and solid particle loading. The two types of polymer solutions represented the low and high spectrum on the viscoelastic properties. These experiments were conducted in plexiglass models with round leakoff sites with a diameter of 1/16 inch. Figure 6.1 is a plot of slurry leakoff rates as a function of the slurry velocity. Guar slurries of 60 and 80 lb/Mgal formed nodes at velocities of 0.33 and 0.25 ft/sec, respectively. However, experiments with 60 lb/Mgal and 80 lb/Mgal

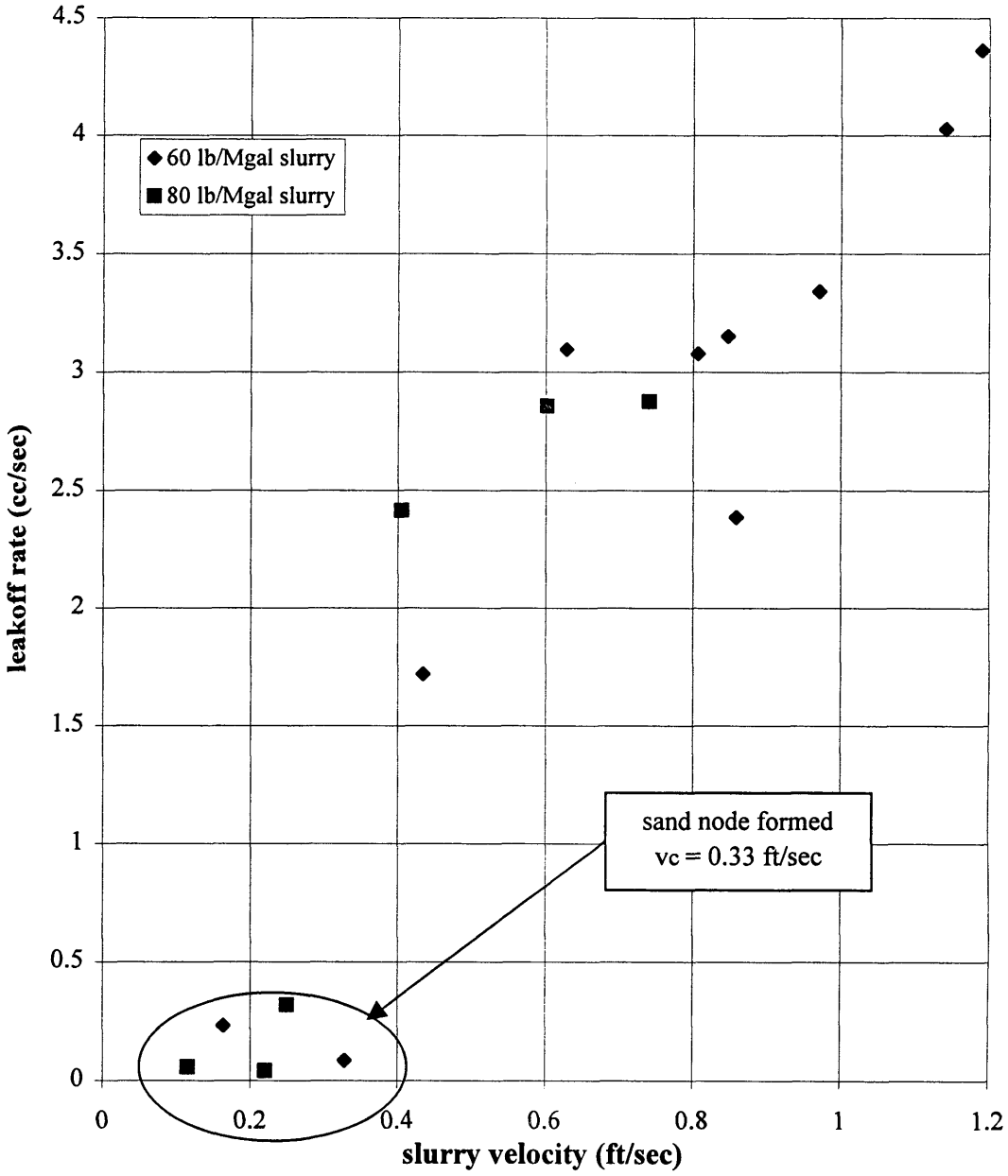

Fig 6.1: Slurry Leakoff Rates For Guar Slurries

polyacrylamide slurries did not develop sand node within the similar range of velocities (Figure 6.2). This was a clear indication that fluid rheology had a direct effect on the slurry leakoff from the leakoff site. Similar experiments were conducted in plexiglass models with slot geometry of 0.05 inch width and 1.0 inch height. For the 60 and 80 lb/Mgal guar experiments, sand node formed at velocities of 0.33 and 0.25 ft/sec, respectively. However, for the 60 and 80 lb/Mgal polyacrylamide slurries, sand nodes did not form.

Rheology effect was further investigated by conducting flow experiments using 40 lb/Mgal and 20 lb/Mgal polyacrylamide slurry. As depicted in Figure 6.3, fluid leakoff greatly decreased for velocities of 0.19 ft/sec and 0.08 ft/sec for 20 lb/Mgal and 40 lb/Mgal, respectively. This behavior was contrary to previous observations in which viscoelastic slurries did not exhibit a sand node formation characteristic; however, because of the reduction in polymer loading slurry viscoelasticity was reduced, thus resulting in sand node formation and slurry leakoff control.

The results of the flow experiments conducted for guar and polyacrylamide slurries indicated that slurry was a significant factor and its magnitude determined the outcome of the flow experiment. Higher viscoelasticity prevented node formation. Once its magnitude was lowered, then it was not a significant factor and a sand node formed. Qualitatively, the viscoelasticity of the polymer solutions is altered by the applied shear rates and additive concentration. An increase of the shear rate increases the normal

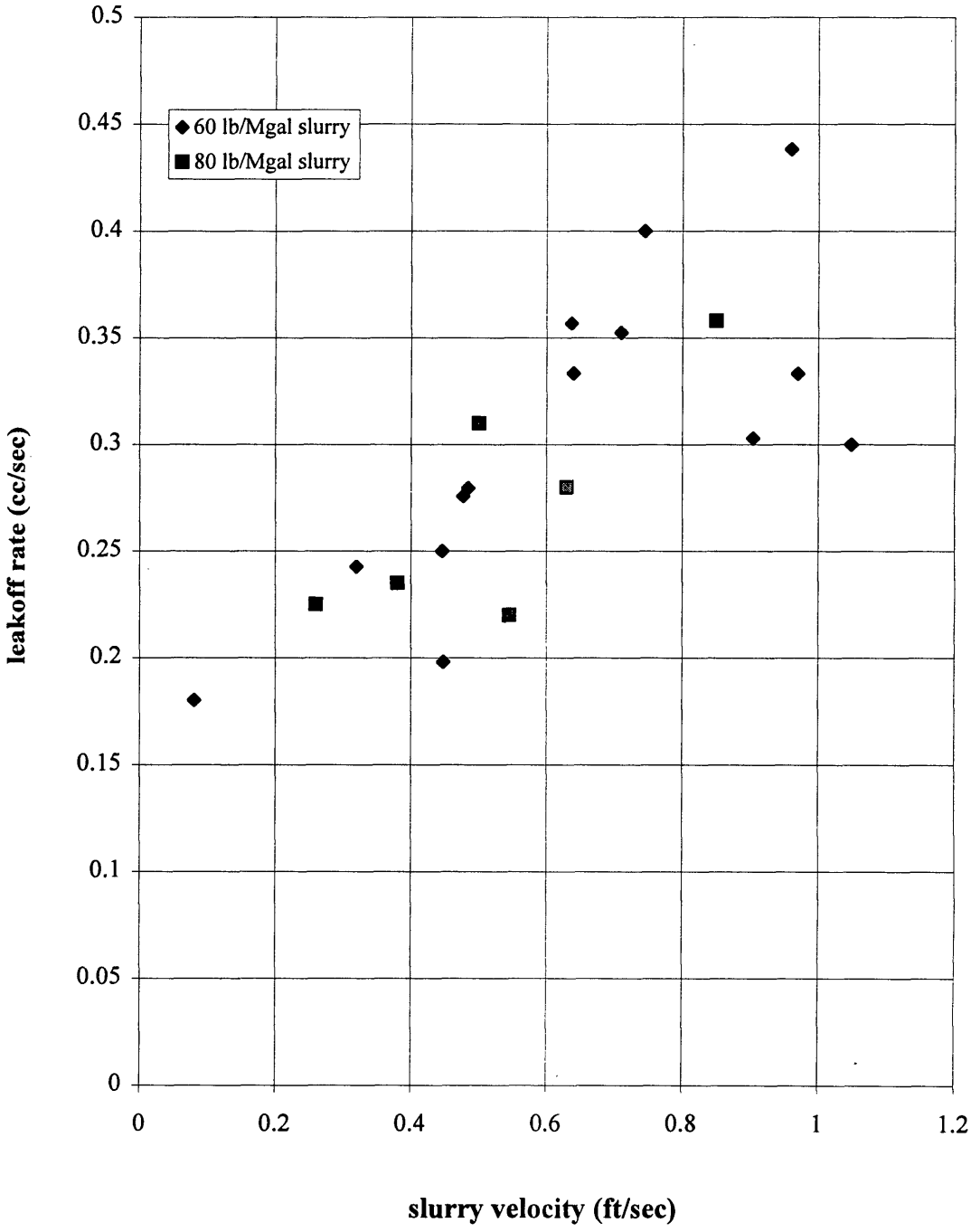

Fig 6.2: Slurry Leakoff Rates For PHPA Slurries
No sand node formed

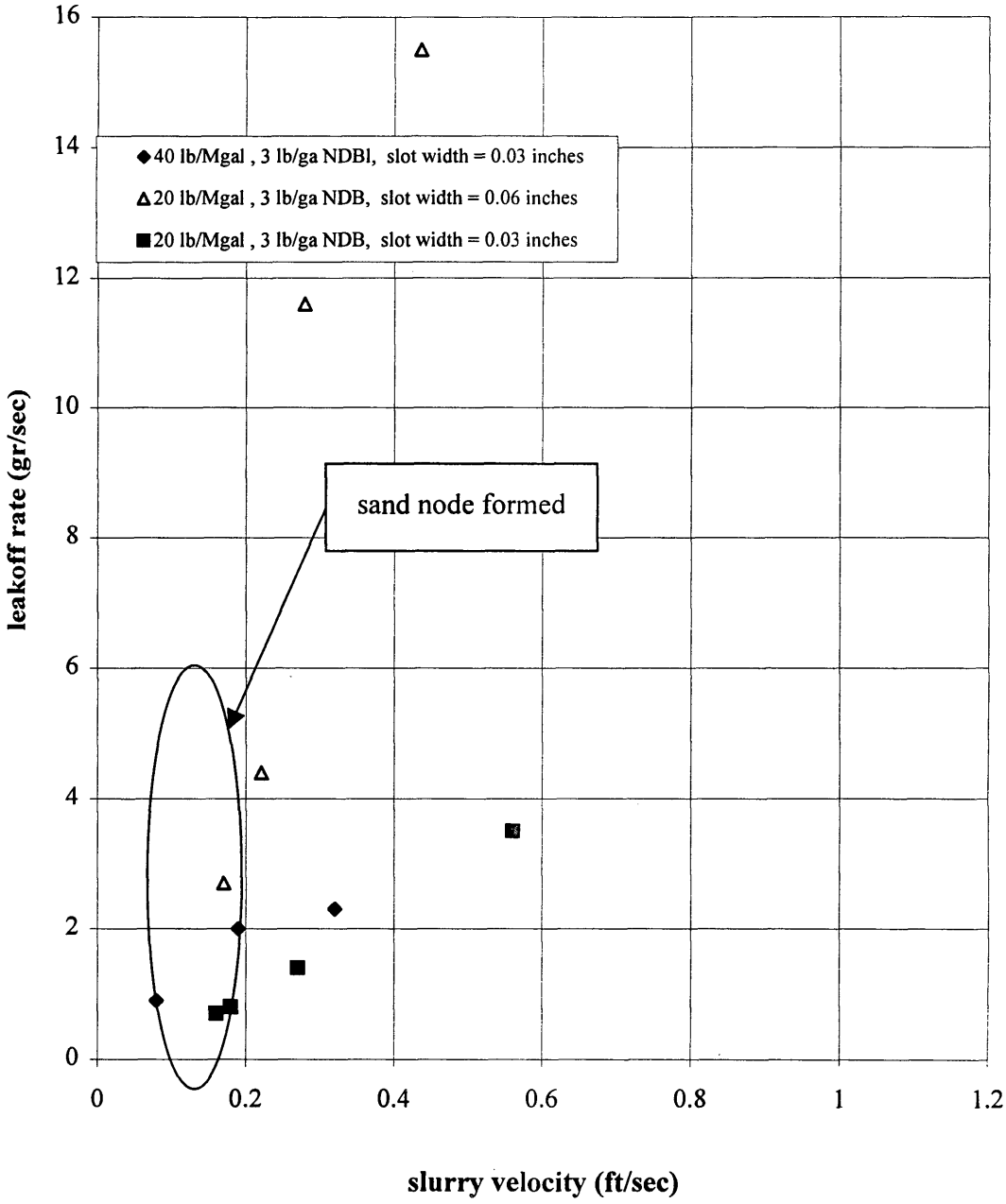

Fig 6.3: Slurry Leakoff Rate For PHPA Slurries

forces, thus enabling the fluid to exhibit higher viscoelasticity and vice versa. Similarly, the addition of the particles reduces the viscoelastic nature of the slurry. The higher the additive concentration, the lower the viscoelasticity of the slurry becomes. The limiting factor will be the particle settling in slurry which would be detrimental for particle suspension and a homogeneous slurry flow.

It is noteworthy that the effects of shear rate and rheology are intertwined. The slurry velocity in the plexiglass model in a way represents the shear rate during the flow experiments. Therefore, it is reasonable to state that velocity affects the viscoelastic properties of the slurry and as a result the velocity and the rheology have a combined effect on the node formation.

Velocity/shear effect on the viscoelastic behavior of a slurry system can be quantified by the magnitude of the normal stresses generated during the flow. The normal stresses are proportional to the square of the shear rate. Slurry velocity also represents fluid flow conditions which ties the effect of convective forces to shear forces; in other words, velocity/shear rate relates and influences slurry viscosity.

6.1.4 Dimensionless Groups (Weissenberg Number and Reynolds Number)

Both the shear stress and normal stresses exist during slurry flow. However, normal stresses become more significant for a viscoelastic solution (i.e. polyacrylamide) compared to a less viscoelastic solution (i.e. guar solution). The relative magnitude of normal stress over shear stress is quantified by Weissenberg number for a given shear rate. Figures 6.4 and 6.5 are plots of the Weissenberg number for guar and polyacrylamide solutions.

Figure 6.4 is a log-log plot of Weissenberg number as a function of frequency for 60 and 80 lb/Mgal guar solutions. When the frequecy increases the normal stresses increase and thus the Weissenberg number increases. It is evident that the increase in polymer concentration increases the Weissenberg number also. At lower frequencies, the solutions will exhibit less significant normal stresses, and this effect is more apparent when the polymer concentration is lower.

Figure 6.5 is a similar plot for polyacrylamide solutions of 20, 40, 60, and 80 lb/Mgal. At low frequencies, the difference in Weissenberg number between the solutions is minor; however, once the frequency increases, the difference in the magnitude of the Weissenberg number increases. The higher the polymer concentration, the higher the magnitude of the normal stresses and the calculated Weissenberg numbers. By comparison it is evident from the Figures 6.4 and 6.5 that Weissenberg number is noticeably larger for polyacrylamide solutions than the guar solutions. The Weissenberg

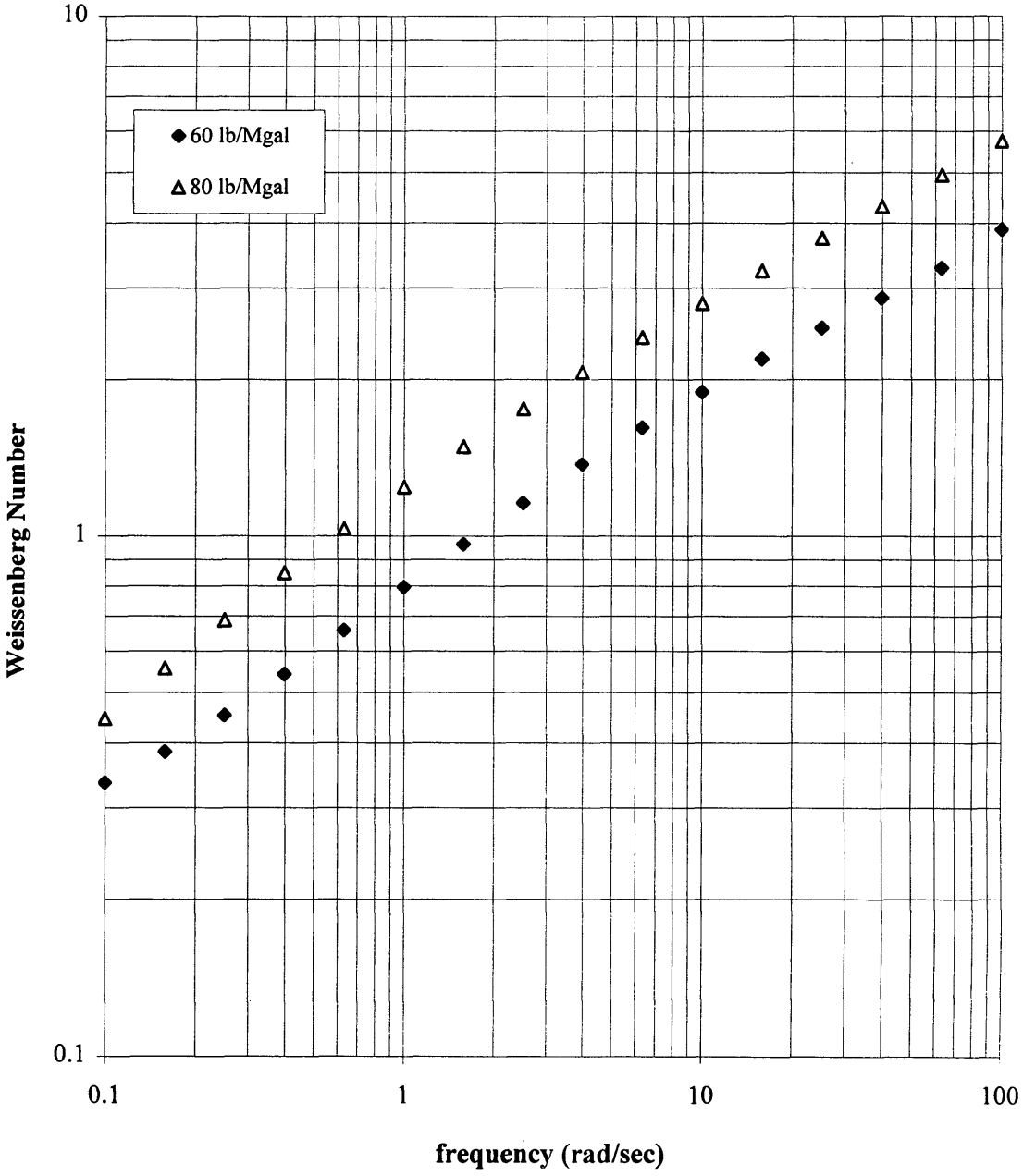

Fig 6.4: Weissenberg Number as a Function of Frequency (Guar Solutions)

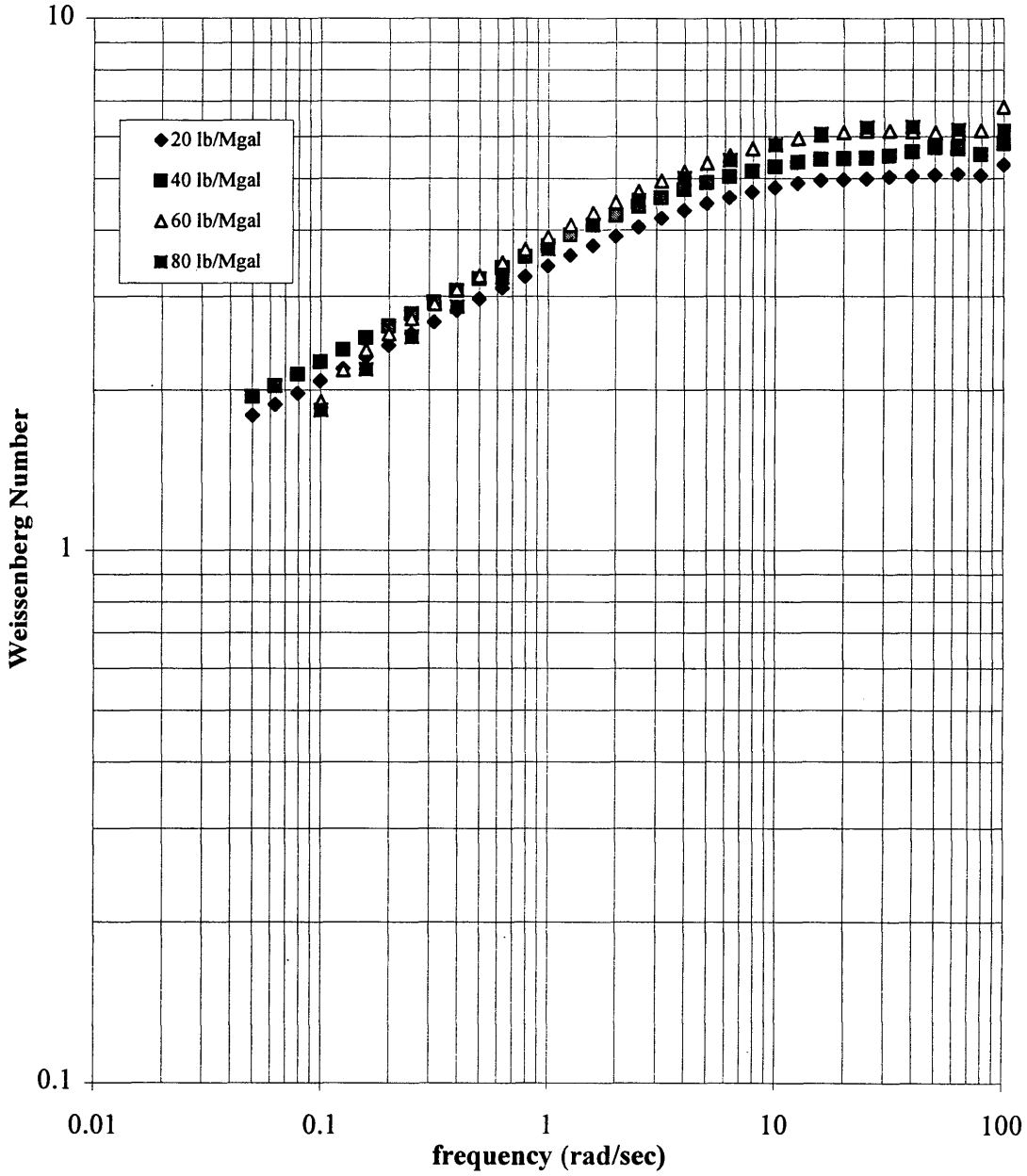

Fig 6.5: Weissenberg Number as a Function of Frequency (Polyacrylamide Solutions)

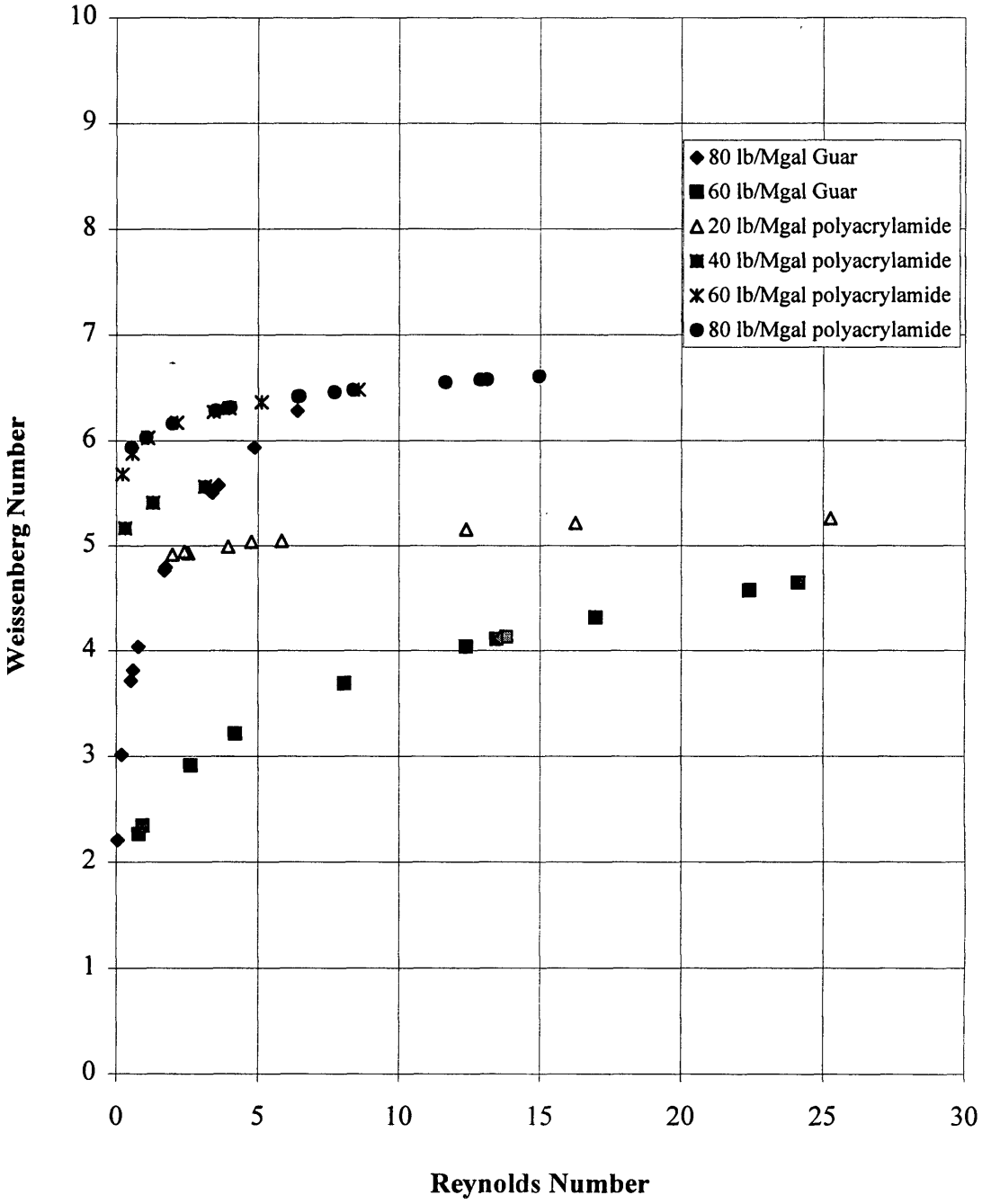

Fig 6.6: Slurry Flow Characterization in the Plexiglass Model

number for 60 lb/Mgal guar and 60 lb/Mgal polyacrylamide at frequency of 1 rad/sec is 0.8 and 3.88, respectively which is a factor of about five.

By regression, Weissenberg numbers were estimated for the polymer solutions for the flow experiments of 60 lb/Mgal and 80 lb/Mgal guar slurries. The experimental observations indicate that sand node formed for guar slurries at Weissenberg numbers below four and for polyacrylamide solutions for less than six. Further discussion concerning the influence of the normal stresses will be presented later.

Reynolds number for each experiment was calculated using equation 6.1. the average slurry velocity, slurry density, hydraulic diameter, and the respective slurry viscosity at the given shear rate.

$$Re = V * \rho * D / \mu$$

Where, Re = Reynolds number
V = average slurry velocity (cm/sec)
ρ = slurry density (gr/cc)
D = hydraulic diameter (cm)
μ = slurry viscosity (poise)

Figure 6.6 depicts Weissenberg number as a function of the slurry Reynolds number for the entire slurry systems used for the flow experiments. This plot links the slurry flow in the plexiglass model to the slurry rheology during the flow. Reynolds number reflects the impact of the external factors while the Weissenberg number indicates the internal effects. There are two distinct behaviors for this plot. For 60 lb/Mgal and 80 lb/Mgal polyacrylamide solutions, the Weissenberg numbers are above

6.0 and stay as such even when the flow rate or the Reynolds number decreases. However, for the 40 lb/Mgal and 20 lb/Mgal polyacrylamide solutions, the Weissenberg number decreases as the Reynolds number also declines.

For polyacrylamide slurries, a sand node formed for Weissenberg numbers less than six. The data indicates that once the velocity reached 0.08 ft/sec for the 40 lb/Mgal PHPA slurry, a sand node formed. A follow up experiment conducted using the 20 lb/Mgal PHPA showed that reduction of the velocity to about 0.19 ft/sec would lead to sand node formation. Furthermore, for guar slurries, when the 60 lb/Mgal slurry reached a velocity of 0.33 ft/sec a sand node formed, and for 80 lb/Mgal guar slurry a node formed at 0.25 ft/sec. The overall results indicate that a sand node would form for these slurries for Weissenberg number and Reynolds number of less than 6 and 3, respectively.

It is evident from these results that slurry viscoelasticity has to be reduced in-order for sand node to form. This is accomplished by either reducing the shear rates or by reducing the polymer concentration or both. This is the reason that a sand node forms for 40 and 20 lb/Mgal polyacrylamide solutions. It is noteworthy that a node formed for 40 lb/Mgal PHPA solution at lower rates (7.7 1/sec) compared to 20 lb/Mgal (20.3 1/sec). The higher polymer concentration pushes the node formation criteria towards the lower viscoelasticity of the polymer solution, which is toward lower shear rates. Therefore, lower slurry velocities are required during the slot flow.

For the 60 and 80 lb/Mgal polyacrylamide solutions, sand nodes did not form for the shear rates of as low as 20 1/sec and 10 1/sec, respectively. These shear rates kept the Weissenberg numbers at high enough values that the node would not form.

For the guar solutions, higher shear rates still accommodated sand node formation. Obviously, guar solutions have lower viscoelastic properties and conversely, in order to prevent node formation, higher shear rates are required to produce significantly high normal stresses and thus high Weissenberg numbers. There are a couple of observations for the guar experiments. First, sand node formed at Weissenberg numbers less than 4 and Reynolds numbers less than 3. The Weissenberg number is calculated for the guar solution rheological property.

The second observation is related to the shear rate at which a sand node formed for 60 lb/Mgal slurry. The shear rate of 37.8 1/sec is higher than the shear rate of 30.1 1/sec for 80 lb/Mgal slurry. This is consistent with the discussion of the effect of the polymer concentration and the resulting normal stresses. The higher the polymer loading, the higher the Weissenberg number and the less chance to form a node for a given shear rate. In other words, the 80 lb/Mgal solution will require lower shear rates in order to form a node. This is evident data for guar and polyacrylamide flow experiments.

Two points should be discussed here. First is the fact that the computed Weissenberg numbers are based on the polymer solutions only. Though the experiments are two-phase flow, only polymer solution Weissenberg numbers are estimated and used.

However, the Reynolds numbers are computed for the slurry flow. This is done using GEFFAR, which enables one to estimate the effect of the particle additions to the viscosity estimations. The second point is related to how additives influence either the Weissenberg number or Reynolds number calculations.

It should be pointed out that the addition of any type of particles, such as sand, reduces the viscoelasticity of the solution. The addition of the sand to the polymer solution will reduce the magnitude of the Weissenberg number for the slurry. Moreover, the density of the additive will inherently affect this value. For example, addition of sand and/or neutral density beads to the same polymer solution will result in different normal stresses exhibited by the slurry and thus a different Weissenberg number. The denser additive will result in a lower Weissenberg number. For the 40 lb/Mgal polyacrylamide slurry which had neutral density beads as its additive, a Weissenberg number of about five was calculated. However, in reality this figure is less than five had we had a way to incorporate the effect of neutral density beads to the polymer solution. This number would be even less if an equivalent concentration of sand to the solution was accounted for. Therefore, it would take higher shear rates before the magnitude of the normal stresses would be significant to prevent formation of sand node for a slurry system

An examination of the G'(t) and G''(t) data for the polymer solutions and the frequency at which the two curves cross each other, referred to as the cross-over point, may shed some light on the node formation phenomena and thus help design successful

slurry treatments. Table III summarizes the cross over frequency and the corresponding shear rate and the relevant critical velocity/shear rate for which a sand node has formed.

Table III: Flow and Rheological Characteristics for Polymer Solutions

Polymer Type	**Concentration** lb/Mgal	$\gamma')_{x\text{-}over}$ rad/sec	$\gamma')_{Node\ Formation}$ 1/sec
PHPA	20	0.20	20.3
PHPA	40	0.11	7.7
PHPA	60	0.17	N.A
PHPA	80	0.16	N.A
Guar	60	6.31	37.8
Guar	80	15.85	30.1

The comparison of the cross-over frequency with node formation shear rate indicates that node forms at shear rates higher than the cross-over shear rates. However, there are two sources of inaccuracy for the estimation of the node formation shear rate. One is related to the calculation of the flow velocity which is based on the pressure drop in the air tank acting as the source of the energy for the flow experiments. The pressure drop due to air expansion in the cylinder has been accounted for while other pressure drops in the flow system were ignored.

The collected pressure data are used to compute an average flow velocity. However, it is important to realize that node formation does not occur due to an average velocity, rather , a unique velocity at or below which node formation takes place. Thus, a

single velocity or shear rate has to be determined. However, in the experimental set-up it was not possible to determine a single flow rate at which a node would form. For example the 40 lb/Mgal PHPA slurry for which sand node formed at an average velocity of 0.08 ft/sec does not accurately reflect the velocity or the shear rate at which the node formed. The node formed at the later stages of the slurry flow, which would reflect a much lower flow velocity and shear rate for the node formation. The actual velocity would reduce the corresponding Weissenberg number.

The second source of inaccuracy is due to neglecting the effect of particle addition to the polymer solution, which inherently affects the slurry rheology and estimation of the slurry cross-over frequency. In reality, the shear rate corresponding to a node forming is in the proximity of the slurry cross-over frequency than the polymer solution cross-over shear. However, the inability to compute the effect of particle addition to the polymer solution and its subsequent effect on normal forces and the Weissenberg number estimation creates an uncertainty which can not be assessed at present.

Qualitatively incorporating the effect of the above mentioned sources of error will collectively give a lower estimate of the Weissenberg number. This can be interpreted that a sand node forms when the normal forces become less significant during the flow conditions leading toward higher critical velocities.

In conclusion, a sand node forms at shear rates which are greater than the G' and G'' cross-over frequency of the polymer solution. For a given slurry system, increase of

polymer loading lowers the magnitude of the critical velocity and vice versa. For guar slurry systems, sand node formed for Weissenberg and Reynolds number less than four and three, respectively. For the polyactylamide slurries, the upper limits for Weissenberg and Reynolds numbers were six and three respectively.

6.1.5 Proppant Concentration Effects

Proppant concentration is an essential element for node formation. Solid particles are necessary to build an impermeable wall to block the leakoff site under favorable flow conditions.

There is direct correlation between the size and the concentration of the particles and the area of the leakoff site. Experiments indicated that a minimum proppant (20-40 mesh) concentration of 3 lb/gal was needed to effectively inhibit fluid leakoff from the leakoff sites with widths of 0.03 inches up to 0.06 inches. However, a factor which has not been taken into consideration is the timing of the blocking. In other words, it would take a longer time for the 0.06 inch opening to be blocked compared to a 0.03 inch opening. This aspect is not covered in any of the results and analysis due to lack of instantaneous leakoff data. Average leakoff data are computed and used for all experiments. Based on observations from the flow experiments it is concluded that the overriding factors for the node formation are the slurry rheology, slurry velocity in the induced fracture, and the additive concentration.

6.2 Mechanism of the Sand Node Formation

As discussed in previous sections, sand node formation at the leakoff site during flow experiments is influenced by the slurry rheology, the shear rate (slurry velocity), gap width, and solid additive particle size and its concentration. Node formation takes place depending on the magnitude of the normal stresses prevalent during the flow.

The position of the particles in the plexiglass model during the flow is affected by the normal stresses. Normal stresses (first normal stress and second normal stress) act perpendicular to the plane of shear, displacing the particles toward the center of the model , and thus creating "sheet flow". This effect is observed for viscoelastic fluids such as polyacrylamide. However, for guar slurries this effect is not significant especially at low shear rates where the particles tend to migrate toward the walls.

The observations from the flow experiments show that the node formation is initiated when slurry velocity falls below a "critical velocity". This velocity is in the range of 0.08 to 0.33 ft/sec (7.7 1/sec to 37.8 1/sec) depending on the slurry rheology and the model specifications. The node formation is initiated when the particles migrate toward the high shear region (toward the walls) and accumulate at the entrance of the leakoff site. While this process continues, sand node grows from the walls adjacent to the natural fracture toward the center of the gap. This process is also accompanied by some compaction as well. Once the node build-up is complete, slurry leakoff reduces considerably and slurry flows downstream.

At high solid concentrations of 5 lb/Mgal in round leakoff sites, a sand node grows radial and across the induced fracture causing bridging. However, for the rectangle shape leakoff site bridging did not occur. The area to flow for the round leakoff site of diameter 1/16 inch is 0.003 square inches whereas the area to flow for the slot width of 0.03 inches (height of 1 inch) is 0.03 square inches. The ratio of the areas is a factor of 10. There might also be a scaling effect on the rate of node build up; however, this aspect was out of the scope of this research and was not investigated.

Sand node formation or lack of it appears to be due to the pattern of particle migration across the leakoff site. Reduction of the shear rate reduces the magnitude of the normal stresses, which in turn enhances the particle migration toward the walls.

For guar slurries, particles migrate toward the high shear gradient region (toward the walls). In the vicinity of the wall, particles experience extremely low velocities and tend to accumulate and finally block the gap width. However, for the viscoelastic slurries, particles migrate to the low shear gradient region (to the center of the model) due to the normal stresses. Velocities are higher in the center compared to the wall region where particles do not have the opportunity to accumulate and form a node. Thus they exit the slot and a sand node does not form for slurries with high viscoelastic properties.

Chapter 7. Computer Simulation

This chapter discusses computer simulation runs generated for hydraulic fracturing of a published field data using the slurry properties in the laboratory experiments. The intent is to identify the fracture and slurry behavior during a fracturing process and compare our laboratory observation to a computer simulation. This approach is a preliminary step and aid for successful planning and design of a typical hydraulic fracture treatment incorporating the need to prevent screen-out by selecting proper slurry injection rate.

This chapter consists of three sections. Section one briefly discusses the spreadsheet developed to generate the PKN (Perkins-Kern-Nordgren) model predictions of fracture dimensions for a given set of rock and slurry data. Next, the simulation results for the 80 lb/Mgal guar and 20 lb/Mgal polyacrylamide slurries are discussed, followed by a discussion of the simulation results and the notes concerning the field applications.

7.1 Spreadsheet Set Up

A spreadsheet was developed using Excel to generate the computer simulations for this work. Rock and treatment data are taken from Chapter 4 (page 92) of The Hydraulic Fracturing Monograph[33]. The slurry data from this research are used for the prediction of the fracture dimensions. Generalized Equation For Fracturing Fluid Actual

Rheology (GEFFAR) formulation is used to compute slurry viscosity. The spreadsheet is set up to calculate fracture length, fracture width, average slurry velocity in the fracture, shear rate, slurry viscosity, and pressure drop gradient.

The PKN model assumes a fixed fracture height independent of the fracture length and constant fluid pressure (p) in vertical cross sections perpendicular to the direction of the fracture propagation. It is also assumed that each vertical cross section deforms individually and is not hindered by its neighbors.

The calculations are set up to compute the fracture length first with the rock and the slurry injection data. For the width (W1) calculations, a slurry viscosity is assumed for a given time and W1 is predicted. Average velocity and shear rates are computed using the injection rate and the calculated W1. Using GEFFAR, slurry viscosity is predicted based on the calculated shear rate and the schedule of the injected slurry for each time step. With the GEFFAR-calculated viscosity, a new width (W2) is calculated. If W1 and W2 are identical then the initial viscosity estimate is correct and the computations are complete; otherwise, the viscosity value is iterated until the two width estimates are identical. For every iteration, viscosity is obtained for the corresponding shear rate using GEFFER formulation.

7.2 Simulation Results

This procedure is used to predict the fracture dimensions for 80 lb/Mgal and 60 lb/Mgal guar slurries, 20 lb/Mgal and 40 lb/Mgal polyacrylamide slurries. These slurries were selected for simulation because a sand node formed during the laboratory experimentation. The simulation results are used as a tool to predict when and where in the fracturing process a sand node would form for the slurry used.

The assumption for the simulations are those assumed in the PKN model development. For the slurries, it was assumed that there is no particle settling at high shear rates when there is shear thinning or for the high additive loading when the slurry experiences low velocities for the given injection rates. This assumption was valid for most of the experiments. Where the assumption did, a neutral density beads were used as the fluid loss additive.

Figure 7.1 is the plot of fracture length and width as a function of elapsed injection time for the 80 lb/Mgal guar slurry with the scheduled injection of pad and additive concentration range of 1 lb/gal to 5 lb/gal. For the given rock and fracture treatment data, the average fracture length and width extend to 562 feet and 0.36 inches, respectively. The corresponding slurry velocity in the induced fracture is shown in Figure 7.2. As expected, once the fracture length extends, the slurry velocity decreases, which is due to increase in pressure drop and area to flow. The figure shows that the velocity decreased from 0.25 ft/sec to about 0.07 ft/sec.

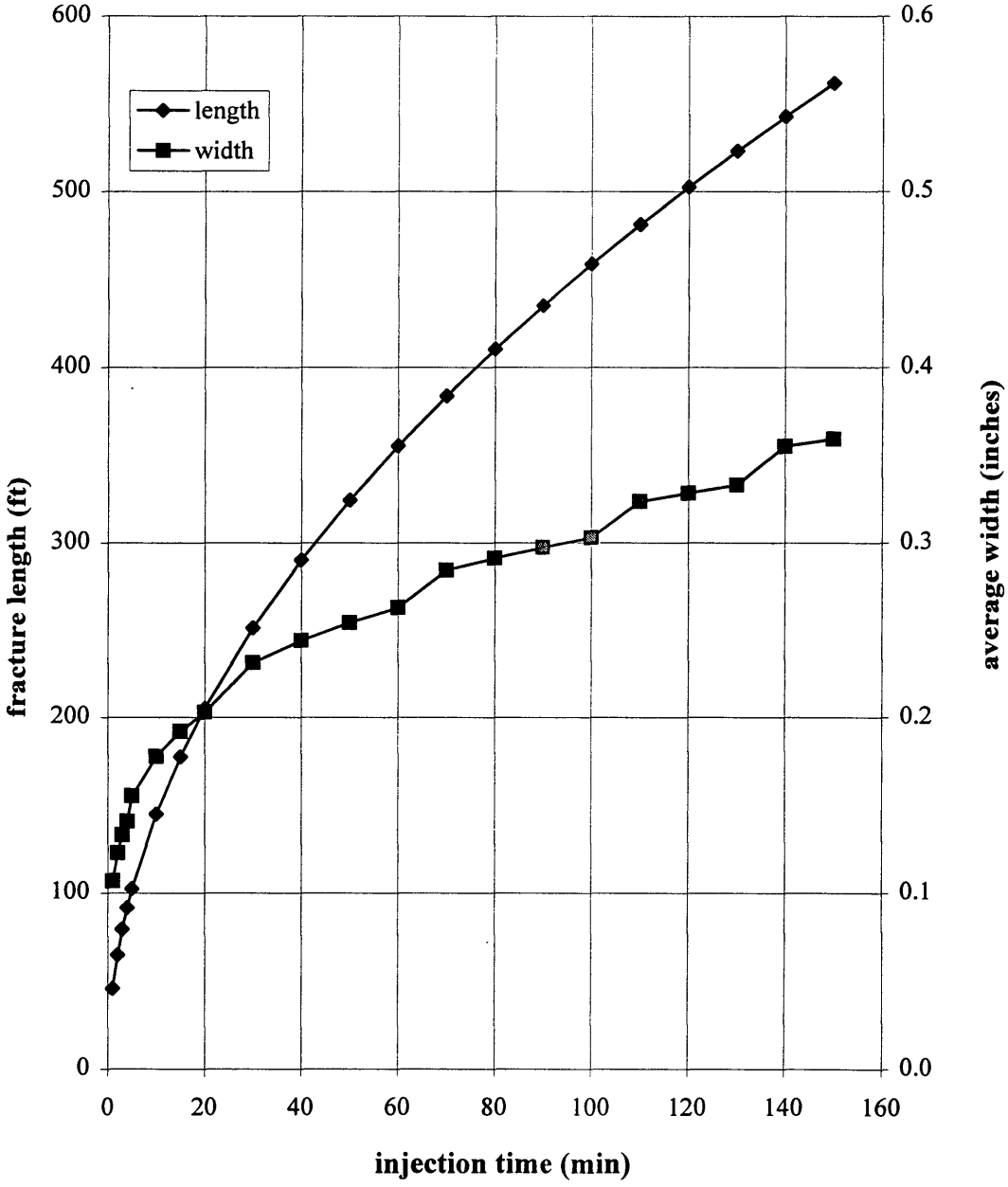

Fig 7.1: Fracture Dimension Prediction Using PKN Model (80 lb/Mgal slurry with constant fluid leakoff)

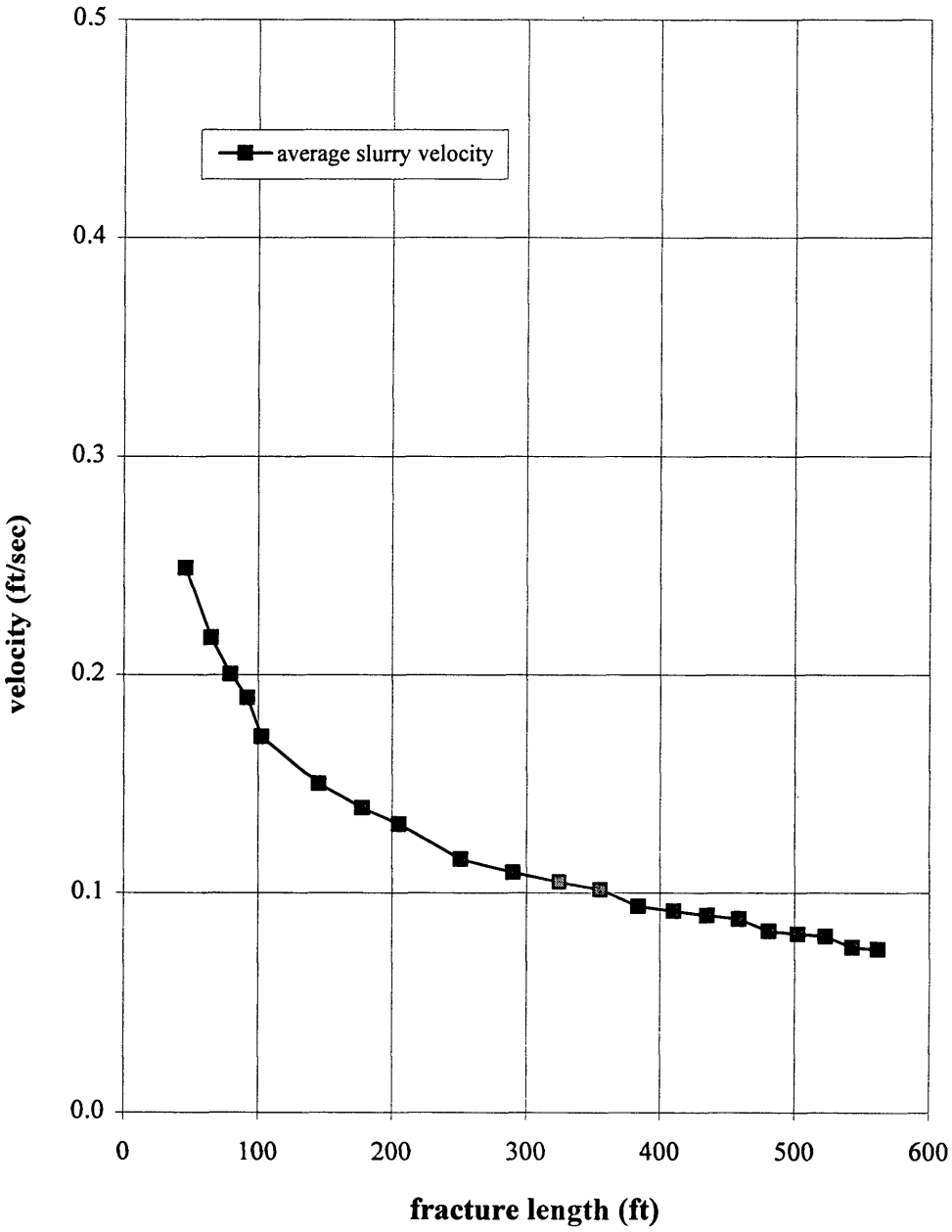

Fig 7.2: Average Slurry Velocity in the Fracture

The rock and the slurry behaviors during the fracturing process are plotted in Figure 7.3. This plot basically captures the fluid flow and the rock partitioning for the duration of the fracturing process. It is clear that the rock or the formation of the interest will widen and the induced fracture would extend while the injected slurry is continuously being loaded with more sand. During this process, slurry velocity decreases and thus the slurry viscosity increases. The significance of this plot is that it is linking the fluid and rock behaviors or the changes in them as the induced fracture extends.

Once the fluid and rock behaviors during the fracturing process are characterized, the simulated slurry flow in the induced fracture can be linked to the rheological characteristics of the injected slurry. This is similar to the approach adopted in Chapter 6 when the laboratory results were analyzed and discussed.

Figure 7.4 depicts calculated Reynolds Number and Weissenberg number for the 80 lb/Mgal slurry with various additive concentration as a function of the simulated slurry velocity in the induced fracture. This plot is a means to identify the region or the window of opportunity when a sand node would form for the given flow conditions and slurry system.

From Figure 7.4, the injected fluid velocity of 0.20 ft/sec refers to Weissenberg number of 4.0 and Reynolds number of about 1.0. At this stage the injected fluid does not have any additives therefore, sand node can not form. However, the later stages starting

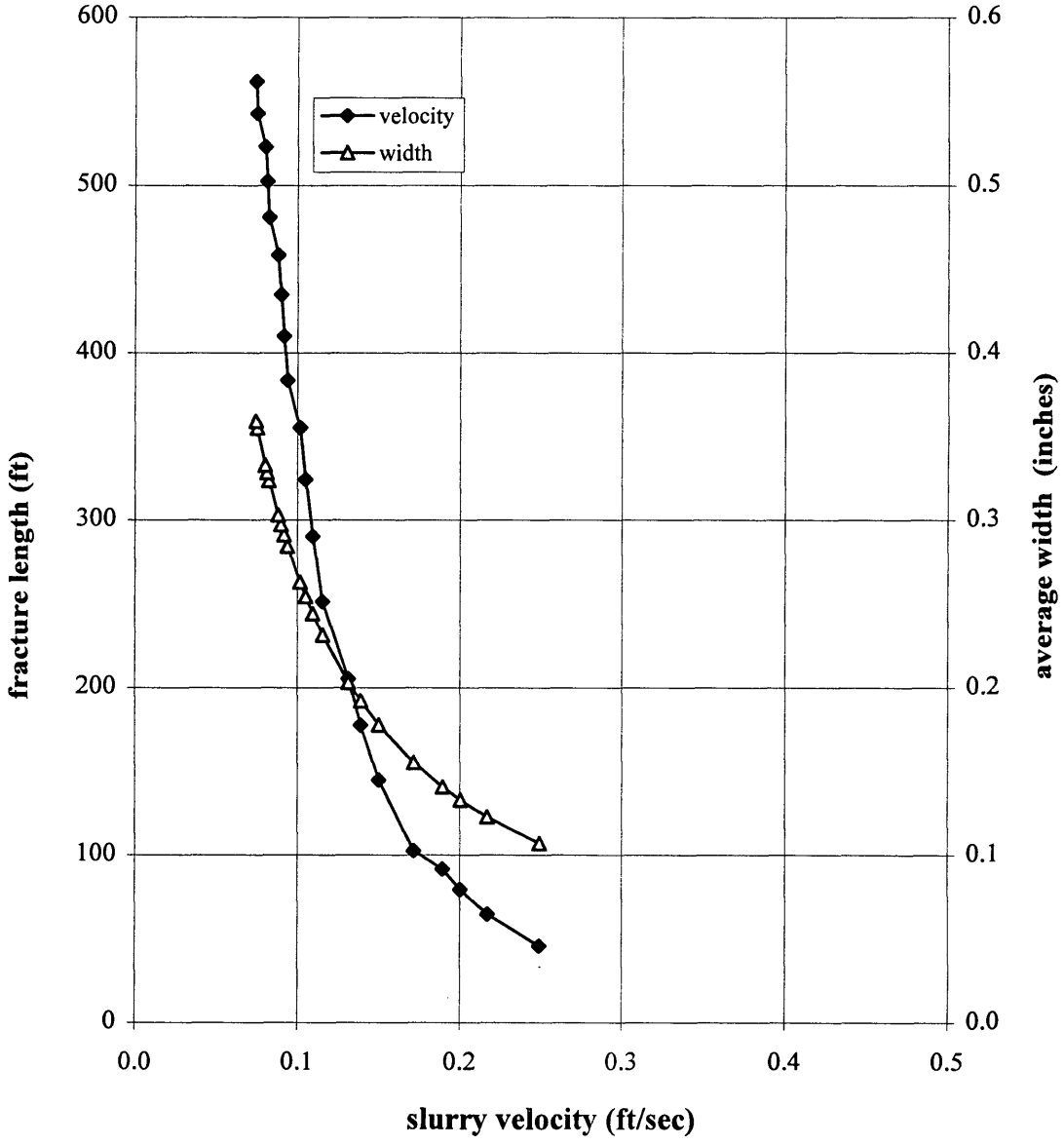

Fig 7.3: Induced Fracture and Slurry Behavior
(Schedualed injection of 80 lb/Mgal guar slurry)

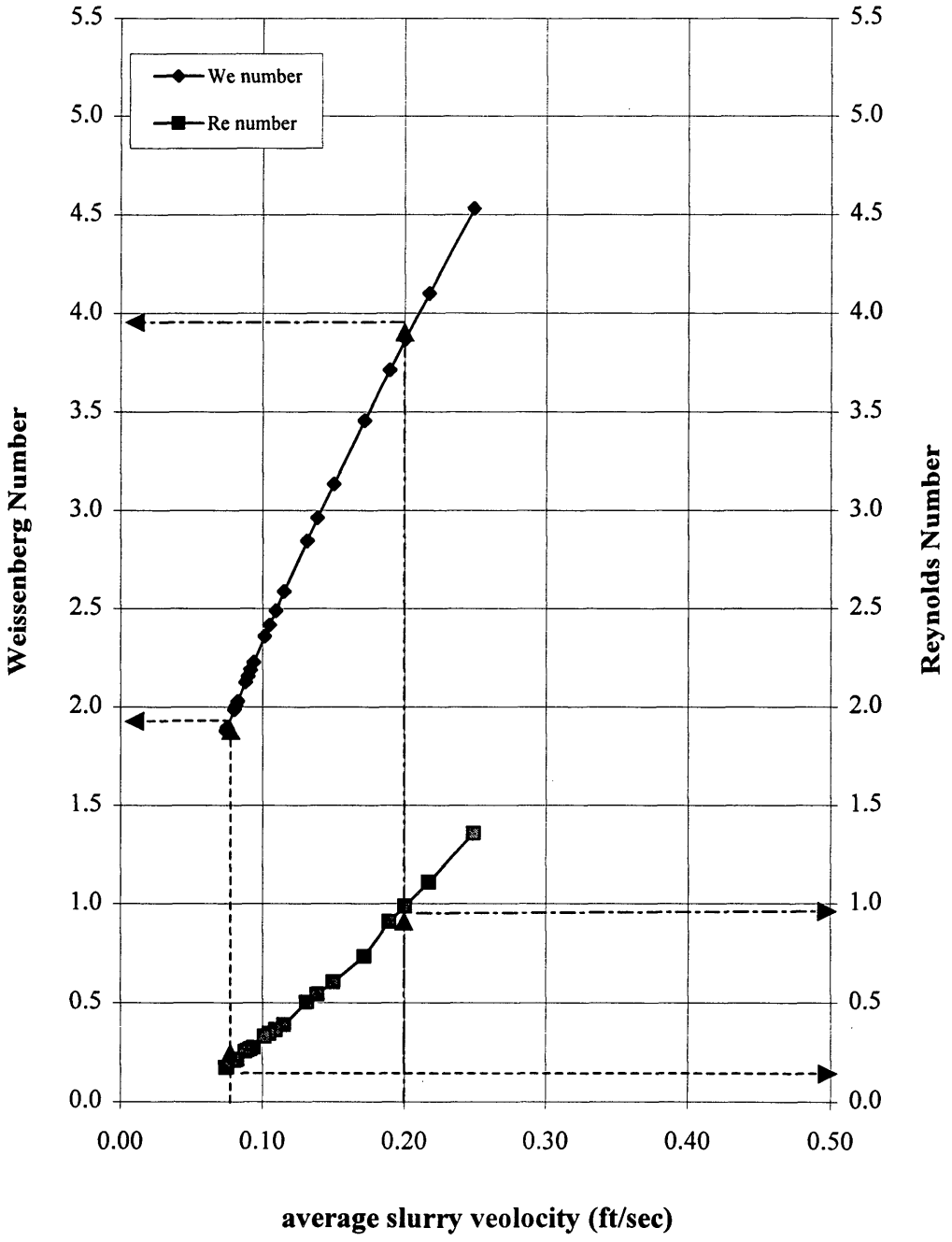

Fig 7.4: Node Formation Prediction under Field Conditions (For 80 lb/Mgal guar slurry)

with slurry velocity of 0.17 ft/sec the additive concentration is increased with 1 lb/gal increments. The injection of 2 lb/gal, 3 lb/gal, 4 lb/gal, and 5 lb/gal slurries start at 0.12, 0.10, 0.08, and 0.07 ft/sec, respectively. As explained in previous section (6.1.5 p.118), a sand concentration of 3 lb/gal is sufficient to form a sand node at the leakoff site.

On Figure 7.4, velocities less than 0.07 ft/sec indicate the flow of 80 lb/Mgal slurry mixed with 5 lb/gal sand. The corresponding Weissenberg number and Reynolds numbers are 1.9 and 0.17. Thus a sand node would form at these conditions for the natural fracture width of up to 0.06 inches

For example, during laboratory experimentation a sand node formed for an 80 lb/Mgal guar solution with 5 lb/gal 20-40 sand additive for Weissenberg and Reynolds numbers less than 4 and 0.80, respectively. This set of laboratory data refers to the average slurry velocity of about 0.25 ft/sec for slot width of 0.06 inches.

Laboratory experiments have also indicated that 3 lb/gal 20-40 mesh sand would be required to build a sand node at the leakoff site, therefore, it is reasonable to assume that for velocities corresponding to the slurry injection of 3 lb/gal which in this case is 0.10 ft/sec, sand node would form at the leakoff sites for the width range of 0.01 to 0.06 inches.

It is important to mention that the ramped slurry injection with the proppant schedule, the initial low sand concentration may not be effective in sealing natural fractures of large width while smaller widths such as 0.01 or 0.02 inch would easily be

sealed off by the 1 lb/gal or 2 lb/gal sand concentrations. It is to say that the 1 lb/gal and 2 lb/gal additive concentration will have impact for the lower range of natural fracture width, however, the 3 lb/gal concentration is effective for the whole range of the natural fracture sizes.

A comparison of Figure 7.4 and Figure 7.5 shows that the Reynolds number is higher for the 60 lb/Mgal slurry system for a similar slurry at a given velocity (i.e. 0.10 ft/sec). This is due to the lower viscosity of the 60lb/Mgal slurry system which makes the Reynolds number greater than the 80 lb/Mgal slurry. In contrast, the Weissenberg number is lower for the 60 lb/Mgal slurry which is due to lower polymer loading of the slurry. These characteristics confirm the laboratory results which show that a sand node formed at lower velocities for the 80 lb/Mgal slurry system (0.25 ft/sec) compared to the 60 lb/Mgal slurry system (0.33 ft/sec).

The results of the computer simulation will be discussed briefly for the 20/Mgal polyacrylamide slurry and will be compared to the results of the 80 lb/Mgal guar slurry. Figure 7.6 is plot of the fracture dimensions obtained for the given rock and the treatment data. The slurry scheduling is kept identical. The length and width for this treatment is 562 feet and 0.20 inches, respectively. The length is invariably the same for all the cases because the formulation only takes the injection rates and the rock data which are held constant for the simulation runs.

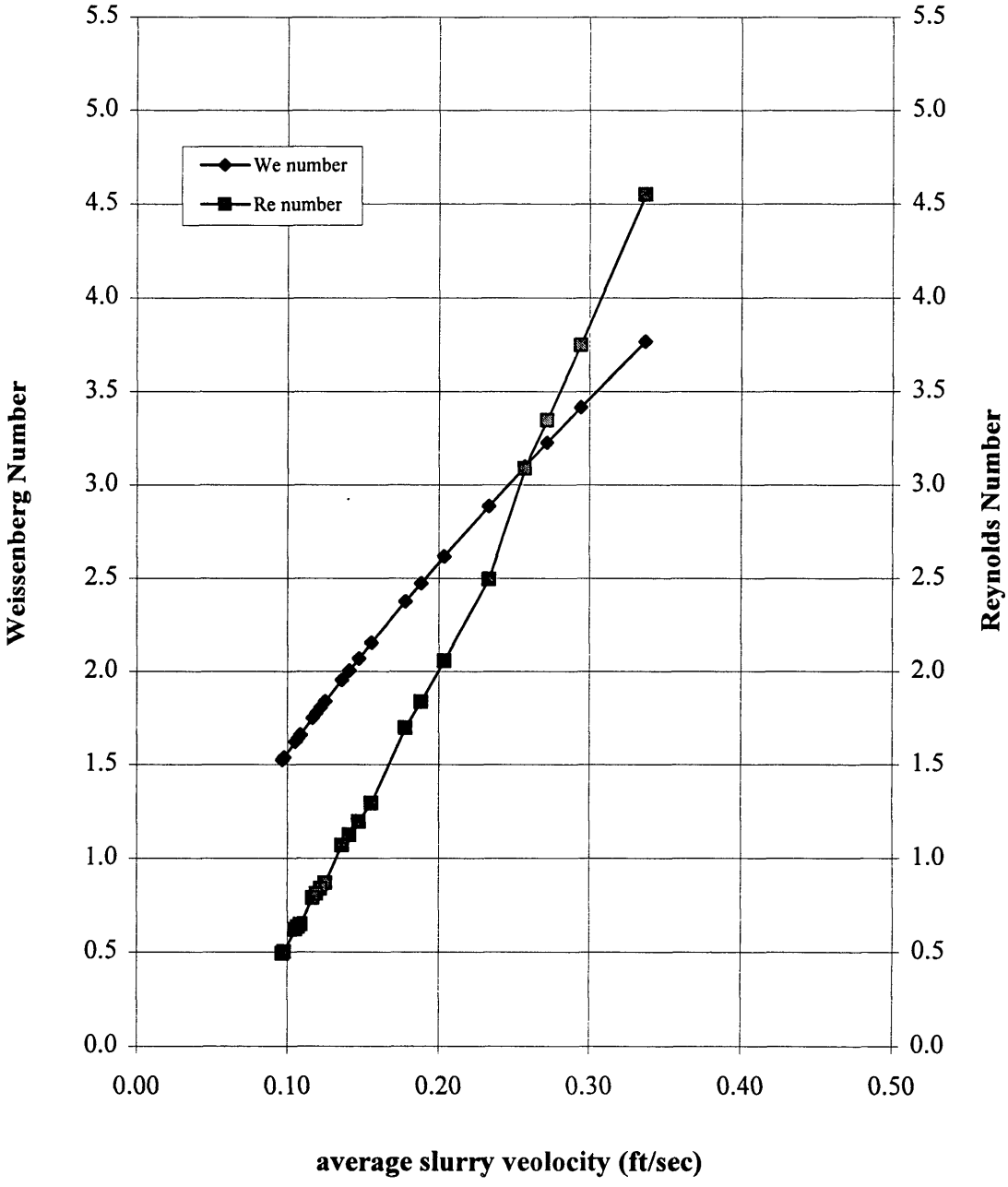

Fig 7.5: Node Formation Prediction under Field Conditions (For 60 lb/Mgal guar slurry)

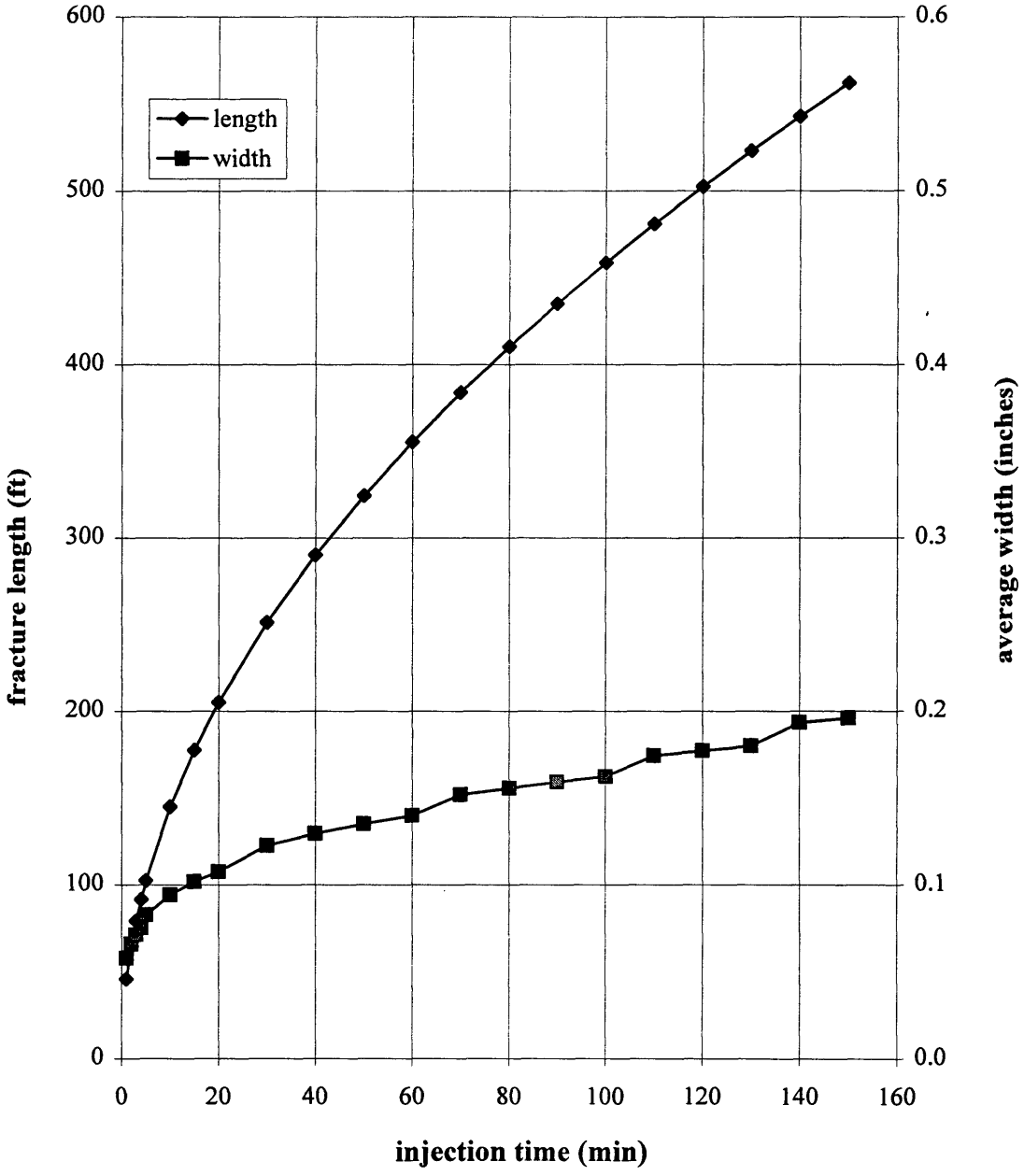

Fig 7.6: Fracture Dimension Prediction Using PKN Model (20 lb/Mgal slurry with constant fluid leakoff)

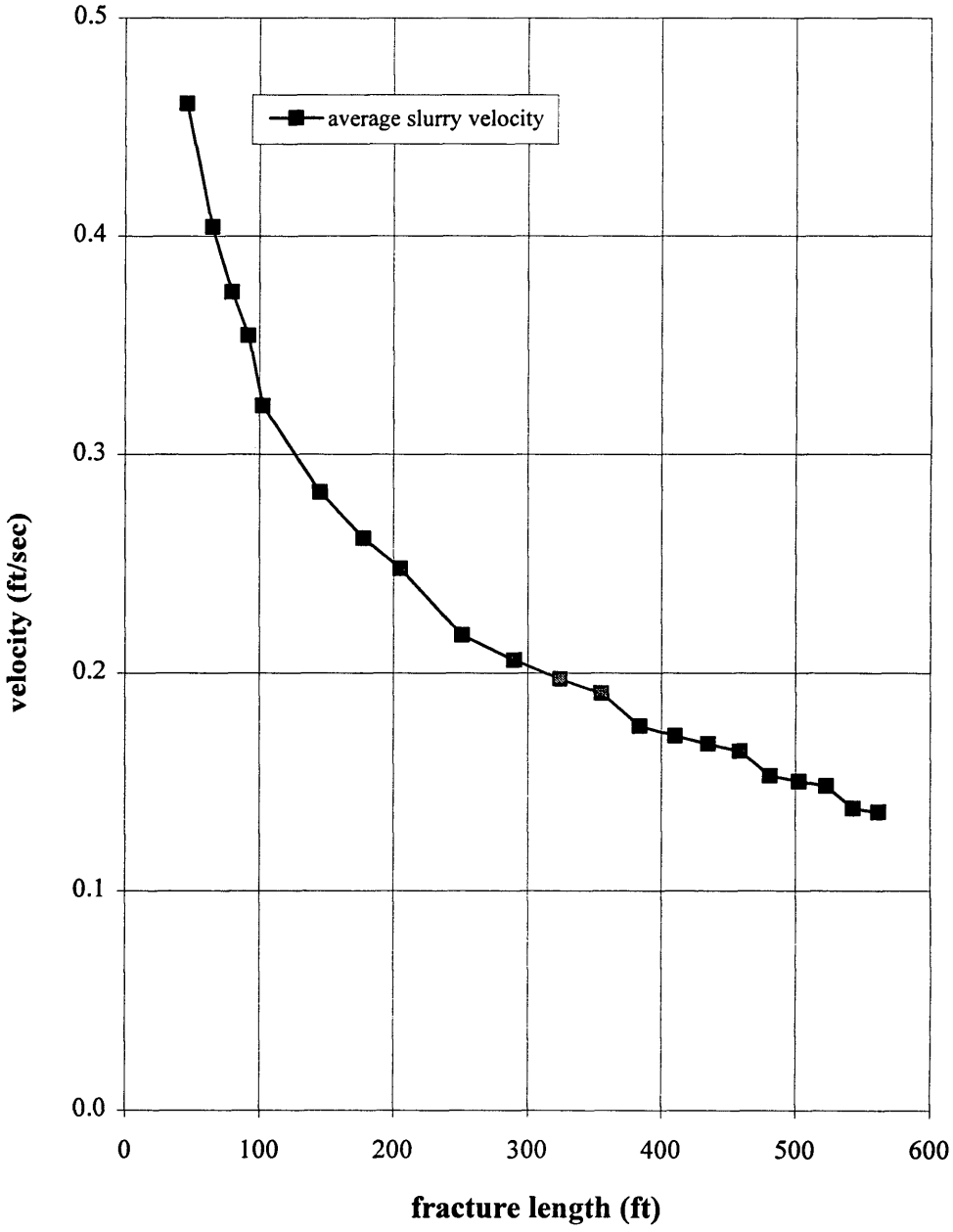

Fig 7.7: Average Slurry Velocity in the Fracture

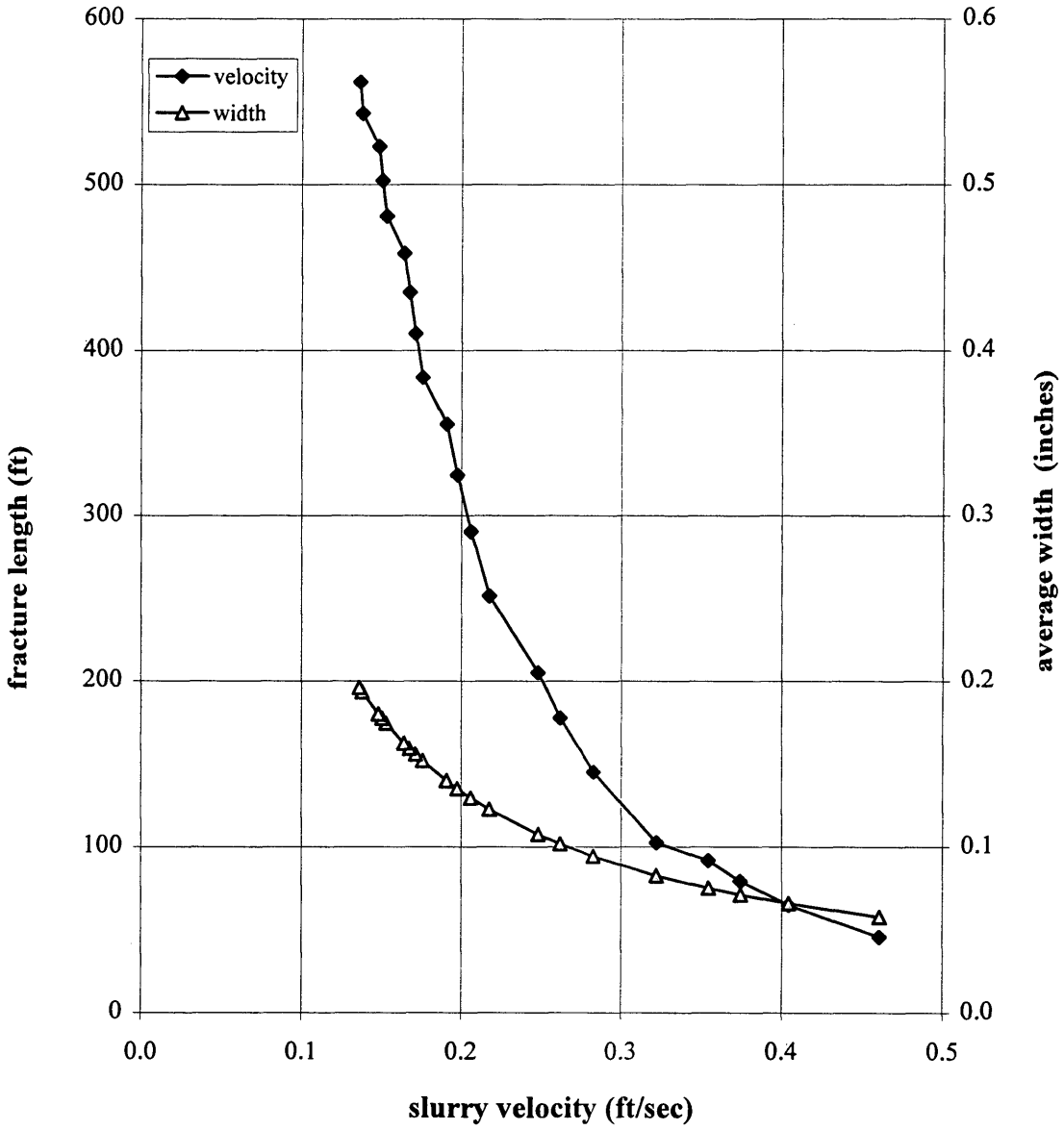

Fig 7.8: Induced Fracture and Slurry Behavior
(Schedualed injection of 20 lb/Mgal PHPA slurry)

Figure 7.7 is a plot of the slurry velocity in the induced fracture. The slurry velocity decreases from 0.46 ft/sec to 0.14 ft/sec during this process. Figure 7.8 is the plot of the induced fracture length and width as a function of the slurry velocity. Based on the simulation, the fracture width grows from 0.06 inches to 0.20 inches. This figure shows that once the fracture extends and widens, the slurry velocity would decrease, resulting in lower shear rates and higher slurry viscosity. In other words, chances for the node formation are enhanced.

Figure 7.9 is a plot of the Weissenberg and Reynolds numbers as a function of the simulated slurry velocity in the induced fracture. According to the laboratory results, sand node formed for the Weissenberg and Reynolds numbers of 4.9 and 2.5, respectively. Therefore, velocities less than 0.17 ft/sec are the region where one would observe node formation. Comparison of this velocity to the 40 lb/Mgal polyacrylamide shows that the required velocity for the latter is 0.08 ft/sec, which is consistent with our previous theoretical discussions of the rheological effects on the node formation.

It is important to mention that the effect of the timing of the sand node formation is not addressed in this research project. This concept was not studied because instantaneous leakoff data had not been collected during the experiments. A sand node would form sooner and quicker for the smaller natural fracture width compared to a larger one and/or for a slurry with higher fluid loss additive concentration than a lower additive loading.

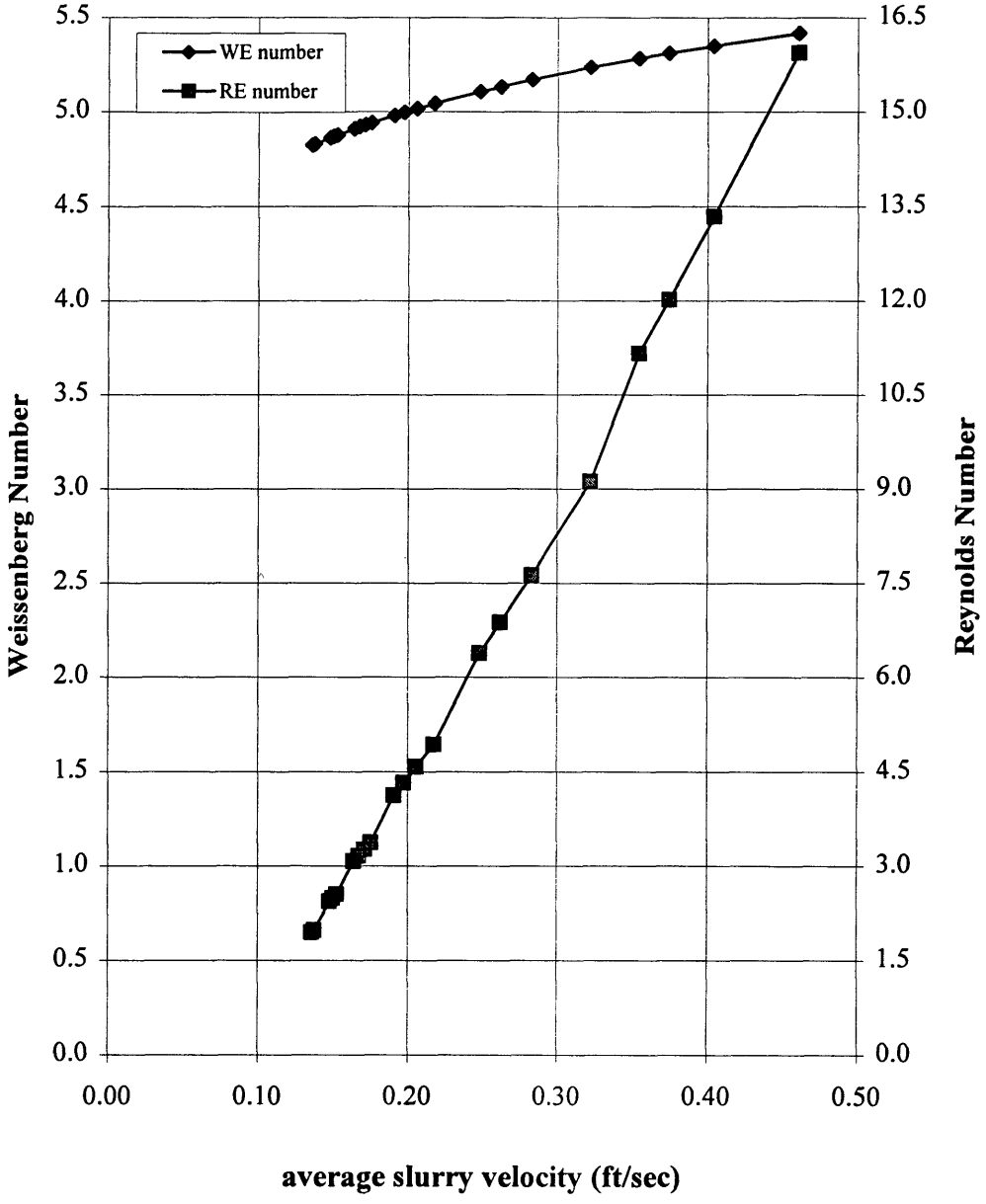

Fig 7.9: Node Formation Prediction Under Field Conditions (For 20 lb/Mgal PHPA slurry)

Once the conditions for sand node formation is specified for the given slurry system / flow conditions, it is advisable to use additives with particle size distribution. A ratio of 25 -75 weight percent combination of large to small particle size would suffice and enhance leakoff control by forming a more impermeable sand node. This will enhance the chances of preventing possible bridge out. In the next section we will have a brief discussion of the simulation results combined with our laboratory results and its implications for a field applications.

7.3 Discussion

Table IV is a summary of the results of the computer simulation combined with the experimental results for the four slurry systems for which sand node formed. Critical velocity and the width data are the results obtained from the experiments. The Reynolds number and Weissenberg number are computed using the simulation estimates for the slurry velocity in the induced fracture and the fracture width.

Table IV: Node Formation Criteria for the Slurry Systems

Slurry Type (Lb/Mgal)	$V_{critical}$ (ft/sec)	We (#)	Re (#)	Fracture Width (inches)
80 Guar	0.25	4	0.8	0.06 & below
60 Guar	0.33	2.9	2.6	0.06 & below
40 PHPA	0.08	5.1	0.3	0.03 & below
20 PHPA	0.17	4.9	2.5	0.06 & below

Table IV is summary of the conditions under which sand node would form. When a slurry exhibits higher viscoelasticity (i.e. 40 lb/Mgal PHPA vs. 20 lb/Mgal PHPA), then the magnitude of the critical velocity for that slurry system is lower. For example, sand node formed at 0.08 ft/sec for the 40 lb/Mgal PHPA compared to 0.17 ft/sec for 20 lb/Mgal PHPA slurry. The corresponding Weissenberg and Reynolds numbers indicate the necessary conditions for fluid flow and rheology characteristics for the sand node formation. The fracture width is the rock characteristic which would be the sufficient condition to form the sand node. The concentration of the additives used for these slurry systems did not exceed 5 lb/gal, however, 3 lb/gal was the cut-off concentration, especially for the fracture width of 0.03 inch and larger. One has to bear in mind that this discussion only considers fluid leakoff in to the natural fractures. There is also fluid leakoff to the matrix, and the assumption here is that the additive would prevent fluid leakoff into the matrix.

Table IV serves as a guideline which directs the laboratory results to field application. Thus, by simulating a hydraulic fracturing scenario, and knowledge of the existing rock fracture characteristics such as the natural fracture height and width, one can determine the optimum additive concentration, slurry rheology to conduct a successful hydraulic fracturing with a controlled fluid leakoff.

Another important concern relates to the rheology of the slurry used. It is obvious that expensive fluids such as polyacrylamide will not be economically attractive

alternative for the field applications. The intent in this project was to investigate the effects of parameters such as rheology. However, the concept has a role in the design of such slurry systems. After all, every slurry system exhibits viscoelastic behavior to some extent. These properties could in one way or another influence the outcome of a field application. Thus, for design purposes, it will be necessary to examine and have some knowledge of the fluid viscoelasticity.

Relating to the same concept is the effect of the sand or particle addition to the polymer solution. As mentioned in the Chapter 6, the addition of fluid loss additives does affect the viscoelasticity of the slurry system; however, this effect was not measurable and was ignored. The addition of the solids to the polymer solution decreases the viscoelasticity of the slurry system which works in favor of the sand node formation effort. So for design purposes, one should qualitatively incorporate that effect for the polymer solution. Weissenberg numbers need not be used very religiously. The estimated shear rates will have a more significant effect which are directly linked to the predicted fracture geometry.

Chapter 8. Conclusions, Implications, and Recommendations

8.1 Conclusions

Based on the laboratory results, by forming a sand node at the leakoff site, slurry leakoff to the formation can be prevented and chemicals are not lost to the formation. As a result cost of the expensive fluids is reduced. Moreover, performance of hydraulic fracturing is improved leading to extension of the induced fracture tunnel and increase in hydrocarbon production. Following is the list of conclusions obtained from this research investigation:

1. Slurry leakoff through a leakoff site representing a natural fracture can be prevented by forming a sand node. It is essential to have solid particles in the slurry to build a wall in order to inhibit slurry leakoff effectively.
2. Fluid leakoff rate is influenced by slurry rheology (viscosity, viscoelasticity), critical velocity, additive concentration, particle size distribution, and the natural fracture width.
3. Weissenberg and Reynolds numbers of 6.0 and 3.0 define the upper limits for the sand node formation in the plexiglass models. The magnitude of the critical velocity is the determinant factor for the node formation for each of the slurry systems.

4. Based on the laboratory experiments for the guar slurries, a sand node formed for shear rates which were at least twice as large as the shear rate corresponding to the cross-over point of the G' and G" data. For the PHPA slurries, this shear rate was at least 7 times the cross-over shear rate.
5. The slurry rheology and the shear rate are the most important parameters for the sand node formation.
6. Fracture dimensions are predicted using the PKN model for a set of rock, slurry and treatment data. Corresponding Weissenberg and Reynolds numbers identify the region where a sand node would form. This approach is a predictive tool to choose slurry scheduling and control slurry leakoff.

8.2 Implications

The main theme of this investigation is the creation of a sand node at a fracture (leakoff site) by controlling velocity, solid additive concentration, and fluid rheology. If the velocity is equal or less than the critical velocity for a given slurry system, then a sand node would form.

A quick way of estimating the critical velocity or the corresponding shear rate is to take the G′ and G′′ data and identify the cross-over frequency. Based on the experiments a sand node formed at shear rates which were at least twice or three times the

cross-over frequency (shear rate) for guar solutions. This shear rate is a factor of 7 or more for the viscoelastic slurry systems.

Following is a step by step method to implement the findings of this investigation for the planning and design stages of the hydraulic fracturing.

1. Determine the critical velocity for the given slurry system. This can be done in laboratory setting by conducting flow experiments or a quick way of estimating the node formation shear rate is to take the cross-over frequency of the G′, G′′ data. Node formation shear rate is two or three times the cross-over frequency for guar solutions and a factor of seven or more for the viscoelastic solutions.
2. By computer simulation, estimate fracture width and slurry velocity in the induced fracture for a given rock, slurry, and treatment data.
3. Estimate the Reynolds number and the Weissenberg number for the slurry flow in the induced fracture channel. For the Reynolds number and the Weissenberg number, slurry velocity and the shear rate is needed (as determined in step 1).
4. Compare the velocities used to estimate Reynolds number and Weissenberg number to that of the critical velocity. If the estimated values are equal or less than the ones for the critical velocity then a sand node would form.
5. Injection rates can be adjusted in order to ascertain the slurry velocity/shear rate to fall in the node formation region.

8.3 Recommendations

Based on our results and observations the following is recommended:

1. The scaling effect, surface roughness, and height increase should be investigated in the laboratory.
2. Instantaneous leakoff data should be collected so that the timing of the node formation can be addressed.
3. Flow experiments should be conducted such that the slurry leakoff to the natural fracture and to the matrix are included. This will resemble the real flow condition in the fracturing process.
4. The natural fracture dilation effect needs to be investigated.
3. Particle size distribution be further investigated.

NOMENCLATURE

a	= slurry viscosity increase exponent
a	= constant
b	= constant
c	= constant
C_v	= volume fraction solids
C_{vmax}	= maximum volume fraction solids
C_n	= C_v / C_{vmax}
d	= diameter of the pipe
G(t)	= relaxation modulus
G'(t)	= storage modulus
G"(t)	= loss modulus
K'	= consistency index
L	= tube length
g	= acceleration of gravity
n'	= flow behavior index
n_o	= flow behavior index
$N_1(\gamma')$	= first normal stress difference
$N_2(\gamma')$	= second normal stress difference
N_c	= dimensionless group for Newtonian fluid
N'_c	= dimensionless group for non-Newtonian fluid
q	= flow rate
N_{Re}	= Reynolds number
Re	= slurry Reynolds number
V_f	= slurry velocity in the induced fracture
$V_{critical}$	= slurry velocity at which sand node forms
Vo	= settling rate velocity
V_N	= velocity
V_ψ	= velocity for prop fractional concentration
ΔP_f	= frictional pressure drop
w	= slot width
W1	= first estimate of the fracture width
W2	= second estimate of the fracture width
We	= polymer Weissenberg number
Wi	= Weissenberg number

α = 0.18

α = 1.277 boundary layer coefficient (for sand)

β = 0.19

β = 0.22

β_p = 2.800 boundary layer coefficient (for sand)

γ_L , γ_H = adjustable parameters to match onset of deviation of low and high shear viscosity from the calculated power law viscosity

γ' = shear rate

$\gamma')_{x\text{-over}}$ = the shear rate at which G ' and G" curves cross over

$\gamma')_{\text{Node Formation}}$ = the shear rate at which sand node forms

ε = shear strain

η = apparent viscosity

η' = complex viscosity (real part)

η'' = complex viscosity (imaginary part)

λ = fluid time constant

λ_{avg} = average fluid time constant

μ = viscosity

μ_o = zero shear viscosity

μ_∞ = apparent viscosity

ρ = fluid density

ρ_p = particle density

$\Delta\rho$ = density difference between the fluid and the particle

τ = shear stress

τ_w = shear stress at the wall

τ_o = apparent yield stress

φ = volume/volume particle concentration

$\Psi_1(\gamma')$ = first normal stress coefficient

$\Psi_2(\gamma')$ = second normal stress coefficient

ω = frequency

REFERENCES

1. Jennings, A.R.: "Fracturing Fluids-Then and Now," JPT (July 1996) 604- 610.

2. Gulbis, J.: "Fracturing Fluid Chemistry," Reservoir Stimulation, Schlumberger Educational Services,. Economides, M.J. and Nolte, K.G.,(eds.),1987.

3. Clark, P. E.: "Stimulation Fluid Rheology-A New Approach," paper SPE 8300 presented at the 54th Annual Fall Conference and Exhibition, Las Vegas, Sept. 23-26, 1979.

4. Shah, S. N., Lord, D. L.,Tan, H. C.: "Recent Advances In the Fluid Mechanics and Rheology of Fracturing Fluids," paper SPE 22391, presented at the International Meeting, Beijing, China, March. 24-27, 1992.

5. Rogers, R. E., Veatch, R. W., Nolte, K. G.: "Pipe Viscometer Study of Fracturing Fluid Rheology," paper SPE 10258 presented at the 1981 SPE Annual Technical Conference and Exhibition, San Antonio, Oct. 5-7, 1981.

6. Lord, D. L., Shackleford, D.: "Real-Time Fracturing Fluid Rheology Measurements With the Helical Screw Rheometer," paper SPE 19734 presented at the 64th Annual Technical Conference and Exhibition, San Antonio, Oct. 8-11, 1989.

7. Shah, S. N.: "Rheological Characterization of Hydraulic Fracturing Slurries," paper SPE 22839, presented at the 66th Annual Technical Conference and Exhibition, Dallas Oct. 6-9, 1991.

8. "Report on the Investigation of the Rheology and Proppant Carrying Capacity of Common Fracturing Fluids", STIMLAB Annual Report, 1995.

9. Hall, C.D., Dollarhide, F.E.: "Effects of Fracturing-FluidVelocity on Fluid Loss Agent Performance," JPT (July 1968) 763-68.

10. Penny, G. S., Conway, M. W., Lee, W. S.: "Control and Modeling of Fluid Leakoff During Hydraulic Fracturing," JPT (June 1985) 1071-81.

11. Hall, B.E., Houk, S.G.: "Fluid-Loss Control in the Naturally Fractured Buda Formation," paper SPE 12152 presented at the 58th Annual Technical Conference and Exhibition, San Francisco, CA, Oct. 5-8, 1983.

13. Woo, G.T., Cramer, D.D.: "Laboratory and Field Evaluation of Fluid-Loss Additives Systems Used in the Williston Basin," paper SPE 12899 presented at the Rocky Mountain Regional Meeting, Casper, WY, May 21-23, 1984.

14. Gulbis, J.: "Dynamic Fluid-Loss Study of Fracturing Fluids," paper SPE 12154 presented at the 58th Annual Technical Conference and Exhibition, San Fracisco, CA, Oct. 5-8, 1983.

15. Roodhart, L.P.: "Fracturing Fluid: Fluid-Loss Measurements Under Dynamic Conditions," paper SPE 11900 presented at the Annual European Petroleum Conference, Aberdeen, England, Sep. 6-9, 1983.

16. Zigrye, J.L., Whitfill, D.L., and Sievert, J.A.: "Fluid Loss Control Differences of Crosslinked and Linear Fracturing Fluids," paper SPE 12153 presented at the 58th Annual Technical Conference and Exhibition, San Fracisco, CA, Oct. 5-8, 1983.

17. Gruesbeck, C.: "Particle Transport Through Perforations," paper SPE 7006 presented at the Third Symposium on Formation Damage Control, Lafayette, LA, Feb 15-16, 1978.

18. Novotny, E.J.: "Proppant Transport," paper SPE 6813 presented at 52nd Annual Fall Technical Conference and Exhibition, Denver, CO, Oct. 9-12, 1977.

19. Hannah, R.R., Harrington, L.J.: "Measurement of Dynamic Proppant Fall Rates in Fracturing Gels Using a Concentric Cylinder Tester," paper SPE 7571 presented at 53rd Annual Fall Technical Conference and Exhibition, Houston, TX, Oct. 1-3, 1978.

20. Clark, P.E., Harkin, M. H.: "Design of a Large Vertical Prop Transport Model," paper SPE 6814 presented at SPE 52nd Annual Fall Technical Conference, Denver, Oct. 9-12, 1977.

20. Subhash, N. Shah.: "Proppant Settling Correlations For Non-Newtonian Fluids Under Static and Dynamic Conditions," Paper SPE 9330 presented at SPE 55th Annual Fall Technical Conference, Dallas, Sep. 21-24, 1980.

21. Clark, P.E., Quadir, J. A.: "Proppant Transport in Hydraulic Fractures: A Critical Review of Particle Settling Velocity Equations," Paper SPE 9866 presented at SPE/DOE , Low Permeability Symposium, Denver, May 27-29, 1981.

23. Roodhart, L. P.: " Proppant Transport in Non-Newtonian Fluids," paper SPE 13905 presented at SPE/DOE Low Permeability Symposium, Denver, May 19-22, 1985.

24. Acharya, A.: "Particle Transport in Viscous and Viscoelastic Fracturing Fluids," paper SPE 13179 presented at the 59th Annual Technical Conference, Houston, TX, Sep. 16-19, 1984.

25. Jin, L., Penny, G.: "Dimensionless Methods for the Study of Particle Settling in Non-Newtonian Fluids," paper SPE 28563 presented at Annual Technical Conference, New Orleans, LA, Sep. 25-28, 1994.

26. Cleary, M.P, Fonseca, A.: "Proppant Convection and Encapsulation in Hydraulic Fracturing: Practical Implications of Computer and Laboratory Simulations," paper SPE 24825 presented at the 67th Annual Technical Conference, Washington D.C, Oct. 4-7, 1992.

27. Clark, P.E., Zhu, Q.: "Fluid Flow into Vertical Fractures From a Point Source," paper SPE 28509 presented at the 1999 Mid-Continent Operations Symposium, Oklahoma City, OK, March 28-31, 1999.

28. Nolte, K.: "Fluid Flow Considerations in Hydraulic Fracturing," paper SPE 18537 presented at the Eastern Regional Meeting, Charleston, WV, Nov. 1-4, 1988.

29. Unwin, A.T., Hammond, P.S.: "Computer Simulations of Proppant Transport in a Hydraulic Fracture," paper SPE 29649 presented at the Western Regional Meeting, Bakersfield, CA, March 8-10, 1995.

30. Barree, R.D., Conway, M.W.: "Experimental and Numerical Modeling of Convective Proppant Transport, " paper SPE 28564 presented at the Annual Technical Conference, New Orleans, Sept. 25-28, 1994.

31. Gauthier, F., Goldsmith, H. L.: "Particle Motions in Non-Newtonian Media," Transactions of the Society of Rheology (1971) 15:2, 297-330.

32. Tehrani, M.A.: "An Experimental Study of Particle Migration in Pipe Flow of Viscoelastic Fluids," J. Rheology (1996) 40, 1057-1077.

33. Gidley, John., Holditch, Stephen., Nierode, Dale., Veatch, Ralph.: "Recent Advances in Hydraulic Fracturing,"Society of Petroleum Engineers, Richardson, TX, 1989, Chapter 3.

34. Bird, R. Byron.: "Dynamics of Polymeric Liquids," New York, Wiley, c1987, pp150.

APPENDIX A

SLURRY LEAKOFF DATA FOR FLOW EXPERIMENTS IN CHAPTER 4

Figure 4.1

velocity(ft/sec)	leak rate(cc/sec)
1.19	4.36
0.86	2.39
0.43	1.72
0.18	0.05
1.14	4.03
0.85	3.15
0.81	3.08
0.16	0.23
0.97	3.34
0.63	3.10
0.33	0.09

Figure 4.2

velocity(ft/sec)	leak rate(cc/sec)
0.62	3.09
0.26	0.11
0.74	2.88
0.40	2.41
0.12	0.06
0.60	2.86
0.22	0.04

Figure 4.3

velocity(ft/sec)	leak rate(cc/sec)
1.05	0.30
0.90	0.30
0.45	0.20
0.45	0.25
0.97	0.33
0.75	0.40
0.64	0.36
0.48	0.28
0.96	0.44
0.71	0.35
0.64	0.33
0.48	0.28
0.32	0.24

Figure 4.4

velocity(ft/sec)	leak rate(cc/sec)
0.26	0.23
0.38	0.24
0.50	0.31
0.55	0.22
0.63	0.28
0.85	0.36

Figure 4.5

velocity(ft/sec)	leak rate(cc/sec)
0.94	31.81
0.71	27.02
0.50	22.60
0.93	30.73
0.80	26.64
0.48	21.59
0.82	30.73
0.66	28.79
0.43	19.39

Figure 4.6

velocity(ft/sec)	leak rate(cc/sec)
0.73	18.64
0.54	16.87
0.34	13.16
0.80	19.65
0.54	17.24
0.34	13.50
0.96	24.62
0.70	20.79
0.55	18.87
0.51	18.07
0.60	15.65
0.47	14.64
0.28	11.16

Figure 4.7

velocity(ft/sec)	leak rate(cc/sec)
1.10	33.33
0.98	30.87
0.67	27.31
0.48	23.61
0.87	28.09
0.71	25.33
0.44	22.14

Figure 4.7 (continued)

velocity(ft/sec)	leak rate(cc/sec)
0.82	20.54
0.52	18.83
0.30	15.68
0.69	17.39
0.35	13.45
0.23	12.44

Figure 4.8

velocity(ft/sec)	leak rate(cc/sec)
0.94	31.81
0.71	27.02
0.50	22.60
0.93	30.73
0.80	26.64
0.48	21.59
0.82	30.73
0.66	28.79
0.43	19.39

Figure 4.9

velocity(ft/sec)	leak rate(cc/sec)
0.73	18.64
0.54	16.87
0.34	13.16
0.80	19.65
0.54	17.24
0.34	13.50
0.96	24.62
0.70	20.79
0.55	18.87
0.51	18.07
0.60	15.65
0.47	14.64
0.28	11.16

Figure 4.10

velocity(ft/sec)	leak rate(cc/sec)
0.96	32.77
0.71	25.39
0.40	15.02
0.79	34.96
0.56	24.36
0.29	13.92
0.87	26.68
0.53	18.71
0.27	10.53

Figure 4.11

velocity(ft/sec)	leak rate(cc/sec)
0.58	18.20
0.38	13.47
0.16	6.25
0.61	19.20
0.34	12.04
0.14	5.47
0.57	18.10
0.27	11.18
0.14	5.50
0.74	21.16

Figure 4.12

velocity(ft/sec)	leak rate(cc/sec)
0.90	11.25
0.70	8.60
0.40	7.39
0.23	4.51
0.16	2.34
0.65	1.15
0.35	0.73
0.83	1.23
0.59	0.96
0.32	0.62
0.13	0.41

Figure 4.13

velocity(ft/sec)	leak rate(cc/sec)
0.55	1.86
0.26	0.77
0.04	0.57
0.58	0.67
0.30	0.50
0.07	0.21

Figure 4.14

velocity(ft/sec)	leak rate(cc/sec)
0.57	10.89
0.27	7.99
0.05	2.51
0.54	1.37
0.25	0.94
0.06	0.36

Figure 4.15

velocity(ft/sec)	leak rate(cc/sec)
0.71	1.81
0.55	1.07
0.31	0.82
0.74	0.63
0.51	0.45
0.17	0.52
0.74	3.12
0.30	1.67
0.57	2.39

Figure 4.16

velocity(ft/sec)	leak rate(cc/sec)
0.86	0.35
0.38	0.43
0.24	0.75
0.79	4.12
0.55	3.39
0.23	1.87
0.81	0.90
0.54	0.48
0.27	0.85

Figure 4.17

velocity(ft/sec)	leak rate(cc/sec)
0.79	1.31
0.48	0.92
0.22	0.56
0.76	1.42
0.49	0.87
0.42	0.86
0.21	0.53
0.14	0.28
0.04	0.12
0.92	1.73
0.71	1.59
0.46	1.10
0.14	0.51

Figure 4.18

velocity(ft/sec)	leak rate(cc/sec)
0.92	34.30
0.64	26.10
0.32	15.10
0.87	32.10
0.64	25.60
0.33	15.80

Figure 4.19

velocity(ft/sec)	leak rate(cc/sec)
0.84	35.5
0.48	23.1
0.12	11.4
0.86	35.2
0.6	26.7
0.32	16.8

Figure 4.20

velocity(ft/sec)	leak rate(cc/sec)
0.29	0.77
0.07	0.25
0.06	0.19
0.04	0.3
0.3	0.68
0.1	0.07
0.05	0.03

Figure 4.21

velocity(ft/sec)	leak rate(cc/sec)
0.20	0.74
0.35	1.10
0.91	2.89
0.04	0.15

Figure 4.22

velocity(ft/sec)	leak rate(cc/sec)
0.67	19.80
0.44	15.50
0.28	11.60
0.22	4.40
0.17	2.70
0.56	3.50
0.27	1.40
0.18	0.80
0.16	0.70

Figure 4.23

velocity(ft/sec)	leak rate(cc/sec)
0.55	29.80
0.20	13.26
0.52	13.60
0.31	8.16
0.28	10.31
0.20	8.02

Figure 4.24

velocity(ft/sec)	leak rate(cc/sec)
0.34	1.10
0.16	0.71
0.06	0.55
0.32	2.30
0.19	2.00
0.08	0.90

Figure 4.25

velocity(ft/sec)	leak rate(cc/sec)
0.20	0.74
0.35	1.10
0.91	2.89
0.04	0.15

Figure 4.26

velocity(ft/sec)	leak rate(cc/sec)
0.26	9.53
0.17	8.72
0.10	6.18
0.07	3.19
0.05	2.96
0.02	1.50
0.28	15.12
0.19	12.50
0.09	6.25
0.03	6.13
0.02	5.75

APPENDIX B

GUAR AND POLYACRYLAMIDE RHEOLOGY DATA FOR CHAPTERS 5 AND 6

Due to the large volume of the rheology data, hard copy of appendix B is not provided in this section. However, the rheology data are provided in a floppy disk. Appendices A and C are included in the floppy disk as well.

APPENDIX C

SIMULATION DATA

Following is the nomenclature for the variables used for the calculations:

U_o = zero shear viscosity

U_l = adjustable parameter to match onset of deviation of low shear viscosity from the calculated power law viscosity

U_h = adjustable parameter to match onset of deviation of high shear viscosity from the calculated power law viscosity

C_v = volume fraction solids

n_o = clean fluid power law flow behavior index

a = slurry viscosity increase exponent ($1.2<a<1.8$)

Estimating fracture dimensions using PKN model. Non Newtonian slurry is used with constant leakoff rates for each stage of injections. Following is the stages and relevant information:

Stage	Fluid Type	C)additive lb/gal	Leakoff Rate ft/min^0.5
I	Pad	0	0.0015
II	Slurry	1	0.0015
III	Slurry	2	0.0015
IV	Slurry	3	0.0015
V	Slurry	4	0.0015
VI	Slurry	5	0.0015

Rock data

Shear modulus G	1450000	psi
Poisson ratio	0.2	
critical stress intensity factor Kc	455	psi/in^0.5
fracture height	129.9	ft
Horizontal stress)min	2750	psi
Horizontal stress)max	3045	psi

Fracture treatment data

injection rate qo	10	bbl/min
time t	200	min
viscosity	100	cp
leakoff rate Kl	0.0015	ft/min^0.5
V sp	0.01	gal/ft^2

Data for non-Newtonian case

80 lb/Mgal guar solution

n	0.252	
K	0.2434	lbf-sec^n/ft^2

Time	Lf	μ	W1	V)f	γ′	μ)GEFFAR	W2	Diff	W)avg
min	ft	cp	inches	ft/sec	1/sec	cp	inches	0.0	inches
1	46	493.5	0.174	0.249	41.3	493.6	0.174	0.0	0.107
2	65	603.7	0.199	0.217	31.4	603.7	0.199	0.0	0.123
3	79	678.4	0.216	0.200	26.8	678.4	0.216	0.0	0.133
4	92	736.4	0.228	0.189	23.9	736.5	0.228	0.0	0.141
5	103	976.8	0.252	0.172	19.6	976.9	0.252	0.0	0.155
10	145	1182.7	0.288	0.150	15.0	1182.8	0.288	0.0	0.178
15	178	1318.8	0.312	0.139	12.8	1318.8	0.312	0.0	0.192
20	205	1422.4	0.329	0.131	11.5	1422.5	0.329	0.0	0.203
30	251	1955.8	0.375	0.115	8.9	1955.9	0.375	0.0	0.231
40	290	2097.1	0.395	0.109	8.0	2097.2	0.395	0.0	0.244
50	324	2210.6	0.412	0.105	7.3	2210.6	0.412	0.0	0.254
60	355	2305.5	0.426	0.101	6.9	2305.6	0.426	0.0	0.263
70	384	2923.6	0.461	0.094	5.9	2923.7	0.461	0.0	0.284
80	410	3008.1	0.472	0.092	5.6	3008.2	0.472	0.0	0.291
90	435	3083.3	0.482	0.090	5.4	3083.4	0.482	0.0	0.297
100	459	3151.0	0.491	0.088	5.2	3151.1	0.491	0.0	0.303
110	481	3909.5	0.524	0.082	4.5	3909.6	0.524	0.0	0.323
120	503	3975.1	0.532	0.081	4.4	3975.1	0.532	0.0	0.328
130	523	4035.4	0.540	0.080	4.3	4035.4	0.540	0.0	0.333
140	543	5029.3	0.576	0.075	3.8	5029.3	0.576	0.0	0.355
150	562	5089.8	0.582	0.074	3.7	5089.8	0.582	0.0	0.359

To generate the viscosity, shear rate can be estimated from the fluid velocity in the induced fracture and shear rate can be computed. The slurry viscosity can be calculated using the polymer solution data and the solid additive volume fraction.

Slurry viscosity estimation scheme using GEEFAR and inputted in the calculations

	G80--0	1 lb/gal	2 lb/gal	3 lb/gal	4 lb/gal	5 lb/gal
Uo	5389.2339	5389.2339	5389.2339	5389.2339	5389.2339	5389.2339
Cv	0	0.042	0.0816	0.1176	0.1509	0.184
a	1.8	1.8	1.8	1.8	1.8	1.8
Ul	3.12	3.12	3.12	3.12	3.12	3.12
no	0.252	0.252	0.252	0.252	0.252	0.252
Uh	1000000	1000000	1000000	1000000	1000000	1000000

	0 lb/gal	**1 lb/gal**	**2 lb/gal**	**3 lb/gal**	**4 lb/gal**	**5 lb/gal**
γ'(1/sec)	**μ(cp)**	**μ(cp)**	**μ(cp)**	**μ(cp)**	**μ(cp)**	**μ(cp)**
41.3	494	568	655	754	869	1011
31.4	604	695	802	923	1062	1237
26.8	678	781	901	1037	1194	1390
23.9	736	847	978	1126	1296	1509
19.6	849	977	1127	1298	1494	1739
15.0	1028	1183	1365	1571	1809	2106
12.8	1146	1319	1522	1752	2017	2348
11.5	1236	1422	1641	1890	2175	2532
8.9	1473	1695	1956	2252	2592	3017
8.0	1580	1817	2097	2414	2780	3235
7.3	1665	1916	2211	2545	2930	3410
6.9	1736	1998	2306	2654	3056	3557
5.9	1913	2201	2540	2924	3366	3918
5.6	1968	2265	2613	3008	3463	4031
5.4	2017	2321	2678	3083	3550	4132
5.2	2062	2372	2737	3151	3628	4223
4.5	2222	2556	2950	3396	3910	4551
4.4	2259	2599	2999	3453	3975	4627
4.3	2293	2639	3045	3505	4035	4697
3.8	2455	2825	3260	3753	4321	5029
3.7	2485	2859	3299	3798	4373	5090

sand loading	density of the slurry(gr/cc)
0	1
1	1.07
2	1.14
3	1.2
4	1.26
5	1.31

Hydraulic diameter = 4 * Hydraulic radius
Area open to flow = Width * Length
Wetted perimeter = 2 * (Width + Length)
Hydraulic diameter = 4 * (Area / Perimeter)

G80 slurry (0,1,2,3,4,5) lb/gal sand

V)f (ft/sec)	γ´(1/sec)	μ(cp)	Width (inch)	d) hyd (cm)	Weissenberg #	Reynolds #
0.249	41.3	494	0.174	0.88	4.53	1.356
0.217	31.4	604	0.199	1.01	4.10	1.109
0.200	26.8	678	0.216	1.10	3.87	0.987
0.189	23.9	736	0.228	1.16	3.71	0.909
0.172	19.6	977	0.252	1.28	3.46	0.733
0.150	15.0	1183	0.288	1.46	3.13	0.606
0.139	12.8	1319	0.312	1.58	2.96	0.543
0.131	11.5	1422	0.329	1.67	2.85	0.503
0.115	8.9	1956	0.375	1.90	2.59	0.390
0.109	8.0	2097	0.395	2.01	2.49	0.364
0.105	7.3	2211	0.412	2.09	2.42	0.345
0.101	6.9	2306	0.426	2.16	2.36	0.331
0.094	5.9	2924	0.461	2.34	2.23	0.275
0.092	5.6	3008	0.472	2.40	2.19	0.267
0.090	5.4	3083	0.482	2.45	2.16	0.260
0.088	5.2	3151	0.491	2.49	2.13	0.255
0.082	4.5	3910	0.524	2.66	2.03	0.216
0.081	4.4	3975	0.532	2.70	2.01	0.212
0.080	4.3	4035	0.540	2.74	1.99	0.209
0.075	3.8	5029	0.576	2.92	1.89	0.174
0.074	3.7	5090	0.582	2.96	1.88	0.172

Estimating fracture dimensions usingPKN model. Non Newtonian slurry is used with constant leakoff rates for each stage of injections. Following is the stages and relevant information:

Stage	Fluid Type	C)additive lb/gal	Leakoff Rate ft/min^0.5
I	Pad	0	0.0015
II	Slurry	1	0.0015
III	Slurry	2	0.0015
IV	Slurry	3	0.0015
V	Slurry	4	0.0015
VI	Slurry	5	0.0015

Rock data

Shear modulus G	1450000	psi
poisson ratio	0.2	
critical stress intensity factor Kc	455	psi/in^0.5
fracture height	129.9	ft
Horizontal stress)min	2750	psi
Horizontal stress)max	3045	psi

Fracture treatment data

injection rate qo	10	bbl/min
time t	200	min
viscosity	100	cp
leakoff rate Kl	0.0015	ft/min^0.5
V sp	0.01	gal/ft^2

Data for non-Newtonian case

60 lb/Mgal guar solution

n	0.28	
K	0.1458	lbf-sec^n/ft^2

Time	Lf	μ	W1	V)f	γ′	μ)GEFFAR	W2	Diff	W)avg
min	ft	cp	inches	ft/sec	1/sec	cp	inches	0.0	inches
1	45.9	147.1	0.128	0.337	76.81	224.82	0.128	0.000	0.08
2	64.9	178.6	0.147	0.294	58.62	272.93	0.147	0.000	0.09
3	79.5	200.0	0.159	0.272	50.06	305.66	0.159	0.000	0.10
4	91.7	216.7	0.168	0.257	44.75	331.25	0.168	0.000	0.10
5	102.6	287.0	0.185	0.233	36.77	381.27	0.185	0.000	0.11
10	145.1	348.3	0.212	0.204	28.07	462.55	0.212	0.000	0.13
15	177.7	389.7	0.230	0.188	23.98	517.72	0.230	0.000	0.14
20	205.2	422.1	0.243	0.178	21.44	560.76	0.243	0.000	0.15
30	251.3	589.8	0.278	0.156	16.39	679.04	0.278	0.000	0.17
40	290.1	638.5	0.294	0.147	14.66	735.05	0.294	0.000	0.18
50	324.4	679.0	0.307	0.141	13.45	781.57	0.307	0.000	0.19
60	355.3	713.7	0.318	0.136	12.53	821.60	0.318	0.000	0.20
70	383.8	925.4	0.346	0.125	10.59	925.37	0.346	0.000	0.21
80	410.3	959.6	0.355	0.122	10.06	959.56	0.355	0.000	0.22
90	435.2	990.6	0.363	0.119	9.61	990.66	0.363	0.000	0.22
100	458.7	1019.5	0.370	0.117	9.23	1019.38	0.370	0.000	0.23
110	481.1	1299.0	0.398	0.109	7.98	1128.25	0.398	0.000	0.25
120	502.5	1329.6	0.405	0.107	7.72	1154.83	0.405	0.000	0.25
130	523.0	1358.3	0.411	0.105	7.49	1179.79	0.411	0.000	0.25
140	542.8	1747.8	0.442	0.098	6.48	1304.24	0.442	0.000	0.27
150	561.8	1779.9	0.448	0.097	6.31	1328.17	0.448	0.000	0.28

To generate the viscosity, shear rate can be estimated from the fluid velocity in the induced fracture and shear rate can be computed. The slurry viscosity can be calculated using the polymer solution data and the solid additive volume fraction.

Slurry viscosity estimation scheme using GEEFAR and inputted in the calculations

	0 lb/gal	1 lb/gal	2 lb/gal	3 lb/gal	4 lb/gal	5 lb/gal
Uo	5515.4521	5515.4521	5515.4521	5515.4521	5515.4521	5515.4521
Cv	0	0.042	0.0816	0.1176	0.1509	0.184
a	1.8	1.8	1.8	1.8	1.8	1.8
Ul	0.931	0.931	0.931	0.931	0.931	0.931
no	0.281	0.281	0.281	0.281	0.281	0.281
Uh	1000000	1000000	1000000	1000000	1000000	1000000

	0 lb/gal	**1 lb/gal**	**2 lb/gal**	**3 lb/gal**	**4 lb/gal**	**5 lb/gal**
γ'(1/sec)	**μ(cp)**	**μ(cp)**	**μ(cp)**	**μ(cp)**	**μ(cp)**	**μ(cp)**
76.8	147	169	195	225	259	301
58.6	179	205	237	273	314	366
50.1	200	230	266	306	352	410
44.7	217	249	288	331	381	444
36.8	249	287	331	381	439	511
28.1	303	348	402	463	533	620
24.0	339	390	450	518	596	694
21.4	367	422	487	561	646	751
16.4	444	511	590	679	782	910
14.7	481	553	639	735	846	985
13.4	511	588	679	782	900	1047
12.5	538	618	714	822	946	1101
10.6	605	697	804	925	1065	1240
10.1	628	722	834	960	1105	1286
9.6	648	746	861	991	1141	1328
9.2	667	767	885	1019	1174	1366
8.0	738	849	980	1128	1299	1512
7.7	756	869	1003	1155	1330	1548
7.5	772	888	1025	1180	1358	1581
6.5	853	982	1133	1304	1502	1748
6.3	869	1000	1154	1328	1529	1780

sand loading	density of the slurry(gr/cc)
0	1
1	1.07
2	1.14
3	1.2
4	1.26
5	1.31

Hydraulic diameter = 4 * Hydraulic radius
Area open to flow = Width * Length
Wetted perimeter = 2 * (Width + Length)
Hydraulic diameter = 4 * (Area / Perimeter)
G60 slurry (0,1,2,3,4,5) lb/gal sand

V)f (ft/sec)	γ˙(1/sec)	μ(cp)	Width (inch)	d) eq (cm)	Weissenberg #	Reynolds #
0.337	76.8	147	0.128	0.652	3.77	4.55
0.294	58.6	179	0.147	0.746	3.42	3.75
0.272	50.1	200	0.159	0.808	3.23	3.35
0.257	44.7	217	0.168	0.854	3.10	3.09
0.233	36.8	287	0.185	0.942	2.89	2.50
0.204	28.1	348	0.212	1.078	2.62	2.06
0.188	24.0	390	0.230	1.167	2.47	1.84
0.178	21.4	422	0.243	1.234	2.37	1.70
0.156	16.4	590	0.278	1.411	2.15	1.29
0.147	14.7	639	0.294	1.492	2.07	1.20
0.141	13.4	679	0.307	1.558	2.01	1.12
0.136	12.5	714	0.318	1.614	1.96	1.07
0.125	10.6	925	0.346	1.756	1.84	1.26
0.122	10.1	960	0.355	1.802	1.81	1.18
0.119	9.6	991	0.363	1.843	1.78	1.13
0.117	9.2	1019	0.370	1.881	1.75	0.87
0.109	8.0	1299	0.398	2.022	1.66	0.88
0.107	7.7	1330	0.405	2.056	1.64	0.85
0.105	7.5	1358	0.411	2.088	1.62	0.83
0.098	6.5	1748	0.442	2.244	1.54	0.67
0.097	6.3	1780	0.448	2.274	1.53	0.66

Estimating fracture dimensions usingPKN model. Non-newtonian slurry is used with constant leakoff rates for each stage of injections. Following is the stages and relevant information:

Stage	Fluid Type	C)additive	Leakoff Rate
		lb/gal	ft/min^0.5
I	Pad	0	0.0015
II	Slurry	1	0.0015
III	Slurry	2	0.0015
IV	Slurry	3	0.0015
V	Slurry	4	0.0015
VI	Slurry	5	0.0015

Rock data

Shear modulus G	1450000	psi
poisson ratio	0.2	
critical stress intensity factor Kc	455	psi/in^0.5
fracture height	129.9	ft
Horizontal stress)min	2750	psi
Horizontal stress)max	3045	psi

Fracture treatment data

injection rate qo	10	bbl/min
time t	200	min
viscosity	100	cp
leakoff rate Kl	0.0015	ft/min^0.5
V sp	0.01	gal/ft^2

Data for non-Newtonian case

40 lb/Mgal polyacrylamide solution

n	0.31	
K	0.020	lbf-sec^n/ft^2

Time	Lf	μ	W1	V)f	γ′	μ)GEFFAR	W2	Diff	W)avg
min	ft	cp	inches	ft/sec	1/sec	cp	inches	0.000	inches
1	45.9	116.1	0.121	0.357	87.69	177.43	0.121	0.000	0.075
2	64.9	139.3	0.138	0.313	67.31	212.91	0.138	0.000	0.085
3	79.5	154.9	0.149	0.290	57.67	236.84	0.149	0.000	0.092
4	91.7	167.1	0.158	0.274	51.68	255.45	0.158	0.000	0.097
5	102.6	219.6	0.173	0.249	42.64	291.66	0.173	0.000	0.107
10	145.1	263.5	0.198	0.218	32.73	350.00	0.198	0.000	0.122
15	177.7	293.1	0.214	0.202	28.04	389.40	0.214	0.000	0.132
20	205.2	316.2	0.226	0.191	25.13	420.02	0.226	0.000	0.139
30	251.3	437.7	0.258	0.168	19.30	503.86	0.258	0.000	0.159
40	290.1	472.1	0.272	0.159	17.29	543.48	0.272	0.000	0.168
50	324.4	500.6	0.284	0.152	15.88	576.34	0.284	0.000	0.175
60	355.3	525.2	0.294	0.147	14.81	604.66	0.294	0.000	0.182
70	383.8	678.1	0.320	0.135	12.54	678.11	0.320	0.000	0.197
80	410.3	702.3	0.328	0.132	11.92	702.35	0.328	0.000	0.202
90	435.2	724.4	0.336	0.129	11.40	724.45	0.336	0.000	0.207
100	458.7	744.8	0.342	0.126	10.95	744.81	0.342	0.000	0.211
110	481.1	946.8	0.368	0.118	9.48	822.44	0.368	0.000	0.227
120	502.5	968.9	0.374	0.116	9.17	841.52	0.374	0.000	0.231
130	523.0	989.5	0.380	0.114	8.90	859.42	0.380	0.000	0.234
140	542.8	1272.0	0.408	0.106	7.70	949.15	0.408	0.000	0.252
150	561.8	1295.3	0.414	0.105	7.50	966.52	0.414	0.000	0.255

To generate the viscosity, shear rate can be estimated from the fluid velocity in the induced fracture and shear rate can be computed. The slurry viscosity can be calculated using the polymer solution data and the solid additive volume fraction.

Slurry viscosity estimation scheme using GEEFAR and inputted in the calculations

	0 lb/gal	1 lb/gal	2 lb/gal	3 lb/gal	4 lb/gal	5 lb/gal
Uo	25000	25000	25000	25000	25000	25000
Cv	0	0.042	0.0816	0.1176	0.1509	0.184
a	1.8	1.8	1.8	1.8	1.8	1.8
Ul	0.07	0.07	0.07	0.07	0.07	0.07
no	0.31	0.31	0.31	0.31	0.31	0.31
Uh	1000000	1000000	1000000	1000000	1000000	1000000
	0 lb/gal	**1 lb/gal**	**2 lb/gal**	**3 lb/gal**	**4 lb/gal**	**5 lb/gal**
γ´(1/sec)	**μ(cp)**	**μ(cp)**	**μ(cp)**	**μ(cp)**	**μ(cp)**	**μ(cp)**
87.7	116	134	154	177	204	238
67.3	139	160	185	213	245	285
57.7	155	178	206	237	273	317
51.7	167	192	222	255	294	342
42.6	191	220	253	292	336	391
32.7	229	263	304	350	403	469
28.0	255	293	338	389	448	522
25.1	275	316	365	420	484	563
19.3	330	379	438	504	580	675
17.3	356	409	472	543	626	728
15.9	377	434	501	576	664	772
14.8	396	455	525	605	696	810
12.5	444	510	589	678	781	909
11.9	459	529	610	702	809	941
11.4	474	545	629	724	834	971
10.9	487	561	647	745	857	998
9.5	538	619	714	822	947	1102
9.2	551	633	731	842	969	1128
8.9	562	647	747	859	989	1152
7.7	621	715	824	949	1093	1272
7.5	632	728	840	967	1113	1295

sand loading	density of the slurry(gr/cc)
0	1
1	1.07
2	1.14
3	1.2
4	1.26
5	1.31

Hydraulic diameter = 4 * Hydraulic radius
Area open to flow = Width * Length
Wetted perimeter = 2 * (Width + Length)
Hydraulic diameter = 4 * (Area / Perimeter)
PHPA40 slurry (0,1,2,3,4,5) lb/gal sand

V)f (ft/sec)	γ˙(1/sec)	μ(cp)	Width (inch)	d) eq (cm)	Weissenberg #	Reynolds #
0.357	87.7	177	0.121	0.615	5.82	3.77
0.313	67.3	213	0.138	0.701	5.73	3.14
0.290	57.7	237	0.149	0.758	5.69	2.83
0.274	51.7	255	0.158	0.800	5.65	2.62
0.249	42.6	292	0.173	0.881	5.60	2.46
0.218	32.7	350	0.198	1.006	5.52	2.05
0.202	28.0	389	0.214	1.087	5.47	1.84
0.191	25.1	420	0.226	1.148	5.44	1.71
0.168	19.3	504	0.258	1.310	5.37	1.51
0.159	17.3	543	0.272	1.384	5.34	1.40
0.152	15.9	576	0.284	1.444	5.31	1.32
0.147	14.8	605	0.294	1.495	5.29	1.26
0.135	12.5	678	0.320	1.625	5.25	1.18
0.132	11.9	702	0.328	1.667	5.23	1.14
0.129	11.4	724	0.336	1.705	5.22	1.11
0.126	10.9	745	0.342	1.739	5.21	1.08
0.118	9.5	822	0.368	1.869	5.17	1.03
0.116	9.2	842	0.374	1.900	5.16	1.00
0.114	8.9	859	0.380	1.929	5.15	0.98
0.106	7.7	949	0.408	2.074	5.11	0.92
0.105	7.5	967	0.414	2.101	5.11	0.91

Estimating fracture dimensions using PKN model. Non-Newtonian slurry is used with constant leakoff rates for each stage of injections. Following is the stages and relevant information:

Stage	Fluid Type	C)additive	Leakoff Rate
		lb/gal	ft/min^0.5
I	Pad	0	0.0015
II	Slurry	1	0.0015
III	Slurry	2	0.0015
IV	Slurry	3	0.0015
V	Slurry	4	0.0015
VI	Slurry	5	0.0015

Rock data

Shear modulus G	1450000	psi
Poisson ratio	0.2	
critical stress intensity factor Kc	455	psi/in^0.5
fracture height	129.9	ft
Horizontal stress)min	2750	psi
Horizontal stress)max	3045	psi

Fracture treatment data

injection rate qo	10	bbl/min
time t	200	min
viscosity	100	cp
leakoff rate Kl	0.0015	ft/min^0.5
V sp	0.01	gal/ft^2

Data for non-Newtonian case

20 lb/Mgal PHPA solution

n	0.32	
K	0.0167	lbf-sec^n/ft^2

Time	Lf	μ	W1	V)f	γ′	μ)GEFFAR	W2	Diff	W)avg
min	ft	cp	inches	ft/sec	1/sec	cp	inches	0.0	inches
1	45.9	42.0	0.094	0.461	146.47	64.20	0.094	0.0	0.058
2	64.9	50.2	0.107	0.404	112.67	76.71	0.107	0.0	0.066
3	79.5	55.7	0.116	0.374	96.64	85.14	0.116	0.0	0.071
4	91.7	60.0	0.122	0.354	86.66	91.68	0.122	0.0	0.075
5	102.6	78.6	0.134	0.322	71.61	104.37	0.134	0.0	0.083
10	145.1	93.9	0.153	0.283	55.08	124.74	0.153	0.0	0.094
15	177.7	104.3	0.165	0.262	47.24	138.46	0.165	0.0	0.102
20	205.2	112.2	0.174	0.248	42.37	149.08	0.174	0.0	0.108
30	251.3	154.7	0.199	0.217	32.61	178.12	0.199	0.0	0.123
40	290.1	166.6	0.210	0.206	29.24	191.81	0.210	0.0	0.130
50	324.4	176.5	0.219	0.197	26.87	203.16	0.219	0.0	0.135
60	355.3	185.0	0.227	0.191	25.08	212.91	0.227	0.0	0.140
70	383.8	238.2	0.246	0.176	21.26	238.17	0.246	0.0	0.152
80	410.3	246.5	0.253	0.171	20.22	246.50	0.253	0.0	0.156
90	435.2	254.1	0.258	0.167	19.33	254.08	0.258	0.0	0.159
100	458.7	261.1	0.263	0.164	18.58	261.06	0.263	0.0	0.162
110	481.1	331.2	0.283	0.153	16.11	287.66	0.283	0.0	0.175
120	502.5	338.7	0.288	0.150	15.58	294.18	0.288	0.0	0.177
130	523.0	345.7	0.292	0.148	15.12	300.30	0.292	0.0	0.180
140	542.8	443.6	0.314	0.138	13.10	330.98	0.314	0.0	0.193
150	561.84	451.46	0.318	0.14	12.77	336.89	0.32	0.0	0.196

To generate the viscosity, shear rate can be estimated from the fluid velocity in the induced fracture and shear rate can be computed. The slurry viscosity can be calculated using the polymer solution data and the solid additive volume fraction.

Slurry viscosity estimation scheme using GEEFAR and inputted in the calculations

	0 lb/gal	1 lb/gal	2 lb/gal	3 lb/gal	4 lb/gal	5 lb/gal
Uo	15000	15000	15000	15000	15000	15000
Cv	0	0.042	0.0816	0.1176	0.1509	0.184
a	1.8	1.8	1.8	1.8	1.8	1.8
Ul	0.05	0.05	0.05	0.05	0.05	0.05
no	0.32	0.32	0.32	0.32	0.32	0.32
Uh	100000	1000000	1000000	1000000	1000000	1000000
	0					

	0 lb/gal	**1 lb/gal**	**2 lb/gal**	**3 lb/gal**	**4 lb/gal**	**5 lb/gal**
γ´(1/sec)	**μ(cp)**	**μ(cp)**	**μ(cp)**	**μ(cp)**	**μ(cp)**	**μ(cp)**
146.5	42	48	56	64	74	86
112.7	50	58	67	77	88	103
96.6	56	64	74	85	98	114
86.7	60	69	80	92	106	123
71.6	68	79	91	104	120	140
55.1	82	94	108	125	144	167
47.2	91	104	120	138	159	186
42.4	98	112	129	149	172	200
32.6	117	134	155	178	205	239
29.2	125	144	167	192	221	257
26.9	133	153	176	203	234	272
25.1	139	160	185	213	245	285
21.3	156	179	207	238	274	319
20.2	161	186	214	246	284	330
19.3	166	191	221	254	293	340
18.6	171	197	227	261	301	350
16.1	188	217	250	288	331	385
15.6	192	221	256	294	339	394
15.1	196	226	261	300	346	402
13.1	217	249	288	331	381	444
12.8	220	254	293	337	388	451

sand loading	density of the slurry(gr/cc)
0	1
1	1.07
2	1.14
3	1.2
4	1.26
5	1.31

Hydraulic diameter = 4 * Hydraulic radius
Area open to flow = Width * Length
Wetted perimeter = 2 * (Width + Length)
Hydraulic diameter = 4 * (Area / Perimeter)
PHPA20 slurry (0,1,2,3,4,5) lb/gal sand

V)f (ft/sec)	γ'(1/sec)	μ(cp)	Width (inch)	d) eq (cm)	Weissenberg #	Reynolds #
0.461	146.5	64	0.094	0.477	5.42	15.94
0.404	112.7	77	0.107	0.543	5.35	13.34
0.374	96.6	85	0.116	0.587	5.31	12.02
0.354	86.7	92	0.122	0.620	5.28	11.16
0.322	71.6	104	0.134	0.682	5.24	9.12
0.283	55.1	125	0.153	0.777	5.17	7.63
0.262	47.2	138	0.165	0.839	5.13	6.87
0.248	42.4	149	0.174	0.886	5.11	6.38
0.217	32.6	178	0.199	1.010	5.04	4.93
0.206	29.2	192	0.210	1.067	5.02	4.58
0.197	26.9	203	0.219	1.113	5.00	4.32
0.191	25.1	213	0.227	1.152	4.98	4.13
0.176	21.3	238	0.246	1.251	4.94	3.37
0.171	20.2	246	0.253	1.283	4.93	3.26
0.167	19.3	254	0.258	1.312	4.92	3.16
0.164	18.6	261	0.263	1.338	4.91	3.08
0.153	16.1	288	0.283	1.437	4.88	2.55
0.150	15.6	294	0.288	1.461	4.87	2.49
0.148	15.1	300	0.292	1.483	4.86	2.44
0.138	13.1	331	0.314	1.593	4.83	1.98
0.136	12.8	337	0.318	1.614	4.82	1.94